

Alma Mater Studiorum – Università di Bologna

DOTTORATO DI RICERCA IN

Scienze Biotecnologiche, Biocomputazionali, Farmaceutiche e Farmacologiche

Ciclo XXXIV

**Settore Concorsuale: 06/A3 - MICROBIOLOGIA E MICROBIOLOGIA CLINICA**

**Settore Scientifico Disciplinare: MED/07 – MICROBIOLOGIA E MICROBIOLOGIA CLINICA**

*A genome editing approach to the study of Parvovirus B19*

**Presentata da:** Alessandro Reggiani  
Matricola n. 880352

**Coordinatore Dottorato**

**Chiar.ma Prof.ssa  
Maria Laura Bolognesi**

**Supervisore**

**Chiarissimo Prof.  
Giorgio Gallinella**

**Esame finale anno 2022**



## ***Abstract***

**Dott.** Alessandro Reggiani

**Supervisor:** Prof. Giorgio Gallinella

**PhD programme:** Scienze Biotecnologiche, Biocomputazionali, Farmaceutiche e Farmacologiche, XXXIV ciclo

**Thesis:** A genome editing approach to the study of Parvovirus B19

The human Parvovirus B19 (B19V) is a small pathogenic ssDNA virus, with a 5596 nt long genome encapsidated within an icosahedral capsid with a diameter of about 22 nm. Viral proteins are subdivided into structural and non-structural depending on their role: the main non-structural one is the NS1, along with three minor proteins of 7.5-, 9- and 11-kDa, while the 2 structural proteins VP1 and VP2 assemble originating the capsid shell.

B19V has a very narrow tropism, with erythroid progenitor cells (EPCs) at the stage of proerythroblasts in the bone marrow constituting the main target for productive infections. However, virus can be detected in several districts with a capacity to persist in tissues possibly lifelong. As a pathogen, the virus can induce anemia and erythroid aplasia, with the risk of development of severe complications in patients already suffering from hemopoietic disorders or immune compromised. Typical clinical manifestations are *erythema infectiosum* in children, also known as fifth disease, and arthropathies in adults, but the virus has the potential to induce *hydrops fetalis*, fetal death and cardiomyopathies as well. Therapeutic strategies are, so far, only symptomatic: blood transfusion can be needed in case of severe anemias, NSAID have been used to treat arthropathies and passive immunization via IVIG administration represents a temporary solution in the case of chronic infections. However, the search for specific antivirals is an active field of research, with screenings that have demonstrated the antiviral activity *in vitro* of different compounds such as hydroxyurea (HU), cidofovir (CDV) and brincidofovir (BCV) via a drug repurposing approach.

The possibility to study *in vitro* B19V has always been limited by the availability of just two cellular systems able to support viral replication, the semi-permissive cell line UT7/EpoS1 and a primary culture of peripheral blood *in vitro* differentiated EPCs, and by the difficulties in obtaining high-titer viral replication, hence the need to use patients-derived viremic sera as a viral stock.

Recently, a new model has been developed in our laboratory: a genotype 1a consensus sequence has been used to generate a genomic clone, named CK, that can replicate *in vitro* after nucleofection of UT7/EpoS1 cells and give rise to an infectious viral progeny that can be propagated by infecting EPCs, with yields comparable to those of native virus. This tool can reduce the need of clinical samples and improve the manageability of B19V model systems, opening the way to genome editing strategies to better characterize viral molecular biology and to study virus-host interactions.

In the first project described in this thesis, with the dual aim of testing the plasticity of B19V genome to rearrangements and focusing the attention on the NS1 protein (which is still largely uncharacterized), a functional minigenome of B19V was developed, able to just express the NS1 protein. This minigenome, originated by the deletion of the right-hand half of the internal region and the generation of a new cleavage-polyadenylation site, proved able to replicate and to express the NS1 protein at levels comparable to those of unmodified clones. Furthermore, the ability of this minigenome to complement the function of NS1-deficient genomes was demonstrated, thus providing a proof-of-concept of B19V genome editing possibility and, at the same time, a useful tool to study the NS1 protein also as an antiviral target.

In the second project, in collaboration with the group of prof. Nicolas Gillet that hosted me in his laboratory at the University of Namur, I addressed the interplay between B19V and the cellular restriction factor APOBEC3B (A3B). This protein is a cytidine deaminase acting on ssDNA, whose footprint on B19V genome was proved by a bioinformatic sequence analysis performed by the hosting lab. To understand whether A3B still exerts activity and a potential antiviral effect on B19V, the UT7/EpoS1 cells were transduced with lentiviral vectors expressing shRNAs to silence A3B expression. Then, the modified cells were used as a model to study viral behavior, comparing them to the *wild type* UT7/EpoS1. No significant role of A3B on B19V was demonstrated, in agreement with the hypothesis of viral adaptation to this cellular restriction factor; on the other hand, the virus ability to alter A3B expression would deserve further investigations.

## *Summary*

1. Introduction.....	1
1.1. Taxonomy.....	1
1.2. Genotypes.....	2
1.3. Virus structure .....	3
1.4. Viral Genome .....	5
1.5. Gene expression and transcription .....	6
1.6. Viral proteins.....	9
1.6.1. Non-structural proteins .....	9
1.6.1.1. NS1 protein.....	9
1.6.1.2. 11-kDa protein.....	10
1.6.1.3. 7.5- and 9-kDa proteins .....	10
1.6.2. Structural proteins.....	11
1.7. Viral Tropism .....	11
1.7.1. Virus receptor and cell binding.....	11
1.7.2. Cell entry and genome replication .....	13
1.7.3. Cellular control of B19V replication .....	16
1.7.4. Cell culture systems .....	16
1.8. Host cell response in permissive systems .....	17
1.8.1. B19V-induced DNA Damage Response.....	17
1.8.2. Cell cycle impairment and arrest .....	17
1.8.3. Cell death .....	18

1.9.	Non-permissive systems.....	18
1.10.	Immune response.....	19
1.10.1.	Humoral immune response.....	20
1.10.2.	Cellular immunity.....	20
1.11.	Epidemiology and transmission.....	21
1.12.	Course of infection and clinical manifestations.....	22
1.12.1.	Early events.....	22
1.12.2.	Late events.....	23
1.12.3.	Clinical manifestations.....	24
1.12.4.	Erythema infectiosum.....	25
1.12.5.	Arthritis and rheumatic diseases.....	26
1.12.6.	Intrauterine infection and fetal damage.....	27
1.12.7.	Myocarditis and cardiac diseases.....	28
1.12.8.	Encephalitis and neurological syndromes.....	28
1.13.	Diagnosis.....	28
1.14.	Treatment and antiviral research.....	29
1.14.1.	Therapeutic options.....	29
1.14.2.	Vaccine development.....	30
1.14.3.	Search for antivirals.....	31
1.14.3.1.	Hydroxyurea.....	31
1.14.3.2.	Nucleotide analogs Cidofovir (CDV) and Brincidofovir (BCV).....	32
1.14.3.3.	G-Quadruplex targeting molecules.....	33
1.14.3.4.	Other compounds.....	36
2.	Aim of the project.....	38
2.1.	Experimental background.....	38

2.2.	Generation of a functional minigenome of Parvovirus B19 .....	41
2.3.	Study of the role of APOBEC3B on B19V genome .....	42
3.	Generation of a functional minigenome of Parvovirus B19 .....	44
3.1.	A replicating B19V minigenome .....	44
3.1.1.	Molecular cloning .....	46
3.1.2.	Comparative functional analysis of the pAs1 clones .....	46
3.1.2.1.	Nucleic acids analysis.....	47
3.1.2.2.	Protein expression analysis.....	50
3.2.	Genome splitting and functional complementation .....	51
3.2.1.	NS Knocked Out genome .....	52
3.2.1.1.	Molecular Cloning.....	52
3.2.1.2.	Functional analysis of NSKO genome .....	52
3.2.2.	NS Spliced minigenomes.....	55
3.2.2.1.	Molecular Cloning.....	55
3.2.2.2.	Functional analysis of <i>NS Spliced</i> minigenomes.....	55
3.2.2.3.	Extracellular vehiculation of minigenomes.....	57
3.3.	Discussion .....	58
4.	Study of the role of APOBEC3B on B19V genome.....	61
4.1.	Test of A3s expression in UT7/EpoS1 .....	62
4.2.	A3B silencing in UT7/EpoS1 cells .....	64
4.3.	B19V–A3B interplay in nucleofected UT7/EpoS1 .....	65
4.4.	B19V–A3B interplay in infected UT7/EpoS1 .....	68
4.5.	Discussion .....	70
5.	Conclusions.....	72
6.	Materials and Methods.....	74

6.1.	Bacterial strains .....	74
6.2.	Bacterial media.....	74
6.3.	Molecular cloning .....	75
6.4.	Bacterial transformation and growth.....	79
6.5.	Plasmid miniprep and midiprep systems.....	80
6.6.	DNA fragments purification.....	80
6.7.	Cells.....	80
6.8.	Endpoint PCRs .....	81
6.9.	Nucleofection of UT7/EpoS1 cells .....	83
6.10.	Infection of UT7/EpoS1 cells or EPCs.....	83
6.11.	Generation of Lentiviral vectors.....	83
6.12.	Lentiviral transduction of UT7/EpoS1 cells.....	85
6.13.	Selection of edited UT7/EpoS1 cells.....	85
6.14.	Nucleic acid extraction .....	85
6.15.	qPCR analysis.....	86
6.16.	RT-qPCR analysis .....	87
6.17.	A3B isoform identification.....	89
6.18.	IIF analysis .....	90
6.19.	Flow cytometry analysis.....	91
6.20.	Southern Blot analysis .....	91
6.21.	Western Blot analysis .....	92
6.22.	Deamination Test.....	93
7.	References.....	94

## ***1. Introduction***

### **1.1. Taxonomy**

Parvoviruses are among the smallest existing pathogens, being non-enveloped viruses with a diameter around 25 nm. Parvovirus B19 (B19V) was discovered in 1975 by Yvonne Cossart and colleagues while screening serum samples for hepatitis B virus, getting its name from the sample number [1].

Recently renamed *Primate Erythroparvovirus 1* by the International Committee on Taxonomy of Viruses (ICTV), it is a single-stranded DNA virus (*Monodnaviria*) belonging to the *Parvoviridae* family. This family was divided in 1993 into two subfamilies, *Parvovirinae*, and *Densovirinae*, containing viruses infecting respectively vertebrates and invertebrates [2]. Now, due to the discovery of novel viruses challenging this classification, a new taxonomy proposal has been approved in 2020, adding the new subfamily *Hamaparvovirinae* and overcoming the traditional host-dependent classification [3].

The 2020 taxonomy revision has confirmed the previous classification of Parvoviruses according to the phylogenetic analysis of the main nonstructural protein, NS1, introducing some improvements to overcome difficult classification of recently discovered viruses. To be classified inside a genus, the NS1 aminoacidic sequence of a virus should have more than 35-40% of identity with the one of viruses in the same genus and less than 30% with parvoviruses in other genera. The identity percentage required rises up to 85% inside the same species. According to the recently modified parameters, ten genera have been defined inside the *Parvovirinae* subfamily: *Protoparvovirus*, *Amdoparvovirus*, *Aveparvovirus*, *Bocaparvovirus*, *Dependoparvovirus*, *Erythroparvovirus*, *Copiparvovirus*, *Tetraparvovirus*, *Artiparvovirus* and *Loriparvovirus* [3] (Figure 1).

## Introduction

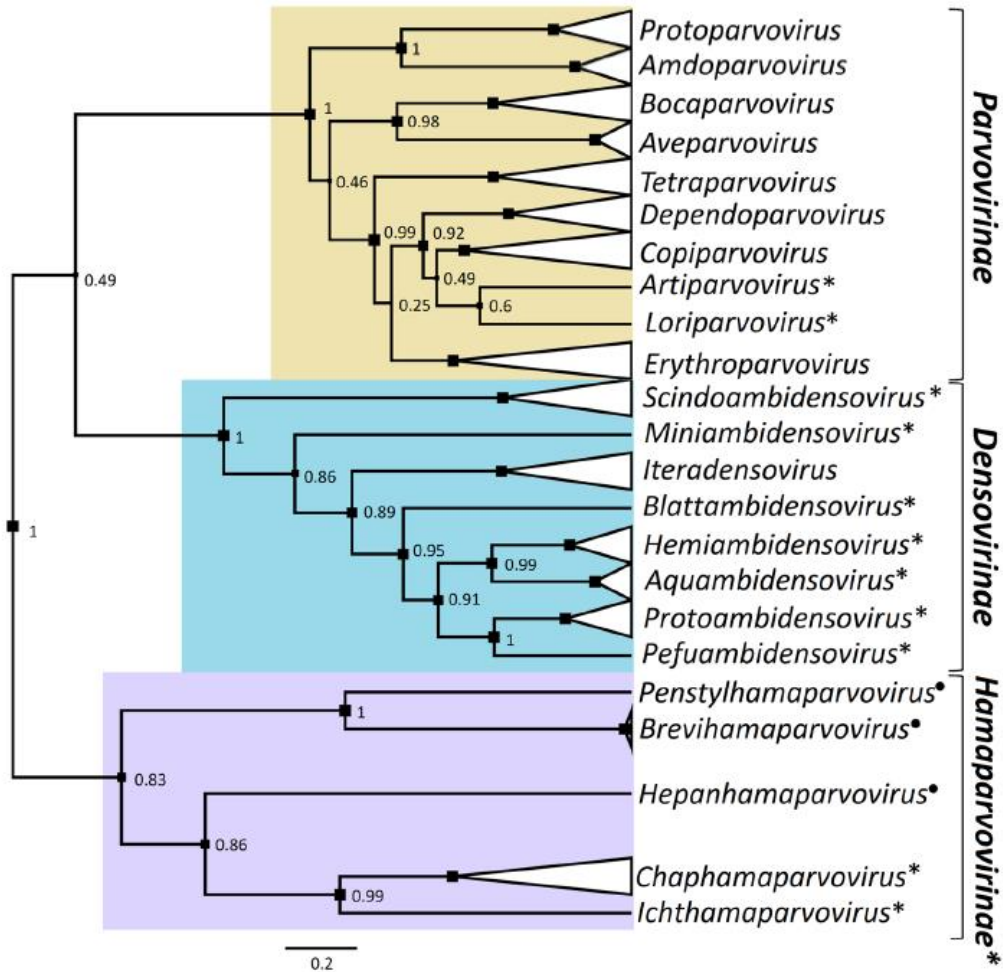


Figure 1: Updated representation of the Parvoviridae taxonomical subdivision [3]

### 1.2. Genotypes

B19V genetic diversity has been a subject of interest both for studying viral evolution and for discovering possible determinants to virus-cell interactions. The development of novel sequencing techniques over the time has expanded the amount of data available, enabling the discovery of new variants that ultimately led to the subdivision of the species into three genotypes [4]. In fact, despite early studies showed a picture of high homology within B19V isolates, usually more than 98%, later on the discovery of some genetically divergent isolates changed the perception about B19V evolution.

Three variants were identified and named genotype 1 for the prototypical isolates, genotype 2 for isolates LaLi- and A6, genotype 3 for isolates V-9 and D91.1-like [4]. Of these, the most common currently circulating is genotype 1, while genotype 2 is considered to have been replaced by genotype one in the late '70s: it is sporadically associated with acute infections, but the ability of B19V to persist in tissues enabled its frequent detection in soft tissues of subjects born before 1972. Genotype 3 is circulating endemically in some geographical regions in Africa, but it has been just sporadically detected in Europe, Brazil, and India [5–7].

The three genotypes, anyway, appear to have similar properties from a biological, pathogenetic and antigenic point of view, constituting a single serotype [8].

The substitution rate is around  $4 \times 10^{-4}$  substitutions per site per year, within the range for RNA viruses. Thus, the evolutionary speed is considerably high, as observed also for canine parvovirus and other ssDNA viruses using the host replicative machinery for their replication [9–11].

### **1.3. Virus structure**

B19V capsid is formed by 60 subunits assembled into a T=1 icosahedral symmetry, with the smaller capsid protein VP2 being the major constituent and the larger VP1 constituting about a 5-10% of the total [12]. The core structure of the virion is formed by the VP common region, arranged in a  $\beta$ -barrel, with eight strands connected by large loops whose variable regions (VRs) at the top determine the topography of the outer surface and give rise to specific structures at the 5-, 3- and 2-fold axes, which have the same overall characteristics in the *Parvovirinae* subfamily (Figure 2).

## Introduction

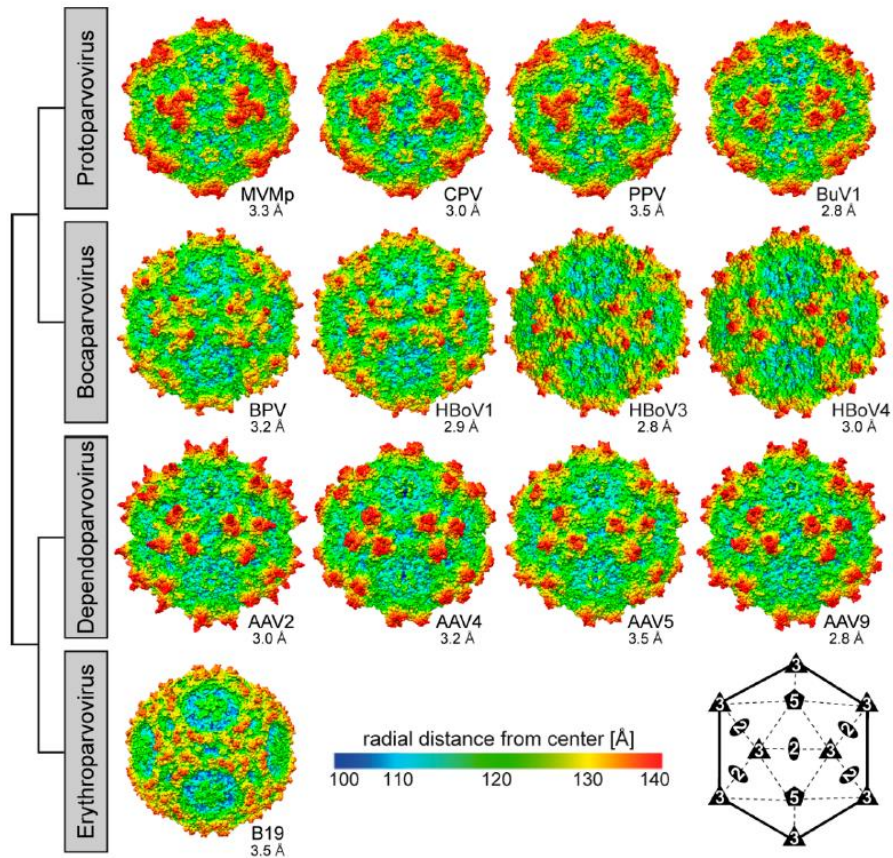


Figure 2: A selection of capsid structures of the Parvovirinae subfamily. The capsid surfaces are viewed down the icosahedral 2-fold axes and are colored according to radial distance from the particle center (blue to red), as indicated by the scale bar. In the lower right-hand corner, a symmetry diagram illustrating the positions of the icosahedral symmetry axes on the capsid surfaces. [13].

First, a channel surrounded by a canyon-like depression at the 5-fold symmetry axis connects the interior to the exterior of the capsid and is believed to be important during genome packaging. Secondly, protrusions are located at the 3-fold axis that may vary in shape and size depending on the genus and loop length and conformation. In B19, two different protrusions are present in this region, but they're generally smoother than in other genera, giving the capsid a more rounded shape.

At last, a second depression, separated from the first one by a raised region known as the 2/5-fold wall, is located at the 2-fold axis. Its depth and width are variable within genera, but the floor is constituted by residues conserved within each genus. All those regions are involved in virus-host interactions, binding receptors, glycans or antibodies. [13,14]

Despite several capsid crystal structures have been made during the years, the N-terminus of the VP1 has not been determined. The main hypothesis is that it can be located in the inner part of the

capsid and exposed if virions are damaged or during the first phase of infection. Moreover, a G-rich stretch makes this region highly flexible, disordered and, therefore, harder to characterize. In any case, it has been shown that the VP1-unique region (VP1u) of B19V is involved in the interaction with a still unknown receptor on the cell membrane and is important for its phospholipase activity (depending on a phospholipase A2 domain, PLA2).

### **1.4. Viral Genome**

B19V genome is a ssDNA molecule, of either positive or negative polarity, 5596 nucleotides long. This molecule can be schematically subdivided into an internal region (4830 nt long) flanked by two Inverted Terminal Repeats (ITRs, 383 nt long) forming a hairpin-like structure (Figure 3).

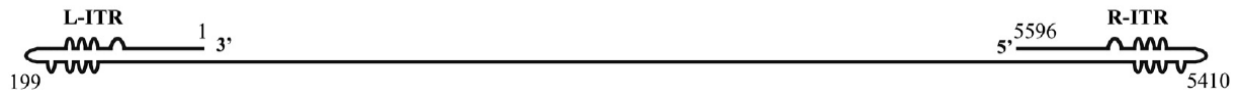


Figure 3: Schematic diagram of a B19V minus strand genome. Bulges and bubbles represent mismatched bases in the ITRs [15]

The ITRs have a fundamental role during the replication, serving as primers for the synthesis of the complementary strand after viral entry and during the rolling-hairpin replication [16]. Their sequence is a non-perfect palindrome (Figure 4), with mismatches and insertions generating bulges and bubbles that, eventually, lead to the existence of two different ITR configurations generally called “flip/flop”, one being the reverse complement of the other. Different combinations of these configurations can give rise to four different genome isomers.

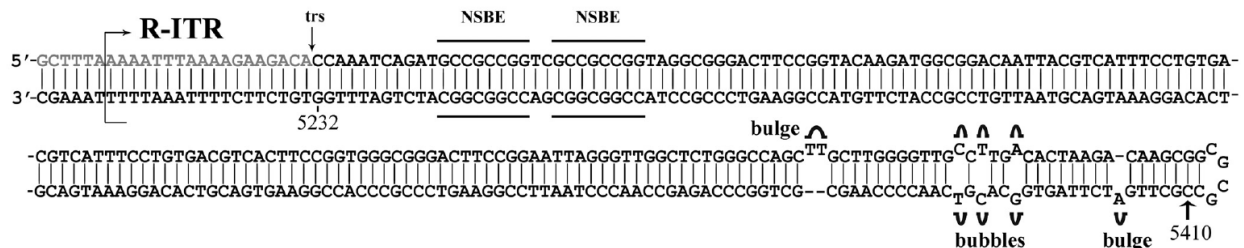


Figure 4: Representation of the right ITR in the flip conformation. Bulges, bubbles, terminal resolution site and NS1 binding elements are annotated [15].

The ITRs contain the NS Binding Elements (NSBEs), an array of four sequence motifs which are necessary for the specific binding of the NS1 protein and its endonuclease and helicase activity.

## Introduction

These NSBEs are 4 8-10 nt long motifs (NSBE 1-4) in the beginning of the ITR: the first two of them (figure 3) are necessary for the binding of the NS1 protein, while NSBE 3 and 4 are dispensable but able to maximize binding affinity and replication rate, suggesting a potential role in binding cellular factors, that has more recently led to consider them as cellular factor binding elements (CFBEs) [17,18]. The terminal resolution site (trs) where NS1 exerts its endonuclease activity is also present in this region, as noted in figure 3.

The internal region contains all the coding sequences for the viral genes (Figure 5): the two main ORFs for the NS1 (in the left side) and the two colinear VP1/VP2 capsid proteins (in the right side), as well as the minor ORFs for the 7.5-, 9- and 11-kDa proteins. Of the three minor proteins, the 11-kDa is the only one already studied, while the others are predicted but not yet characterized.



Figure 5: Schematic representation of B19V genome ORFs

## 1.5. Gene expression and transcription

B19V genome is transcriptionally active in its double-stranded replicative form (dsRF), which has a single promoter at map unit 6 (P6), with a transcription start site at nt 531 [19,20]. Some upstream enhancers (nt 180-490) can bind cellular transcription factors CREBP, C-Ets, GATA, YY1 and Oct-1, which strengthen the promoter activity [21,22]. Moreover, the viral protein NS1 can bind the NSBEs at nt 337-354 to transactivate the P6 via its C-terminal domain [23–25].

A single pre-mRNA is synthesized and a complex system of alternative splicing and polyadenylation is used to express at least 12 different mature mRNA transcripts [20,26,27].

The pre-mRNA contains two splice donor sites (D1 and D2) each followed by two alternative splicing acceptor sites (A1-1/2 and A2-1/2). In addition, it harbors two proximal (pA)p1/2 (with a utilization ratio of 90:10) and a distal (pA)d polyadenylation site. The activity of these splicing and polyadenylation signals, especially for the ones close to the center of the genome, are finely regulated by a number of intron and exon splicing enhancers (2 ISEs and 3 ESEs) and through a

competition mechanism between the splicing and polyadenylation machinery when binding this region [26,28,29].

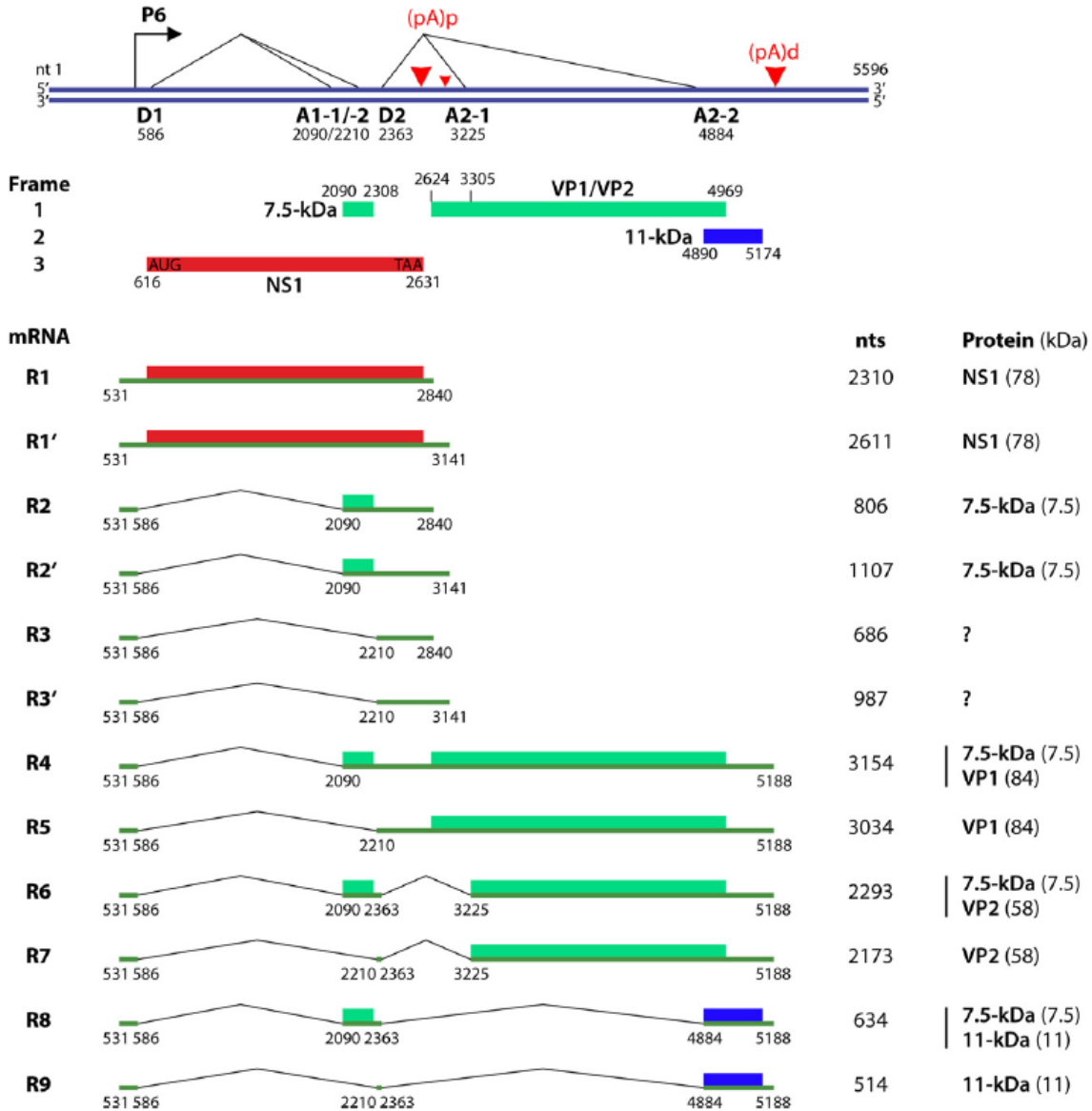


Figure 6: B19V transcription map. Schematic diagram of the duplex replicative form (RF) of the B19V genome. It is capable of expressing viral genes, replicating, and producing progeny virions. The P6 promoter, the RNA initiation site, splice donor sites (D1 and D2), splice acceptor sites (A1-1, A1-2, A2-1, and A2-2), and proximal/distal polyadenylation sites (pA)p/(pA)d are indicated, along with the nine major mRNAs (R1 to R9). Different ORFs are depicted in different-colored boxes [30].

All viral transcripts share at the 5' end a common 55 nt long leader sequence (Figure 6). It is possible to distinguish the transcripts as unspliced mRNA transcripts and spliced ones. Unspliced mRNA transcripts (R1 and R1') that polyadenylate at (pA)p encode the NS1 protein while those

## Introduction

spliced at A1-1 (R2 and R2') and use (pA)p sites can encode only the 7.5-kDa protein. The mRNA transcripts polyadenylated at (pA)d and that undergo one or two splicing events encode respectively for VP1 (R4 and R5) and VP2 proteins (R6 and R7). The 11-kDa protein is encoded by a transcript where three introns have been spliced out (R8 and R9). It is interesting to notice that the 7.5-kDa protein could be encoded by all the even transcripts (R2, R2', R4, R6, R8), even though its actual expression has still to be verified. In the same way, the 9-kDa protein could be encoded by several transcripts, like the ones polyadenylated at the (pA)p2 site, but it is not known whether the protein is actually expressed. At last, transcripts using the A1.2 acceptor site which are polyadenylated at the (pA)p (R3 and R3') are considered as non-coding RNAs, whose function is unknown.

B19V transcripts levels are regulated in several ways: in the absence of viral DNA replication, most of the transcripts polyadenylate at (pA)p leading to the expression of NS1 in both B19V permissive or non-permissive cells [31]. Viral DNA replication facilitates the read-through of (pA)p and overcomes the blockade to express mRNAs that polyadenylate at (pA)d encoding for the VP1, VP2 and 11-kDa proteins [29]. Therefore, this fine regulation in the frequency utilization of RNA processing signals leads to an expression profile where two different patterns can be distinguished. First an early phase, when cleavage at the proximal site leads to a higher relative production of mRNA for NS protein; then a late phase, when cleavage at the distal site is more frequent leading to higher relative abundance of mRNA for VPs and 11-kDa proteins (Figure 7) [32]. Hence, replication of the genome facilitates the generation of sufficient full-length transcripts that encode the viral capsid proteins and 11-kDa nonstructural protein [29].

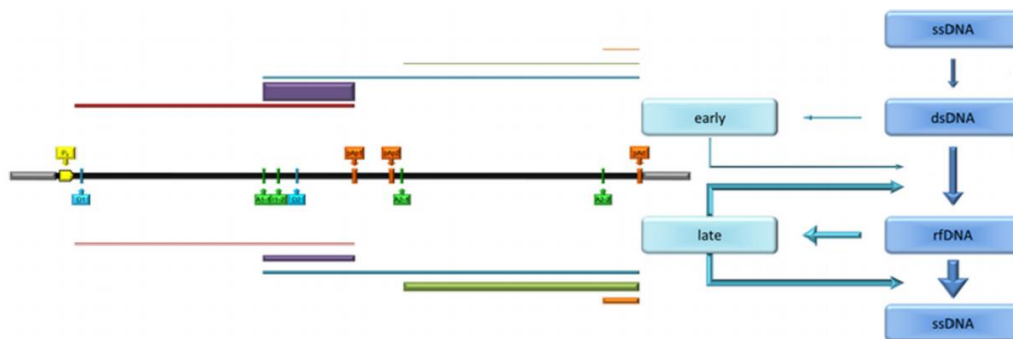


Figure 7: A model for B19V replication and expression. Viral genome can be present in four consecutive states, connected by three state transitions: input ssDNA, initial dsDNA, replicating rfDNA, and product ssDNA. Two functional profiles are identified as “early” (from dsDNA) and “late” (from rfDNA), characterized by a differential abundance and relative composition of transcriptome (see transcription map in figure 5 for comparison). Each profile is involved in regulative loops on genome state transitions.

## 1.6. Viral proteins

B19V genome has the potential to code for four non-structural proteins (NS1, 7.5-, 9- and 11-kDa) and two structural proteins (VP1 and VP2) [14]. Due to the limited dimension of its proteome, B19V has evolved an optimal adaptation to the environment of particular host cells [16].

### 1.6.1. Non-structural proteins

#### 1.6.1.1. NS1 protein

The NS1 protein (Figure 8) is the main non-structural protein encoded in the left half of B19V genome and locates mostly in the nucleus [33] for the presence of two predicted NLS: KKPR (177-179) and KKCGKK (316-321) [23]. It's 671 aa long for a molecular weight around 78 kDa and has three domains that enable its functions on B19V genome [12,20]. The amino-terminal is the DNA binding and endonuclease domain, with the endonuclease motif between aa 137 and 145 [17]; an ATPase and NTP-binding domain is in the center, with helicase functions [34]; a transactivation domain a the C-terminus [35].

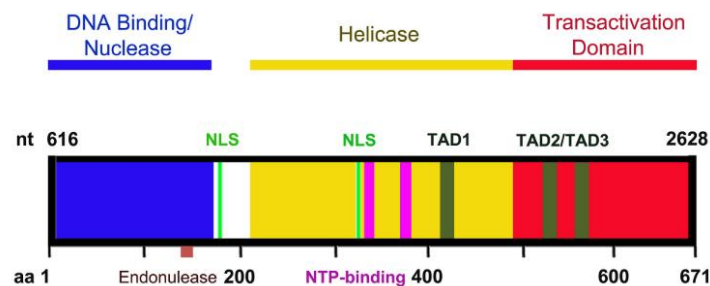


Figure 8: Representation of the NS1 protein and its domains. Endonuclease and NT-binding motifs, nuclear localization sites (NLS) and putative transactivation domains (TADs) are also noted.

NS1 is fundamental during B19V replication, using its N-terminal domain to bind the NSBEs on the ITRs in the dsRF, generating a nick in the trs that allows the prosecution of the rolling hairpin mechanism, presumably using its helicase activity [17,23]. Another important role of the NS1 is the transactivation of the P6 promoter, in assistance with transcription factor Sp1/Sp3, to initiate a loop that regulates viral gene expression [36].

## Introduction

Moreover, NS1 is involved in the interaction with the host (Figure 9): in fact, it has been shown to transactivate several cellular genes (such as tumor necrosis factor alpha (TNF- $\alpha$ ), interleukin 6 (IL-6) and p21, which is involved in the cell cycle arrest), to induce apoptosis in different cell lines (with an involvement of its NTP-binding motif) and to induce cell cycle arrest and DNA Damage Response (DDR) [30,34,37].

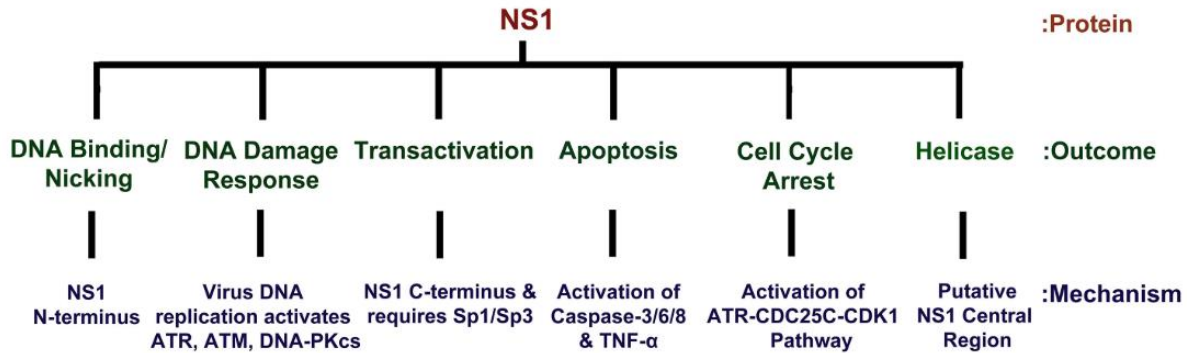


Figure 9: Schematization of the different functions of the NS1 protein [23]

### 1.6.1.2. 11-kDa protein

This minor non-structural protein is encoded in the extreme right region of B19V genome. It is expressed at high levels during B19V infection, even 100 times more than NS1, and is a stronger apoptosis inducer than NS1 [38,39]. It's not fundamental for viral replication, but it has been shown to have a role in facilitating viral replication by interacting with the cellular growth factor receptor-bound protein 2 (Grb2) via a proline-rich domain, thus disrupting extracellular signal-regulated kinase (ERK) signaling, leading to an increase in viral replication [40].

### 1.6.1.3. 7.5- and 9-kDa proteins

B19V genome has the potential to encode also two small non-structural protein of 7.5 and 9 kDa respectively. The 7.5-kDa has been shown to be expressed in an infected cell line in an early report, but no function is known at the present day [41]. The 9-kDa, sometimes named X protein, is predicted to be an 81 aa long protein encoded in a small ORF in the region of VP1u, on another frame [14]. No actual demonstration of its existence has been achieved so far, but the position of the ORF with respect to the (pA)p2 site (which is the same of the 11-kDa ORF compared to the

(pA)d) and some data on its conservation [42] seem to indicate a potential role of this predicted ORF in B19 genome.

### **1.6.2. Structural proteins**

The two capsid proteins, VP1 and VP2, of 84 and 58 kDa respectively, are encoded by a single ORF that give rise to two different transcripts using alternative splicing [43]. The two proteins share the whole sequence of the VP2, but VP1 has an additional N-terminal domain known as VP1-unique region (VP1u). The relative amounts of the minor VP1 protein and the major VP2 protein in the viral capsid are partially regulated by the presence of multiple AUG codons upstream of the commonly used translation initiation codon of the VP1 protein [44]. These spurious triplets, which have been shown to be responsible for the reduced translation efficiency of the VP1 mRNAs, are removed by splicing events from the VP2 mRNAs, drastically increasing the synthesis of the VP2 protein [43].

VP proteins are produced in the late phase of viral gene expression, when the replication process is ongoing. Translated in the cell cytoplasm, they are imported in the nucleus using a non-conventional NLS motif at the C-terminus of VP2 [45], where they self-assemble into viral particles with a ratio of 1:20 [33]. Previous studies, based on the use of heterologous system, demonstrated that VP2 alone is able to assemble into virus-like particles (VLPs), which resemble the icosahedral structure of the B19V capsid. On the contrary, the VP1 protein is not capable of self-assembly, unless the N-terminus region is deleted [46,47].

The N terminus (aa 1 to 100) of VP1u plays a crucial role in virion binding and internalization during B19V entry into cells [48], whereas the central portion of VP1u (aa 128 to 160) contains a motif with PLA2 activity [49]. This PLA2 motif is possibly used during intracellular trafficking to escape late endosomes for nuclear entry, as for other parvoviruses [50].

## **1.7. Viral Tropism**

### **1.7.1. Virus receptor and cell binding**

B19V tropism, considering cells that can be productively infected, is very narrow and basically limited to a main target, represented by erythroid progenitor cells (EPCs) located in the bone

## ***Introduction***

marrow, where the virus can exert a cytotoxic effect that causes a block in erythropoiesis, sometimes leading to a clinically relevant transient or persistent erythroid aplasia. This cellular target is a heterogenous population with proliferating cells at different stages of differentiation, with different phenotypical and functional properties.

One of the main determinants in B19V infection is its interaction with cell receptors. The glycolipid globoside (globotetraosylceramide, Gb4), determinant of the minor blood group P, has been considered to be the specific receptor for a long time [51]. In fact, rare persons with the p phenotype, that lack globoside on the plasma membrane of erythrocytes and EPCs, were shown to be naturally resistant to B19V infections [52]. Though necessary, globoside expression was not sufficient for a productive infection, suggesting the existence of some coreceptor. Some proposal about the identity of these coreceptor has been made throughout the years, spanning from  $\alpha 5\beta 1$  integrin to Ku80, but their correlation with the host range of B19V has proven weak.

However, Gb4 role during viral entry has recently been questioned [53]. From this study, it turned out that Gb4 is essential for viral productive infection but exerts some post entry effect: indeed, Gb4 knocked-out cells can still be infected by B19, which reaches the nucleus but remains transcriptionally inactive. Further investigation about the role of Gb4 demonstrated its role in endocytic trafficking, since its interaction with B19V is regulated by pH conditions: while the early endosome is a perfect environment for this interaction, due to its acidic pH, the neutral conditions in extracellular milieu do not favor it. The pH dependency of this interaction should favor interaction with globoside in the endosome rather than directly on plasma membrane, thus contributing to the narrow tropism of B19V [54].

Due to this recent evidence, the main receptor for B19V entry in the cells seems to be a still unknown molecule interacting with a receptor binding domain (RBD) in the N-terminal region of the VP1u, characterized by a rigid helical fold: the distribution of this putative receptor seem to correlate better with cell susceptibility and its blocking by soluble VP1 strongly reduces B19V entry in the cells [48,55,56]. These results suggest a prominent role of the VP1u and its receptor, whose interaction would trigger the endocytosis into the EPCs allowing a productive viral replication in the bone marrow.

### 1.7.2. Cell entry and genome replication

Since VP1u represents a dominant antigenic target for neutralizing antibodies [48], it is reasonable to assume that it is not exposed to the external environment until viral attachment [57]. Upon this step, a conformational change occurs in the VP1 protein, leading to the exposure of VP1u. It is unclear whether this modification is due to Gb4 interaction as originally suggested [57], but VP1u exposure leads to its binding to a specific, unknown, cell receptor, and to the display of a PLA2 domain, which could increase the permeability of the cell membrane mediating internalization of the virion through clathrin-mediated endocytosis [56,58].

Virions are eventually released in the cell cytoplasm through an endosomal escape mechanism that may involve the PLA2 activity of VP1u, since PLA2 sequences alter and induce curvature of membranes by modifying the lipid head groups to change their packing within the membrane. However both the contribution of other viral or cellular factors and the details of the mechanism of escape are unknown [59].

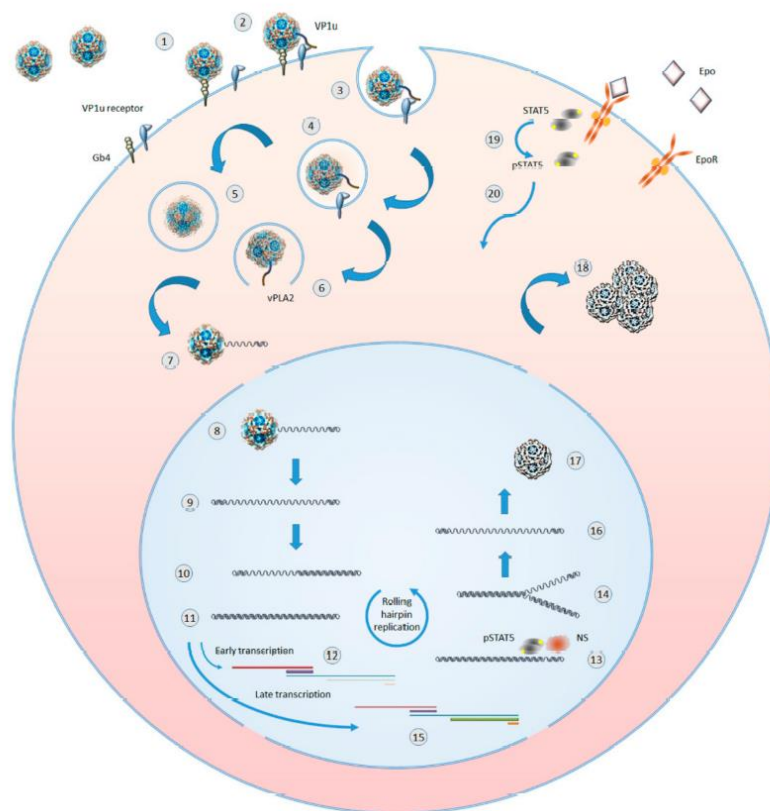


Figure 10: Outline of B19V replicative cycle in erythroid progenitor cells. 1: virion binding to globoside. 2: extrusion of VP1 unique (VP1u) region and binding to an erythroid specific receptor. 3: clathrin-mediated endocytosis. 4: virions in endosomal

## **Introduction**

*vesicles. 5: virion processing within endosomes. 6: VP1u-associated viral phospholipase (vPLA2) mediated virion escape from endosomes. 7: partial uncoating and externalization of viral ssDNA. 8: translocation in the nucleus and complete uncoating. 9: parental ssDNA and onset of macromolecular syntheses. 10: hairpin-primed second strand synthesis. 11: formation of dsDNA replicative intermediate. 12: early phase of transcription on the parental template, mainly of mRNAs for NS protein. 13: dsDNA nicked by NS and priming of replication in coordination with cellular proteins. 14: replication by a rolling hairpin mechanism, via self-primed single-strand displacement mechanisms. 15: late phase of transcription on the replicative intermediates, mainly of mRNAs for VP and 11kDa proteins. 16: progeny ssDNA released from the replicative intermediates. 17: encapsidation of progeny ssDNA molecules in newly formed virions. 18: accumulation of virions before their release via cell lysis or apoptosis. 19: Epo binding by Epo receptor (EpoR), EpoR activation, and STAT5 phosphorylation. 20: pSTAT translocation in the nucleus where it is essential for formation of a functional replicative complex [60].*

Following endosomal escape and prior to nuclear entry, a significant proportion of the incoming capsids rearrange and externalize the viral genome without capsid disassembly. Uncoating releases viral ssDNA of either positive or negative polarity into the nucleus. The uncoating mechanism is unknown: it is thought to occur with a limited capsid rearrangement prior to nuclear entry capsid disassembly [61].

It has to be noticed that only a small proportion of internalized virions reaches the nucleus, as endosomes can fuse with lysosomes.

Once the viral genome is free in the nucleus, cellular DNA repair mechanism begin the synthesis of the second strand, generating a dsDNA that can act as template both for transcription and replication. The early phase of transcription leads mainly to the production of NS that, acting together with cellular factors, promotes the genomic replication through a rolling-hairpin mechanism (Figure 11).

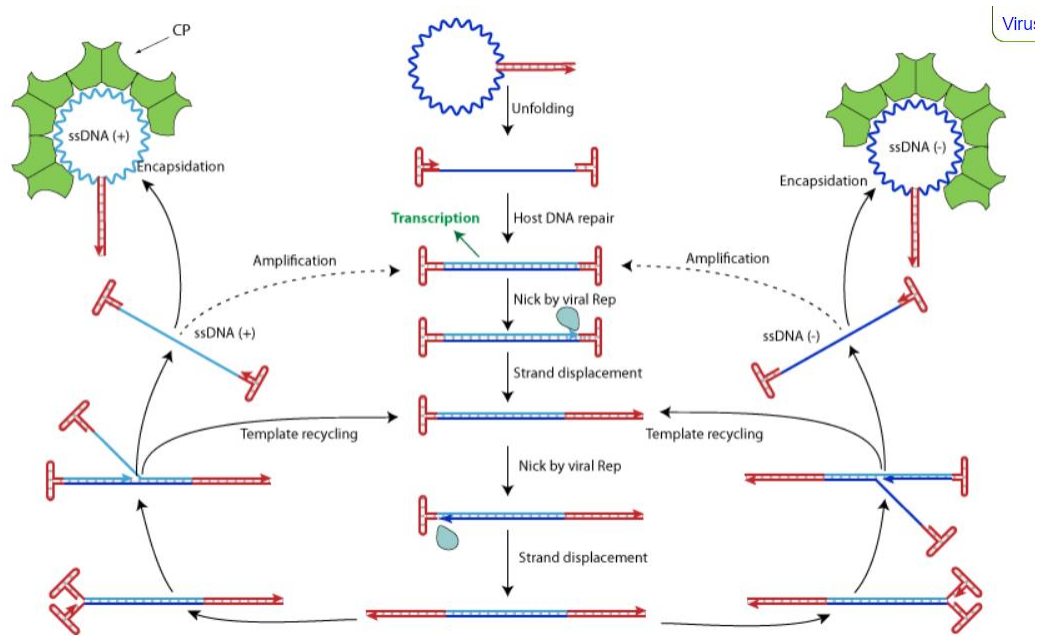


Figure 11: Schematization of the rolling-hairpin replication in AAVs. In the case of B19, the Rep protein is substituted by NS1. [ViralZone]

After its synthesis in the early phase of transcription, NS1 binds the NSBEs (5'-CCGGCGGC-3') in the viral Ori on the dsRF of B19 introducing a nick at the trs that generates a 3'-OH used by cell machinery to do strand displacement while extending the linear dsDNA molecule. The two ITRs can then reform the hairpin structure, and the 3' terminal of one strand acts as primer to the synthesis of the second one, while a complete ssDNA genome copy is displaced and ready to be encapsidated. Since the two hairpins are symmetrical, the amount of positive and negative ssDNA generated is comparable.

In the meantime, the dsRF is transcriptionally active [16], relying again on cell machinery. The (pA)p block is overcome by the replication [29], so mRNAs encoding the late genes are exported to the cytoplasm to be translated. The VPs assemble as trimers in the cytoplasm and are then transported into the nucleus, where they form an empty capsid that will host a genome copy possibly through an NS1-dependent encapsidation mechanism [30]. Complete virions are then accumulated in the cytoplasm, and will be released by cell lysis or apoptosis [60].

## ***Introduction***

### ***1.7.3. Cellular control of B19V replication***

B19V very narrow tropism implies that the presence of globoside and of VP1u receptor is not enough to support viral replication: B19V has been associated to the alteration of several cell-signaling pathways that are used to increase replication efficiency [35,62–64].

Not having its own DNA polymerase, B19V only relies on cellular machinery. It has been shown that the virus induces a block in the late S/G2 phase with a 4N DNA content [65,66], and that several S-phase factors, such as DNA Pol  $\delta$ , PCNA, RFC1, cyclin A and MCM, colocalize at B19V replication centers [63]. Moreover, erythropoietin (Epo) is essential for the differentiation of EPCs and both them and the semi-permissive cell line UT7-EpoS1 rely on Epo for *in vitro* growth. Epo is a hormone produced by renal interstitial fibroblast that is used to regulate erythropoiesis, along with IL-6, IL-3 and stem cell factor (SCF) [64,67].

Epo, in particular, plays a direct role in the cell permissiveness to B19V, since EPCs differentiated from CD34+ HSCs are not permissive in the absence of Epo: in fact the activation of EpoR activates three subsequent major pathways, MEK/ERK, PI3K and JAK2-STAT5, with the latter one being essential for B19V replication [30]. Phosphorylated STAT5 (pSTAT5) seems indeed to bind a binding site in the viral Ori, recruiting the MCM complex to initiate DNA replication [68]. Hypoxia is another factor that has been shown to enhance viral replication. When infecting EPCs under hypoxic condition, thus recreating an environment more similar to the *in vivo* target in the bone marrow, viral gene expression, replication and production are enhanced [23]. This importance of hypoxia is not related to a better viral entry or trafficking, nor to a role exerted by HIF-1 [62], but to an upregulation of STAT5 and downregulation of MEK in both infected EPCs and UT7/EpoS1 cells transfected with the infectious clone M20 [62].

### ***1.7.4. Cell culture systems***

B19V is cultured *in vitro* mainly in just two systems, EPCs or a cellular line named UT7/EpoS1. EPCs can be obtained from different sources, spanning from the bone marrow to fetal liver and umbilical cord blood, but the most common and easiest to use is peripheral blood. Starting from peripheral blood mononuclear cells (PBMCs), CD36+ EPCs can be obtained through *in vitro* differentiation [32,69], representing the optimal model to study B19V, especially if kept under hypoxia conditions. This system, though, has the strong limit of relying on blood supply, since this

primary cells are a differentiating heterogenous population that can be infected in a really narrow window of time [32]. It is therefore useful to work with a cell line. Several megakaryocyte-erythroid or leukemia cell lines have been tested (M-02, JK-1, Ku812Ep6, UT7/Epo) and, based on viral replication and protein expression, UT7/EpoS1 cells appeared to be the best compromise between efficiency (much lower than EPCs) and manageability [14,30].

## **1.8. Host cell response in permissive systems**

### **1.8.1. B19V-induced DNA Damage Response**

B19V infection triggers a DNA damage response (DDR) by phosphorylating all the upstream kinases of each of the three repair pathways: ATM (ataxia-telangiectasia mutated), ATR (ATM and Rad3 related), and DNA-PKcs (DNA-dependent protein kinase catalytic 19 subunit) [70]. These proteins and their downstream effectors (Chk2, Chk1, and Ku70/Ku80 complex, respectively), localize within the B19V replication center. None of the viral proteins is involved in triggering the DDR, which is instead the result of the replication of the viral genome and not of its mere expression [35].

NS1 is essential for DNA replication and is required for inducing the DDR during B19V infection. Viral DNA replication is a prerequisite for a B19V-induced DDR, and DNA replication intermediates could be potential inducers of the DDR.

### **1.8.2. Cell cycle impairment and arrest**

B19V infection results in a rapid arrest of cell proliferation in the primary CD36+ EPCs and UT7/Epo-S1 cell systems; in vivo, this leads to the block of erythropoiesis, thus to anemia. The mechanisms and the stages at which this process occurs are diverse and still under investigation. B19V infection of CD36 EPCs and UT7/Epo-S1 cells induces arrest in late S/G2 phase, a cell cycle status with 4N DNA content [65]. The arrest in in G2/M phase is demonstrated by accumulation of cyclin A and B1 in the cytoplasm, phosphorylated cdc2, and an up-regulated kinase activity of the cdc2-cyclin B1 complex, similar to that in cells treated with the mitotic inhibitor [65].

In addition, stable G2 arrest is induced by the interaction between NS1 and repressive E2F transcription factors (E2F4 or E2F5) [35]. The E2F proteins play a role in regulating cell cycle

## ***Introduction***

progression. Activating E2Fs (E2F1 to E2F3a) are downregulated, while repressive E2Fs (E2F4 to E2F8) are upregulated; moreover, NS directly interacts with E2F4 or E2F5 [71], enhancing their nuclear import, which induces a stable G2 arrest by target gene repression, through a p53-independent manner. The transactivation domain at the C terminus of NS is required for NS-induced G2 arrest [35].

Parvovirus B19 not only induces G2 arrest but also G1 arrest. NS-transfected UT7/Epo-S1 cells show cell cycle arrest at the G1 phase; in this case, NS significantly increases expression of p21/WAF1, a cyclin-dependent kinase inhibitor that induces G1 arrest. This transactivation requires the cellular transcription factor Sp1-NS interaction [37].

Taken together, these findings show that the viral genome and/or its replication is capable of inducing S-phase arrest, while NS1 per se induces G2-phase arrest. Therefore, B19V infection-induced late-S-phase arrest is a compromise outcome of genome replication-induced S-phase arrest and NS1-induced G2-phase arrest [63]. While S-phase arrest enriches S-phase factors that favor viral DNA replication, G2 arrest halts erythropoiesis of erythroid progenitors and eventually kills the cells.

### ***1.8.3. Cell death***

Cell death occurring to the erythroid progenitors infected in the bone marrow leads to a transient aplastic crisis [72], due to block in the erythropoiesis caused by the specific infection of the erythroid progenitors at the BFU-E and CFU-E stage (Burst/Colony Forming Unit Erythroid, respectively). It was shown that different apoptotic pathways are activated by different viral proteins: both infection and transfection with NS1 expression induce activation of caspase -3, -6 and -8 leading to apoptotic death with DNA fragmentation [73,74]; TNF- $\alpha$  pathway of extrinsic apoptosis has been associated with B19V infection both in UT7/EpoS1 and in CD36+ EPCs [75]; the 11-kDa protein is a proven strong apoptosis inducer with caspase-10 involvement [39].

Thus, it appears clear how several components act synergistically to induce an apoptotic cell death.

## **1.9. Non-permissive systems**

B19V infection of non-erythroid cell types is possible, but largely considered as non-productive. The presence of globoside and its role in the first attachment to the cell could explain the ability

of B19V to bind several cell types, but the absence of the erythroid-specific receptor implies that a different mechanism for cell entry is required [76]. Antibody-dependent enhancement (ADE) of infectivity has been demonstrated for some cellular types such as tonsillar B cells, U937 monocytic cells and endothelial cells [76,77], but other cell lines can be infected as well [78,79]. Within these systems, B19V probably undergoes the sole step of double-strand DNA conversion and basal expression of NS and VP proteins. Unlike permissive/semi-permissive systems, NS here triggers activation of the STAT3/PIAS3 pathway, thus the upregulation of immune response genes (IFNAR1 and IL-2) and downregulation of genes associated with antiviral defense (OAS1 and TYK2) [80].

B19V DNA can be detected in a myriad of tissues in different districts even decades after the primary infection, including spleen, liver, tonsils testes and brain [81,82], although it not clear whether virus is present as episomal DNA or can be integrated into the host genome [83,84]. However, the mere detection of viral DNA is not enough to correlate viral infection with possible pathologies, since virus can be present in the tissue but silenced through methylation of CpG sites on viral ITRs [85]. Nonetheless, in some cases viral genome can be transcriptionally active even in absence of replication evidence, as it has been shown for human fibroblasts [86], with the potential to induce pathological effects [87]. B19V presence in various tissues has also been associated to inflammatory and autoimmune consequences, possibly due to the NS1 protein [88]. However, due to viral prevalence and to the almost ubiquitous expression of globoside, associations between B19V and pathologies should not rely just on the detection of viral DNA, but also take into account the transcriptional activity of viral genome and the expression of viral proteins, despite technical difficulties.

### **1.10. Immune response**

The innate immune response against Parvovirus B19 is still poorly known. Some studies have shown the activation of TLR9 triggered by a CpG oligonucleotide localized in the P6 promoter, as well as increased levels of defensins and TLR4, -5, -7 and -9 upon transfection of non-permissive COS7 cells with B19V NS1 and VP2. However, these results have to be validated and deserve further investigation [30].

Much more is known about the adaptive immune response towards B19V.

## ***Introduction***

### ***1.10.1. Humoral immune response***

B19V is able to elicit a strong humoral response. IgM antibodies, which are produced at 8 to 12 days post-infection, can last for 3 to 6 months [89,90]. IgG production begins a few days later, taking advantage over IgM that vanish to an undetectable level in the following weeks and months. IgA antibodies were detected as well, probably protecting nasopharyngeal mucosa [91].

Both IgM and IgG responses are directed against the capsid proteins, with most of the neutralizing epitopes of VP1 localized in the VP1u, despite its inaccessibility in native virions and possibly due to the presence of the receptor binding domain, or the VP1-VP2 junction region, eliciting a stronger response than VP2 epitopes [30,92]. While neutralizing epitopes in the VP1u region mapped to the N-terminus are mainly linear, VP2 epitopes are conformational [92,93].

Antibodies against viral non-structural proteins have also been detected both in acute and persistent infections, with anti-NS1 IgG usually associated with persistent infections, while anti-NS1 IgM could also appear during acute infections [94,95]. Despite its expression 100 times higher compared to the NS1, antibodies targeting the 11-kDa protein (as well as the 7.5-kDa) were not detected [39].

### ***1.10.2. Cellular immunity***

In PBMCs from healthy individuals naturally infected with B19V, both B-cell and CD4+ T-cell mediated responses recognize VP1/VP2 capsids, with antigen presentation through class II HLA molecules. B19V-specific T helper cell proliferation can be detected in infected patients as well [96].

A remarkable CD8+ T cell response has been documented in patients dealing with an acute infection by B19V, lasting several months, even after viremia clearing [97]. Ex vivo measurement of B19V-specific CD8+ T cell responses confirmed that the HLA-B35-restricted peptide derived from the NS protein is much more present during acute infections rather than in persistent infections, where VP1/2 response becomes predominant [98]. Both the VP1/2 and VP2-only capsids elicit IFN- $\gamma$  and IL-10 release by T-helper cells, indicating VP2 as the major target for B19V-specific T helper cells years after virus infection [30]. Cytokine responses to B19V infection are of the Th1 type, with IL-2, IL-12, and IL-15 being detected in acutely infected patients, correlating with the sustained CD8+ T cell response [99].

On the whole, the B19V specific T-cell responses are peculiar, combining characteristics typical of viruses capable of lytic infections as well as capable of establishing a persistent infection, with the requirement for continuous surveillance by the immune system. Finally, the presence of a long-lasting immune response, which is assumed to protect the host from secondary infections, set the rationale for the development of a vaccine, even if the ability of B19V to persist in tissues and the generation of non-neutralizing immune response in some subjects are issues to be addressed, that could limit vaccine application to the more-at-risk subjects.

### **1.11. Epidemiology and transmission**

Parvovirus B19 is widely and worldwide diffuse in the population. Seroprevalence studies indicate that the virus is actively circulating in all areas of the world, albeit with some regional differences, with generally more than one-half of the adult population having been exposed.

The prevalence of specific antibodies is age-dependent, going from less than 20% in children under 5, to 15-40% in children from until 18 years old and to 40-80% in adults. Nevertheless, the antibody titer, assumed to be life-lasting and protective, can vanish thus allowing reinfection. Typically, the infection spreads among 5 to 15 years old children, but adults are also susceptible [30].

The main route of transmission of the virus is the respiratory route, even if the prodromal symptoms are not related: fever, headache, malaise and myalgia. Due to the viremic phase in the course of infection, the virus can be present in blood at high titers, posing a risk of iatrogenic transmission of the virus via blood, blood components, and blood products: for this reason both FDA and European authorities have imposed a limit to the DNA levels measured in plasma pools [100,101].

B19V outbreaks occur mostly in the winter and spring, with major epidemics occurring every few years. Due to the relative ease of spread of the virus, outbreaks of B19V-induced childhood rash (*erythema infectiosum*) are most common in schools and day care centers, affecting up to one-half of schoolchildren and one-fifth of susceptible staff. Generally, the risk of contagion occurs during the acute phase of infection, when the viral load is at its highest, but symptomatology is not manifest. Moreover, the viral load doesn't necessarily correlate with illness severity [89].

## **1.12. Course of infection and clinical manifestations**

B19V infection is associated with a broad range of clinical manifestations (figure 10), whose characteristics depend on the specific virus-host interplay; hence, the outcome of the disease relies on the physiological status of the person and its capacity of immune response. Many studies come from epidemiological data, especially during B19V outbreaks in well-defined cohorts, but also from controlled infections on volunteers infected by nasal inoculations.

### ***1.12.1. Early events***

After taking contact with the respiratory epithelium, the virus reaches the bloodstream starting a primary viremic phase. The mechanism of this passage is not known yet. It is debated whether the virus gets access to the vessels via transcytosis through the respiratory epithelium or after drainage in the lymphatic circle involving tonsils: viral DNA has been detected in tonsils [102,103], which could represent the true entry portal besides being a site for viral persistence[14].

Then, normally undetected, the virus gets to its primary target organ, the bone marrow, where it infects erythroid progenitors exerting cytotoxic effects. In this phase, the bone marrow can show erythroid aplasia and the presence of characteristic giant erythroblasts, considered to be pathognomonic of B19V infection [14]. The effects on bone marrow derive from the ability of virus to induce cell-cycle arrest, block of erythroid differentiation and eventually apoptosis of susceptible and infected cells, and from the dimension and turnover rate of the erythroid compartment. The more undifferentiated precursors, being relatively resistant to infection, ensure the transience of the erythropoietic block and the possibility to relieve it by a neutralizing immune response. A balance is reached between cell population dynamics and viral replication, considering also possible stresses on the erythropoietic compartments and the immune response [104].

In a healthy individual with a physiological erythropoiesis and an effective immune response, infection is limited, with mild to no symptoms. Levels of hemoglobin are only marginally reduced, and clearance of infection may take 3-4 months. Low viral titers can be detected for years after primary infection, indicating a viral persistence, which does not imply a chronic course of infection sustained by active viral replication [103,105].

If the balance between cell turnover and viral replication is altered by pre-existing individual defects in the erythropoiesis or in the immune response, the infection can become manifest as pure red cell aplasia (PRCA) [106].

Infection by B19V can also lead to an acute episode of profound anemia, that presents as the classical aplastic crisis in patients with underlying hematological disorders, such as hemoglobinopathies and thalassemia. On the other hand, if the immune system has not the capability to control, neutralize, and clear viral infection, this can become chronic, with active viral replication and the involvement to different degrees of erythroid compartment. These situations can be typical of congenital or acquired immunodeficiencies, such as HIV infection, in the course of chemotherapy or in the course of immunosuppressive treatments [107–110].

The distinctions between a normal course and active chronic infections are smooth, and again we should take in mind that our picture of B19V as a virus capable of acute, self-limiting infections has been replaced with a more complex picture of a virus capable of establishing long-term relationship with the host, in a mutual adaptation [14].

### ***1.12.2. Late events***

A secondary viremic phase is sustained by the bone marrow that releases the viral progeny, leading to an active infection. In this phase, the infection becomes systemic, with viral titers than can reach  $10^{12}$  viruses/mL. The canonical clinical manifestations are *erythema infectiosum* (or fifth disease) in children and arthropathies in adults [111,112], but the range of symptoms is broad due to secondary target cells reached by B19V. In peripheral tissues, the pathogenic process may depend on the direct cytotoxic/proapoptotic effect of the virus, or on the host inflammatory response to viral proteins, such as NS or VP1u. In the systemic phase, cells of mesodermal tissue are mainly involved; of these, endothelial cells, which are normally nonpermissive, may constitute a reservoir and sometimes support an active viral replication [113].

Another general assumption is that some typical manifestations of infection, such as the erythema, are due to immune complex formation and deposition, with development of inflammatory responses [14].

## ***Introduction***

### ***1.12.3. Clinical manifestations***

The range of clinical manifestations associated to B19V infection has been constantly increasing, to involve almost all organs and tissues and including systemic syndromes, and descriptions of clinical presentations have progressively stressed atypical aspects (Table 1). Categories broadly include: I) hematological disorders other than those involving the erythroid series, rare and in some case severe, often on an immunopathological basis; II) organ specific involvement (myocarditis, hepatitis, encephalitis, glomerulonephritis, etc.) on a sporadic basis; III) association to systemic disease, possibly by triggering autoimmune mechanisms; IV) infection in the immunodeficient patient; V) association to malignancies (e.g., pediatric leukemia/lymphoma, thyroid cancers). The sporadic nature of these associations makes problematic both a definite assessment of a causal relationship, and the individuation of pathogenetic mechanisms, and calls for accurate diagnostic evaluation.

*Table 1: Clinical manifestations of parvovirus B19 infection*

Category	Frequent	Sporadic	
Hematological	Transient anemia	Bone marrow necrosis and fat embolism	
	Aplastic crisis	Myelodysplastic syndrome	
	Chronic anemia	Thrombocytopenia	
	Chronic Pure Red Cell Aplasia		Granulocytopenia
			Pancytopenia
			Idiopathic Trombocytopenic purpura
			Hemophagocytic Lymphohistiocytosis
Specific tissue/organ disease	Erythema infectiosum	Petecchial purpura	
	Mono or poly-arthritis	Henoch-Schonlein purpura	
	Chronic arthralgias		Papular-purpuric glove-and-socks syndrome
			Acute Myocarditis/pericarditis
			Chronic inflammatory myocarditis
			Myositis
			Hepatitis
	Glomerulonephritis		
	Meningitis		

		Encephalitis
		Peripheral neuropathy
		Thyroiditis and thyroid neoplasia (?)
Systemic	Aspecific febrile illness	Chronic fatigue syndrome
		Vasculitis
		Scleroderma
		Lupus erythematosus
Infection in Pregnancy	Intrauterine infection (30-50%)	Mirror syndrome
	Fetal anemia	Meconium peritonitis
	Fetal hydrops	Fetal malformations
	Fetal death	Congenital anemia
		Neurodevelopmental delay (?)

#### 1.12.4. Erythema infectiosum

*Erythema infectiosum* is the classical acute manifestation of parvovirus B19 infection, characterized by mild constitutional symptoms and a blotchy or maculopapular rash beginning on the cheeks and spreading primarily to exposed extremities, hence the name “slapped-cheek disease” (Figure 12).

Categorized in the 19<sup>th</sup> century as “5<sup>th</sup> disease” among a series of childhood rash illnesses, it was supposed to have a viral origin and was associated with B19V shortly after the latter was discovered [112].

Usually, prodromal symptoms do not precede the rash, that generates suddenly in otherwise well children thus resulting the first and sometimes only clinical manifestation.

Arthralgia and myalgia are generally more common among the adult population rather than children.

Some clinical variants in the manifestation of the 5<sup>th</sup> disease can regard the pattern of the cutaneous rash, which has been addressed as “glove-and-socks syndrome”, and the involvement of the lymphatic system, with lymph nodes enlargement and hepatosplenomegaly that can mimic mononucleosis [114–117]

## ***Introduction***



*Figure 12: Typical rashes in the fifth disease left – "slapped-cheek" ; right – "glove-and-socks"*

### **1.12.5. Arthritis and rheumatic diseases**

B19V can cause acute arthritis or arthralgias and occasionally chronic arthropathies [118,119]. Arthritis and arthralgias are more common clinical manifestations in adults, more frequent in females than males and often presenting without concurrent symptoms. In adults, the typical onset is acute, symmetrical, and involving mainly the small joints of hands and feet; in children, on the opposite, they can develop at lower frequencies (<10%), accompanying or following the classical erythema but usually asymmetric and pauciarticular. Chronicization has been reported for children but is more frequent in adult patients [14]. Arthralgia and arthritis can persist for months or years after parvovirus infection and may be debilitating, but usually without joint erosion or development of rheumatoid factor [120].

In vitro, synoviocytes are not permissive to B19V, although they can respond to infection and assume an invasive phenotype, suggesting a parallel role in the pathological processes within synovia [121]. Any pathogenetic mechanisms linked to B19V would require the expression of viral genes, such as the NS protein with its transactivating activity or the VP1 protein with its phospholipase activity, able to activate and maintain an inflammatory response targeted to the synovial tissue. A common concurrent phenomenon is the production of autoantibodies in the course of infection, that can also act as a possible trigger to the induction of autoimmune diseases. In the acute phase of infection, heterologous, cross-reactive, and self-reactive antibodies can normally be produced [122,123].

**1.12.6. Intrauterine infection and fetal damage**

Maternal infections are of major concern, due to B19V ability to cross the placental barrier and infect the fetus. The villous trophoblasts of the placenta expresses high levels of globoside especially in the first trimester, then decreasing progressively along with the risk of fetal infection [124]. Even if trophoblasts are not permissive to the virus, they bind viral capsid via the globoside thus facilitating transcytosis of virus to the fetal circulation [125].

On the other hand, endothelial placental cells can support viral replication, contributing to placental and fetal damage [126]. Once it has reached the fetal circulation, the virus can infect erythroid progenitor cells in liver and/or bone marrow, depending on the gestational age. The block in fetal erythropoiesis can be severe, as a result of the physiologically expanded erythropoietic compartment combined to an immature immune response, and lead to fetal anemia, tissue hypoxia, possible development of nonimmune hydrops, and/or possible fetal death [127]. Contrary to adult, fetal cardiomyocytes are reported to possess the viral receptor and be susceptible to infection, hence direct infection of these cells may induce fetal myocarditis further contributing to fetal damage [128].

The natural course of fetal infection is affected by several factors. First, the gestational stage plays a role because it determines both the expression levels of globoside in the placenta and the pattern of erythropoiesis in the fetus: higher risk of fetal death or miscarriage are more frequent in early infections, while hydrops is more typical of mid-pregnancy infections. [14,30] Second, the immune status of the mother: the presence of anti-B19V IgG in the mother's blood are supposed to be protective against fetal infection, thus limiting the major risks to seronegative pregnant women who are exposed to a primary infection [129]. Finally, the newborn can incur in perinatal infection; in this case, pure red cell aplasia is the only congenital lesion described [30].

In general, the overall risk of intrauterine infection is estimated at around 1% of pregnancies, depending also on the presence of epidemics. The fetal transmission regards around 30% of the infected women, with a risk of fetal death assessed around 10-12.5% (higher in the first 20 weeks and then decreasing). In any case, it should be considered that B19V infection could be asymptomatic in the mother but address the fetus and that, in absence of specific antiviral drugs, therapeutic options are of the more severe cases are limited to symptomatic treatments.

## ***Introduction***

### ***1.12.7. Myocarditis and cardiac diseases***

In recent years, B19V has been detected at increasing frequencies in endomyocardial tissues. B19V has been directly involved as an etiologic agent in sporadic acute myocarditis both in pediatric and adult populations [130,131]. Active B19V infection has been shown in myocardial endothelial cells, so B19V probably acts by inducing endothelial dysfunction, which in turn triggers inflammatory responses in the cardiac tissue [132,133]. The definition of a possible role of B19V in the development of chronic cardiomyopathies and cardiac dysfunction is instead matter of ongoing debate [134,135]. The frequency of B19V DNA detected in cardiac bioptic samples is constantly high, and a marked cardiotropism should be mentioned as one of the main characteristics of B19V. A positive association and a role of B19V in the development of inflammatory chronic cardiomyopathies has been proposed because of significant higher mean viral loads or the presence of viral mRNAs, suggesting active viral replication and expression

### ***1.12.8. Encephalitis and neurological syndromes***

Occasionally, fifth disease patients suffer from neurological symptoms, and diverse neurological complications, such as encephalitis, stroke, neuropathy and meningitis have been associated to B19V [136–138]. Neurological complications can occur in immunocompetent patients, children or adult, in case of acute or chronic parvovirus infection, but they can be more frequent among immunocompromised persons with underlying diseases. IVIG administration has been employed to treat B19V-associated neurological syndromes [139], but its efficacy is of difficult evaluation as a result of the spontaneous improvement of many patients.

## **1.13. Diagnosis**

A clinical diagnosis of B19V can just be hypothesized, because the symptoms are generally unspecific and the typical symptoms associated with B19V can be due to other pathogens as well. Thus, a multiparametric approach based both on molecular and immunological methods represents the best way to achieve a B19V infection diagnosis, also considering the peculiar lifecycle of the virus, that can reach high titer levels during viremia, can show a delayed clearance of virus from circulation and then remain persistent in tissues.

Serum or plasma samples are the elected sample to quantify viral DNA as well as IgM or IgG levels, but bone marrow aspirates, bioptic specimens or amniotic fluid are suitable if required.

Nowadays, the gold standard for the molecular detection of B19V is an internally-controlled qPCR, able to identify all genotypes and to obtain a calibrated and standardized quantification of viral target. These requirements can take advantage of international standards and proficiency panels [14,140].

Moreover, *in situ* hybridization and immunohistochemical techniques can be used for the detection of viral DNA and proteins, respectively. These methodologies have the advantage of identifying target cells and allowing discrimination between productive and non-productive infections [14].

Immunological methods are another important tool to determine a proper diagnosis, carrying out a parallel detection of IgG and IgM and interpreting the result to presume an active, recent or past infection. Since protein expression in prokaryotic systems usually leads to misfolded proteins, it can just be used to produce linear antigens such as VP1u or NS. For conformational antigens such as VP2 or VLPs (viral-like particles) made up with VP2 alone, VP2+VP1 or VP2+VP1u, heterologous expression and purification from eukaryotic systems is usually needed [14].

### **1.14. Treatment and antiviral research**

B19V infection is normally considered a benign clinical situation: the virus is widely diffused and, in most cases, infection is asymptomatic or unnoticed. Sometimes, clinical situations can be more complex and require therapy, such as in patients with underlying hematological disorders or in patients with immune system deficits. In addition, the risk of infection in pregnancy with its potential effects on the fetus has not to be overlooked. Therefore, not only a prompt and accurate diagnosis of infection is required, but a comprehensive approach including prophylactic, therapeutic, and monitoring actions should be considered [14].

#### ***1.14.1. Therapeutic options***

Blood transfusions can be needed to treat anemias in case of transient aplastic crisis, PRCA or persistent infections. Intrauterine transfusions can be useful in cases of fetal infections and hydrops, if the hemoglobin levels fall below a threshold level when measured by non-invasive

## ***Introduction***

Doppler ultrasonography [60]. Moreover, invalidating arthropathies can be treated with non-steroidal anti-inflammatory drugs (NSAID), even if with limited efficacy.

In patients struggling with immunodeficiency of whichever origin, the main issue is the lack of immune response against the virus, that can lead to chronicization of the infection. In these cases, IVIG (intravenous immunoglobulins) administration can be considered, even if no standard scheme has been defined. It has to be considered, though, that this treatment usually is not enough to clear the infection and tends to wane with the degradation of the antibodies, thus requiring following cycles. Henceforth, the cause of the immunodeficiency should be addressed where possible, enabling the activation of the patient's own immune response [14,60].

### ***1.14.2. Vaccine development***

The development of a vaccine targeting B19V is a complex matter. Theoretically, it would be of great usefulness, since B19V is a virus infecting only human host, transmitted by direct interpersonal contact and able to elicit a protective and prolonged immune response. However, its benign nature of virus with usually self-limiting infections and, on the other end, its ability to persist in tissues even when a strong immune response is present question the real need of a general vaccination [14].

A rationale would be the protection of populations more exposed to a major risk, such as people dealing with hemopoietic disorders and women of childbearing age, that would decrease the need for screening and follow-up and avoid a small but still existent number of fetal losses.

From a technical point of view, such a vaccine is feasible. The capsid proteins VP1 and VP2 are considered good immunogens, and their ability to form VLPs even after heterologous expression makes these VP2+VP1 VLPs good candidates as vaccine proteins, [141]. A first approach has been attempted, by expressing these proteins via a baculovirus-mediated expression system: in the animal models, a good immunogenicity and relative safety were shown [142], but phase II studies highlighted a relevant reactogenicity in human [143]. To overcome this issue, a different approach was followed, by expressing VLPs of VP2 and VP1 (either *wild-type* or lacking the PLA2 activity) in *Saccharomyces cerevisiae*. These VLPs are highly homogenous and can be purified from a safe organism, thus removing potential causes of reactogenicity present previously [144].

More recently, another approach has led to the development of a fusion protein between B19V VP1u RBD and pneumococcal surface protein A (PspA), that has been proven immunogenic in mice, inducing the production of both anti-RBD and anti-PspA antibodies. These results would make this fusion protein a good candidate for the development of a dual vaccine targeting B19V and *S. pneumoniae*.

### **1.14.3. Search for antivirals**

So far, no antiviral drugs targeting B19V have been approved. The rationale of a specific antiviral therapy would be mainly the treatment of chronic infections in patients undergoing immunosuppression, or limiting the inflammation in the acute disease.

The virus offers many targets for an antiviral effect, with the NS1 and the VP1u region being the more obvious. Blocking the activity of the NS1 protein, which is fundamental both for viral replication and for transactivation of the promoter, would arrest the viral lifecycle, thus limiting the infection. On the other hand, the PLA2 activity of VP1 is required for viral entry and/or endosomal escape, so it would be a perfect antiviral target. Another approach could be blocking the virus-receptor interaction with a competitor.

Unluckily, none of these targets has been structurally characterized (the N-terminal region of the VP1 is the most flexible and badly known portion of the protein), so a rational drug design is difficult to consider.

Other roads have been thus tested so far, such as drug repurposing/retargeting, serendipity or high-throughput screening, leading to the *in vitro* identification of some active molecules.

#### **1.14.3.1. Hydroxyurea**

Hydroxyurea (HU) is an DNA synthesis inhibitor that targets cellular ribonucleotide reductase enzyme, acting as a virostatic agent if combined with deoxynucleoside analogs: the assumption is that HU prevents the production of deoxyribonucleotides, leading to an increased deoxynucleotide analog incorporation in viral genome [60]. Interestingly, HU is the only disease-modifying drug used for the treatment of sickle-cell disease (SCD) affected patients [145], who are more subject to B19V severe complications. Tested *in vitro* in both UT7/EpoS1 and EPCs systems, with a complete inhibition obtained at more than 1mM and EC<sub>50</sub> values of 96.2  $\mu$ M and 147.1  $\mu$ M in

## ***Introduction***

UT7/EpoS1 and EPCs respectively [146], while cytostatic effects, measured as 50% reduction of viability, occurred at 581.9  $\mu\text{M}$  and 584.8  $\mu\text{M}$ , respectively. However, a loss of membrane integrity was measured only for EPCs treated with HU concentrations higher than 500  $\mu\text{M}$ , but never reaching the 50% of cell damage, thus confirming the mainly cytostatic effects of the drug. Moreover, B19V transcriptional activity decreased in both systems at the highest tested concentrations ( $\geq 1\text{mM}$  for UT7/EpoS1 and  $\geq 10\text{ mM}$  for EPCs). Further data from this study confirmed that the effective concentrations of HU inhibiting B19V replications are in the range of those obtained for other human viruses, while remaining below the range of cell toxicity. In treated SCD patients, where HU peak plasma concentrations can reach 250-400  $\mu\text{M}$  [147] (so enough to decrease viral replication), a protective effect against Parvovirus B19 infection was shown, at least with regards of disease severity [148]. Hence, HU should not be withdrawn in B19V infected SCD patients, since it can exert a dual beneficial effect, acting both on the disease and on a virus that can cause severe complications in the same population.

### **1.14.3.2. Nucleotide analogs Cidofovir (CDV) and Brincidofovir (BCV)**

Another strategy was aimed to evaluate the putative effect of known antiviral compounds against B19V. CDV is an acrylic phosphonate nucleoside that showed activity against all non-retrotranscribing human dsDNA viral families, including those using cellular DNA polymerases. Despite being single-stranded, B19V genome entirely relies on host cell machinery to replicate its genome, thus having the potential to be inhibited by a nucleotide analogue inserted in newly formed DNA.

This hypothesis was proven right [149]: in UT7/EpoS1 CDV was able to achieve complete inhibition of replication in a short infectious cycle at 500  $\mu\text{M}$  and  $\text{EC}_{50}$  values in the range 7.45–41.27  $\mu\text{M}$ , depending on the MOI in the range 10–10<sup>4</sup>. Viral transcription was less affected, but a progressive reduction in the number of FISH or IIF positive cells was correlated to increasing concentrations of CDV.

In EPCs treated in the same way, CDV was less active and unable to achieve a complete inhibition although reducing viral release at the highest tested concentration (500  $\mu\text{M}$ ), highlighting the importance of the cellular environment for the effectiveness of this compound. However, CDV in that concentration proved to be much more effective if cells were extendedly exposed to it, during a longer time course of infection (up to 8 days) or consecutive short term infections, achieving a

reduction of viral replication of 82% and 99% respectively, compared to the 62% inhibition of the initial experimental setup [150].

Going further in this direction, the antiviral activity of the CDV lipid-conjugate Brincidofovir was tested, based on a more potent activity showed against dsDNA viruses, with a better bioavailability and no toxicity.

Both in EPCs and UT7/EpoS1, experimental work confirmed a stronger activity of BCV compared to CDV, leading to a complete inhibition of viral replication that was not achieved in CDV treated EPCs. The specific antiviral effect due to the active enantiomeric form BCV (S) compared to BCV (R) was confirmed as well by a better selectivity index [151].

These results indicated BCV, but not CDV, as a good candidate to evaluate for B19V treatment in humans. However, a following phase 3 clinical trial evaluating the use of BCV in cytomegalovirus prophylaxis has shown an increased risk of serious adverse events and mortality in BCV compared to placebo recipients, thus leading to its withdrawal from clinical trials [152]. Recently, a benefit-risk assessment has led to BCV approval to the treatment of smallpox, in case of variola virus use as a bioweapon [153].

### **1.14.3.3. G-Quadruplex targeting molecules**

Non-canonical DNA structures have been recognized as important features in the regulation of biological processes, including DNA replication, transcription and translation. Particularly, G-Quadruplex structures (G4) have been emphasized for their ability to disrupt the double-helix and to be targeted by stabilizing or destabilizing molecules.

The basic unit in a G4 is the G-tetrad, constituted by 4 guanidine residues kept together by Hoogsteen hydrogen bonds, connected by loops of various length and sequence and stabilized by a monovalent cation, with more G-tetrad can stack one on another generating the final G4 (Figure 13). It has to be noted that these structures can be generated intra- or inter-molecularly, and with different strand orientations [154,155].

## Introduction

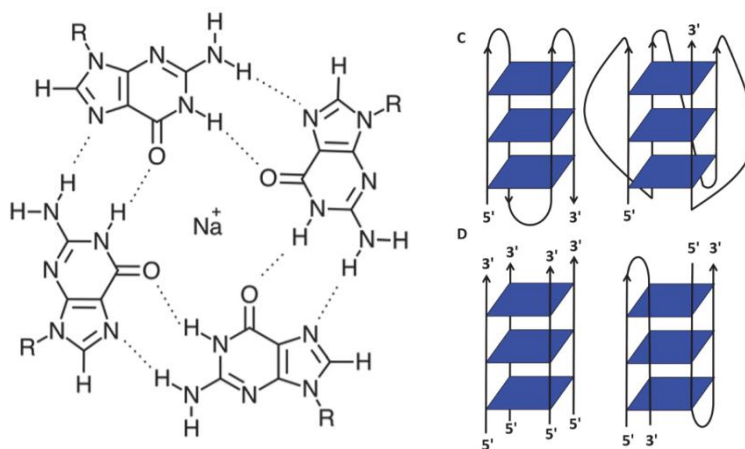


Figure 13: Guanine disposition in a G-tetrad and schematization of possible G4 structures [154]

Methodological developments have enabled the predictability of specific G-Quadruplex structures from the primary sequence. Recently, a survey conducted on viral genomes by regularly expressed patterns search has led to the generation of a database (G4-virus) reporting the presence, distribution and statistical significance of potential quadruplex sequences (PQSs) [156]. In some cases, these PQSs have been experimentally validated, as well as the role of specific G4 ligands such as BRACO-19 (N,N'-(9-[[4-(dimethylamino)phenyl]amino}acridine-3,6-diyl)bis(3-pyrrolidin-1-ylpropanamide) or pyridostatin (PDS) as antiviral agents .

Among others, B19V was indicated as host of PQSs, asking for an experimental validation of this prediction and, as a consequence, for the investigation of potential G4-targeting antiviral agents. Thus, a closer bioinformatic analysis was performed using the QRGS (Quadruplex forming G-Rich Sequences) mapper, based on different algorithms, which led to the identification of 3 PQSs in the ITRs of B19V (PQS 113, 140 and 068) showing a high, low and null G-score (Figure 14) [157].

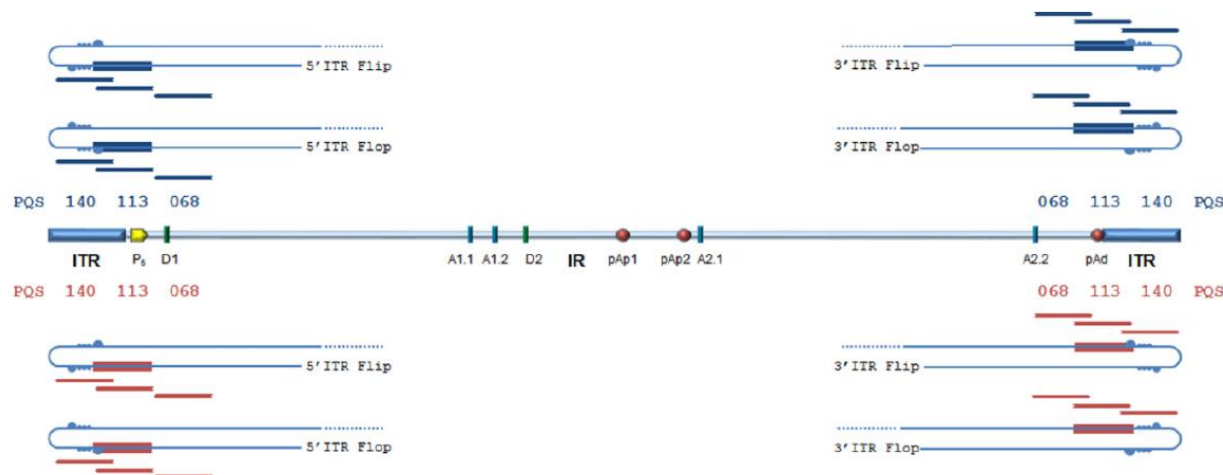


Figure 14: B19V genome symmetry and PQSs. ITRs are shown in the hairpin configuration for the positive and negative strands in the different “flip-flop” isomers. The potential G4 structures predicted by QGRS Mapper are located within the terminal sequences (shown as boxes), 50 to the dyad symmetry, either on the plus strand (blue) or minus strand (red). PQSs partially overlap with the asymmetries leading to the flip/flop isomers (bubbles). Oligonucleotides used in circular dichroism (CD) experiments (PQSs) are shown in context (blue/red stripes) [157].

Oligonucleotides containing each of these PQSs have been used, along with a positive control made by the HIV LTR-II, in a circular dichroism (CD) spectroscopic analysis: this technique is routinely used to evaluate secondary structures of nucleic acids and, in this context, to evaluate the propensity to form G4s. Results didn’t show any peculiar signature usually attributed to the G-Quadruplex for the 3 PQSs (Figure 15), nor BRACO-19 seemed to show any stabilization of G4 structures, although some interaction was seen with all of them [157].

Moreover, neither PDS nor BRACO-19 showed any specific effect on viral replication, while a little decrease in the viral DNA amount was attributed to the cytotoxicity of the two compounds. In summary, these data did not support the efforts made by the bioinformatic predictions, suggesting the hypothesis that B19V ITRs secondary hairpin structure fundamental role for viral replication could prevents the formation of G4 even if theoretically possible based on the primary sequence [157].

## Introduction

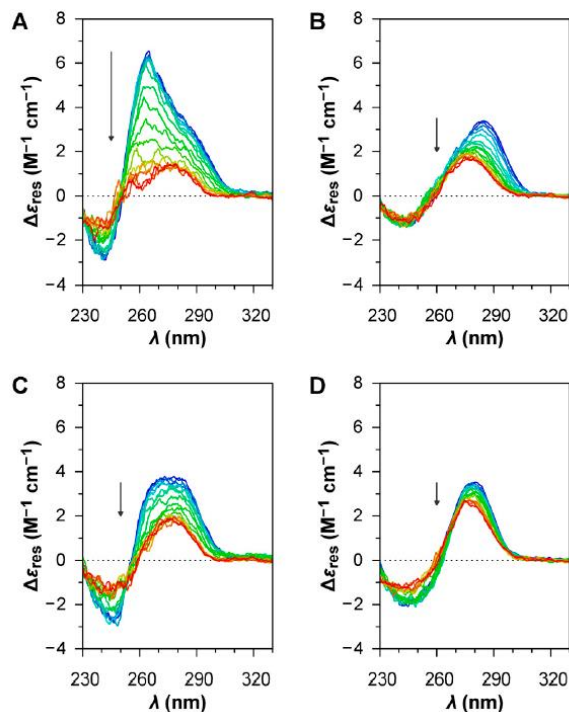


Figure 15: CD spectra of the oligonucleotides under investigation ( $2 \mu M$ ) during the heating ramps of the melting assays. (A) HIV LTR-II; (B) PQS 113; (C) PQS 140; (D) PQS 068. The arrows indicate the evolution along the heating ramp from 15 to 95°C [157].

### 1.14.3.4. Other compounds

Recently, an NS1 target based approach was followed in some studies by developing an *in vitro* assay to screen for compounds able to inhibit the endonuclease activity of this protein.

The first of these studies [158] screened 96 molecules via a fluorophore-based biochemical assay, leading to the identification of three flavonoid promising compounds suitable to be tested in a cell based assay. However, these subsequent tests showed a limited activity of the three molecules in the cells and low selectivity indexes especially in EPCs (1.5–1.8), even if corroborating the hypothesis of mechanism of action blocking the endonuclease activity.

Then, a larger high-throughput screening (HTS) was performed on more than 17000 compounds [159]. This screening was subdivided in subsequent steps: at first, an *in vitro* biochemical approach was followed, identifying 84 hits that were confirmed to inhibit NS1 endonuclease dose-dependently; then a B19V replication inhibition in EPCs was aimed to identify compounds having more than 50% inhibitory activity at  $10 \mu M$ ; finally, another EPCs based assay was aimed to assess the selectivity indexes of these molecules. A purine derivative (P7) was determined to have

promising features, with an EC<sub>50</sub> of 1.46 μM and a CC<sub>50</sub> of 71.8 μM, that could be used for further studies.

Overall, these results show how much the cell environment can impact on the activity of a molecule, that can show very different behaviors moving from an *in vitro* assay to cell-based assays, with further differences depending on the cell type. Moreover, all these approaches are really time consuming and with unpredictable hit rates. Thus, in perspective, an important goal would be a better characterization of the viral targets, that could pave the way to a structure-based drug design or screening.

## **2. Aim of the project**

### **2.1. Experimental background**

The experimental work with Parvovirus B19 has been subject to several limitations. On one hand, the available cellular systems are not many and difficult to manage: the UT7/EpoS1 cell line, which is the most used in this narrow field, is considered as “semi-permissive”, allowing viral replication but a low efficiency in virion release; PBMC *in vitro* differentiated EPCs represent a better model of a natural infection [160,161], with higher replication rates and viral particle release, but they have the limits of a primary culture, depending on blood supplies and lasting in culture just a couple of weeks, with all the heterogeneity that this factors induce.

On the other hand, viral availability as well has been a limiting factor for a long time: B19V is not adapted to grow in culture, thus requiring plasma or serum samples from infected patients to have a concentrated viral stock.

In this context, the generation of B19V genomic clones represented a goal that could enable further work of molecular biology that was not feasible before. At present, just two genomic clones have been developed: pM20 and, from our laboratory, the pCK clones. Clone pM20 was established in 2004, has been shown to possess replicative activity, and has been mainly used in nucleofection experiments [162]. More recently, a synthetic biology approach was followed by our laboratory. To this purpose, firstly, 49 available sequences were used to build a B19V genotype 1a consensus sequence, named EC (GenBank accession KY940273). These sequences comprised more than 70% of the genome sequence and were representative of isolates collected in different settings. Within this dataset, the average coverage of 40.2 hits/nt was different between ITRs, that just had a coverage of 5.8 hits/nt, and the internal region, with 46.0 hits/nt. From the global alignment, the Information Content (IC) per position was derived using a Position Weight Matrix (PWM) (Figure 16). The EC consensus sequence was then used to generate 4 classes of genomic clones with progressively truncated ITRs [163].

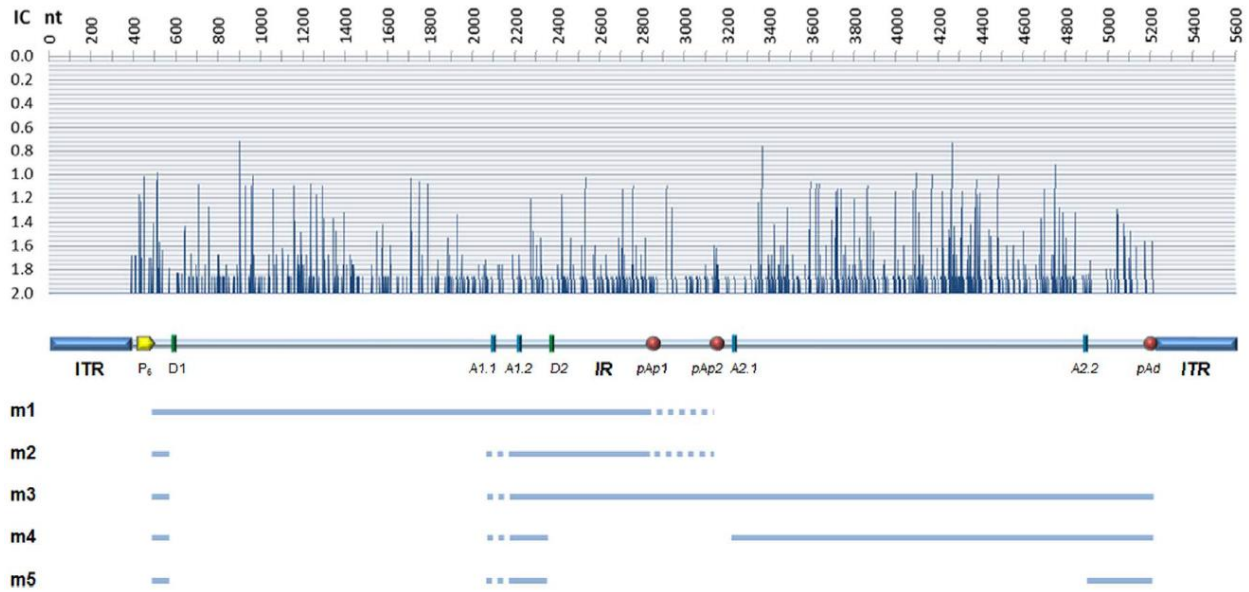


Figure 16: Sequence diversity and functional map of B19V genome. Top: information content (IC) profile of the position weight matrix (PWM) obtained from the alignment of a set of 49 B19V whole genome sequences (supplemental sequence dataset). For each position ( $w$ ), and  $j \in \{T, C, G, A\}$ , the  $IC(w)$  was calculated as:  $IC(w) = 2 + \sum_j p_{wj} \log_2 p_{wj}$ ; Center: a schematic diagram of B19V genome indicating the two inverted terminal regions (ITR), and the internal region (IR) with the distribution of is-acting functional sites (P6, promoter; pAp1, pAp2, proximal cleavage-polyadenylation sites; pAd, distal cleavage-polyadenylation site; D1, D2, splice donor sites; A1.1, A1.2, A2.1, A2.2, splice acceptor sites); Bottom: simplified transcription map of B19V genome, indicating the five classes of mRNAs (m1-5) with respective alternative splicing/cleavage forms. [163]

The pCK clones were designed in order to I) clone the genome in a complete and functional form, trying to reduce the system's complexity and instability; II) elucidate the properties of the ITRs and their role in the functional competence of the genomic clone; III) avoid sequence errors due to the stochastic effect of sampling a particular isolate; IV) optimize the experimental workflow, to yield a higher quantity of collected virus and achieving a viral stock whose infectivity should be comparable to that of native virus [163].

Thus, 4 plasmids were generated containing a viral insert from nucleotide 136 to nucleotide 5461, removing the exterior parts of the terminal regions to achieve a better stability, and considering the flip/flop (or 1/0) isomerism in the ITRs: pCK10/01/11/00.



comparable to native virus. Also, the strong importance of the ITRs in the maintenance of replication competence was demonstrated.

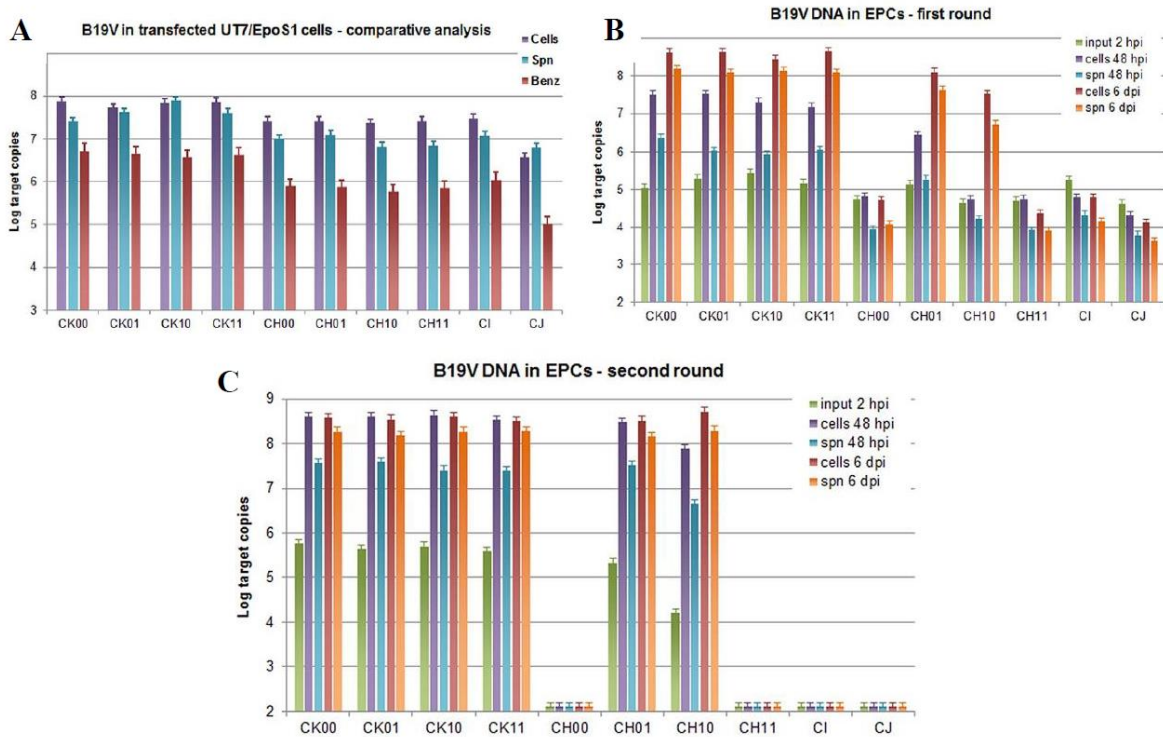


Figure 18: Comparative analysis of genomic clones. A) Quantitative analysis of viral DNA in UT7/EpoS1 cells and their post-transfection supernatant, with or without Benzonase treatment; B) viral DNA quantification, at different time points, in EPCs infected with 6dpi supernatants; C) second round of infection of EPCs, with 6dpi supernatants from infection showed in plot B [163].

Overall, this work established a new model system based on a cloned synthetic B19V genome of known sequence that can be nucleofected in UT7/EpoS1 cells and then used to infect EPCs to generate new viral stock, while studying its interaction with host cells. Henceforth, not only the need for patients-derived samples is strongly reduced, but a whole new series of projects could be designed in order to study the importance of each viral protein or genomic region by editing the consensus genome.

## **2.2. Generation of a functional minigenome of Parvovirus B19**

Going further in the analysis of B19V genome and taking advantage of the molecular clones previously described, an interesting question to be solved is the flexibility of such a system to genetic manipulations. Theoretically, this tool would allow to introduce a wide spectrum of rearrangements into B19V genome, in order to simplify the study of the virus under various

## *Aim of the Project*

aspects, spanning from genome expression to virus-host interactions. However, whether these modifications could be feasible without altering the functionality of the genome it is still to be discovered.

Furthermore, many of B19V proteins still need a good characterization. Apart from those almost just predicted, a proper structural model has been achieved just for the VP2, because the high flexibility in the VP1u region has prevented the generation of a high-resolution crystal structure of this portion. For the non-structural proteins, the situation is even worse, because no crystal structure has ever been obtained neither for NS1 nor for the 11-kDa.

Nevertheless, these proteins are fundamental in the viral replication process and tools to focus the study on each one would be greatly helpful to better understand their role in the viral lifecycle, their interactions with cellular partners and, in perspective, to look for potential antiviral drugs targeting them.

In this context, and based on the experimental background described above, the main project during my PhD was aimed to develop a B19V replicon system able to express the NS1 protein in a simplified genomic environment, then to use this minigenome to study the activity of the NS1 to transactivate the viral promoter. Moreover, to split the expression of the viral proteins on different genomic units subsequently trying to obtain a complete functionality in complementation experiments.

Such a system would present several advantages: first, it would enable us to study the effects of NS1 alone in nucleofected cells; second, NS1 expression wouldn't be subject to a phase transcription shift due to viral replication if the late genes are removed from the minigenome; third, the generation of a second modified genome maintaining the viral promoter would constitute a good tool to study NS1 transactivation ability, with the potential to become useful in the study of NS1 inhibiting compounds; last, it would serve as a proof of concept of the plasticity of B19V genome, that could be then furtherly modified in a perspective of transgene expression.

### **2.3. Study of the role of APOBEC3B on B19V genome**

Viruses and their hosts are in a continuous evolutionary arms race. During millions of years of evolution, many different alarm and defense systems have been evolved by human and other mammalians. Pattern recognition receptors (PRRs) are immune sensors able to detect “pathogen-associated molecular patterns” (PAMPs), thus initiating signal cascades that lead to the production

of type I interferons (IFNs), activating the expression of interferon-stimulated genes (ISGs) [164]. These restriction factors (RFs), many of whom can also be constitutively expressed, are meant to provide quick response towards viral pathogens at every step of their replication cycle. RFs usually target highly conserved viral features or lifecycle steps, thus to confer a broad-spectrum protection. However, viral pathogens as well have evolved mechanisms to avoid, or even exploit, host restriction factors [165].

The APOBEC3s are a family of deaminase enzymes acting on ssDNA sequencing by transforming deoxycytidine into deoxyuridine [166]. Seven APOBEC3 genes are encoded in the human genome, all located in a gene cluster on chromosome 22, named A3A, A3B, A3C, A3DE, A3F, A3G, A3H. Moreover, the diversity of the A3s can be extended by mechanisms of read-through transcription, alternative splicing and internal transcription initiation.

Subcellular localization differs between the A3s, with A3DE/A3F/A3G becoming cytoplasmic, A3B being nuclear and A3A/A3C/A3H cell-wide during interphase [166].

Even if present in almost every cell type, A3s are interferon inducible genes highly expressed in immune cells and, as showed by a recent study [167], the nuclear enzyme A3B is expressed during the G2/M phase in erythroid cells.

Due to their deaminase activity, APOBECs are well known to exert an antiviral effect [168]: several viruses are restricted by APOBEC3s and some have evolved, in a mutual adaptation evolutionary mechanism, proteins dealing with these cellular countermeasures (as it happens for HIV-1 and its Vif protein).

A recent bioinformatic analysis performed at the University of Namur in Belgium has studied viral genomes looking for a footprint left by A3s activity [42], checking the depletion of 5'-TC motifs, which are the preferential target of all A3s except A3G that prefers 5'-CC. It turned out that Parvovirus B19 seems to be strongly depleted of 5'-NTC motifs, where the deaminated cytosine is the third base of a codon. In such a context, a C to T transition would result in a synonymous mutation at a protein level, being well tolerated by a viral host.

Thus, to verify this hypothesis of B19V as a virus strongly subject to A3B action, I was hosted at the University of Namur for a visiting period of six months.

Aim of my project there was to edit the UT7/EpoS1 cell line silencing the expression of A3B, in order to study the potential differences in viral behavior in presence or absence of this protein and, at the same time the differences in A3B expression caused by viral nucleofection or infection.

### ***3. Generation of a functional minigenome of Parvovirus B19***

#### **3.1. A replicating B19V minigenome**

Parvovirus B19 lifecycle is strongly dependent on the host cell environment, with just a few cell types permissive to its infection and propagation. However, once a permissive cell type has been infected or nucleofected in proper conditions, much relies on how the viral genome and the pre-mRNA are processed during the replication and post-transcription steps, respectively.

Along the years, several studies have led to the identification of the fundamental signals and features regulating these mechanisms and, more recently, the development of new genomic clones has paved the way to genome editing and engineering, while still much work is required to achieve a proper characterization of viral proteins, their interaction with cellular partners, and the identification of specific antiviral molecules.

In particular, viral replication strongly depends on the preservation of the ITRs, which serve as primers for the synthesis of the second strand [16], at least to the site of dyad symmetry if the flip/flop heterogeneity is maintained [163]. Furthermore, this region contains at least two NS1 binding elements (NSBEs) [17], binding elements for cellular proteins [23] and the terminal resolution site at which the NS1 nicks the viral genome during the rolling-hairpin replication. All of these elements are required to consent replication of the viral genome, which is assumed to occur through a rolling-hairpin mechanism [169].

Viral expression is regulated by complex mechanisms that, eventually, lead to a two phase early/late expression pattern [32,170]. The utilization of two internal polyadenylation sites (pA)p1 and (pA)p2 [26] competes with the splicing machinery acting on the A1-1 and A1-2 acceptor sites [171], with the ongoing replication that moves this equilibrium advantaging the splicing [29]. Therefore, prevalent proximal cleavage with production of NS1 protein in the early phase is followed by replication of viral genome, which in turn promotes expression of the structural capsid proteins in the late phase. On a protein level, the NS1 protein is thus the principal effector of the main biological processes occurring during viral lifecycle, being fundamental during viral replication also for its role in transactivating the viral P6 promoter and inducing expression of other cellular proteins [80].

A main focus of our work was to manipulate the viral genome in its cloned, functionally competent form, by reducing its complexity to a simple replicon unit. In its design, the EC consensus genome

## Generation of a functional minigenome of Parvovirus B19

of B19V [163] was edited generating a minigenome, where the genome terminal regions had to be maintained in a form able to sustain viral replication, while the internal region could be clipped to include only the left-side genetic set, containing the coding sequence for the functional NS1 protein. To this purpose, the genomic region comprised between the (pA)p1 and )pA)d sites was deleted. A new cleavage and polyadenylation site named (pA)s1 was generated, by putting close one to the other the upstream element necessary for (pA)p function, as described in [26], and the (pA)d sequence joined by a useful BamHI RE site (Figure 19). A graphic summary of all the minigenomes generated in this work, and further detailed below, can be found in Figure 20.

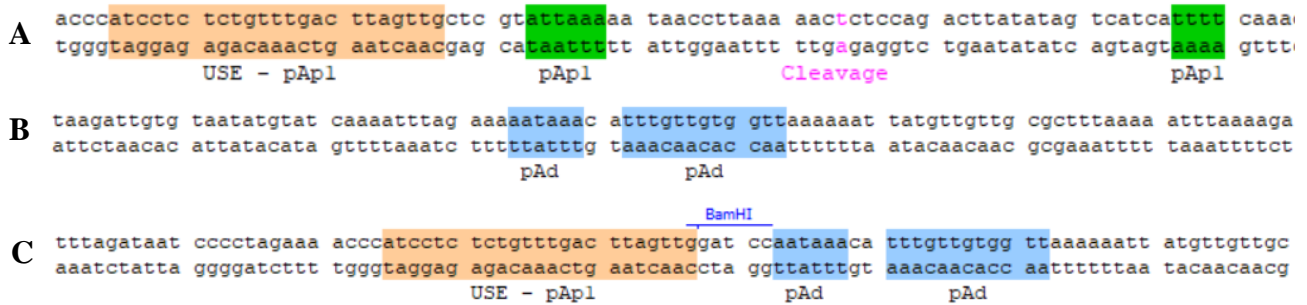


Figure 19: Sequence of the three polyadenylation sites: A – (pA)p1; B – (pA)d; C – (pA)s1

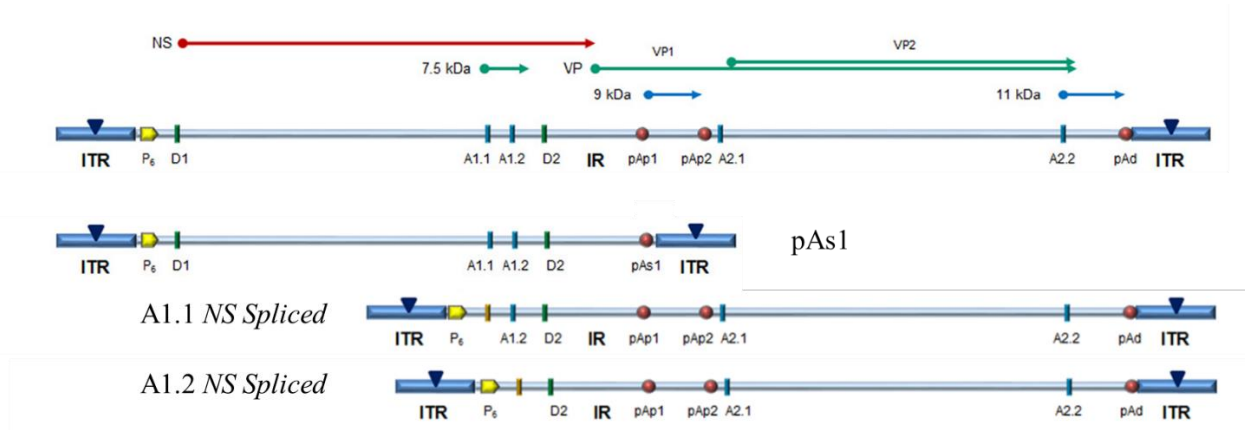


Figure 20: Maps of the different minigenomes generated in this work. Further detail is provided in the main text and in figures 21 and 30

## Generation of a functional minigenome of Parvovirus B19

### 3.1.1. Molecular cloning

To obtain the designed B19V minigenome, a DNA fragment of the newly defined sequence was synthesized and used to modify by replacement the sequence in the genomic clones already present in the lab. With the aim of preserving the ITRs in their entirety, as a first approach cloning in the pCK10 clone was attempted, by substituting the original sequence with the pAs1. Despite several efforts and different cloning strategies, this only allowed the production of unstable plasmids where only the left ITR was included. This unexpected result could possibly be due to an excessive instability at a plasmid level introduced by the reduced ITR distance. Instead, cloning in the pCH10 clone, whose viral insert extends up to the site of dyad symmetry for both ITRs, successfully led to the generation of a stable plasmid containing the modified minigenome, named pCH10 pAs1 (Figure 21).

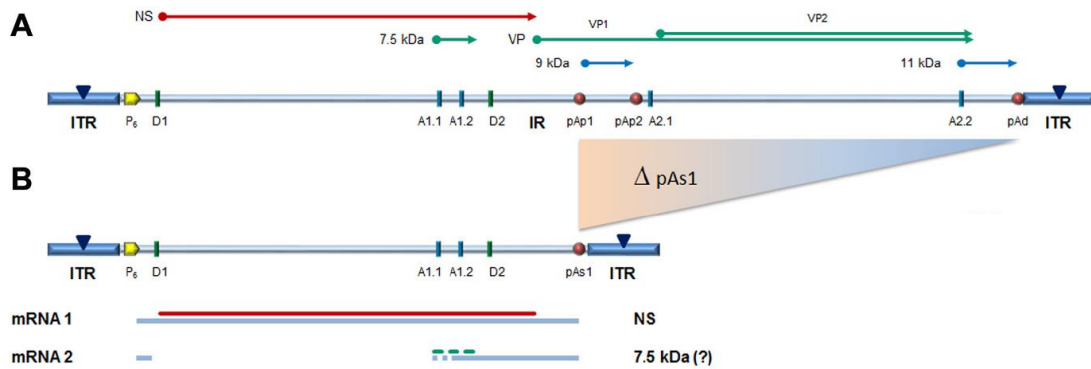


Figure 21: A) Map of B19V genome. ITR: inverted terminal repeats (▼, site of dyad symmetry). IR: internal region and relevant cis-acting functional sites (P<sub>6</sub>, promoter; pAp1, pAp2, proximal cleavage-polyadenylation sites; pAd, distal cleavage-polyadenylation site; D1, D2, splice donor sites; A1.1, A1.2, A2.1, A2.2, splice acceptor sites). Coding sequences for viral NS, VP and smaller non-structural proteins are aligned to map. Δ: deletion to create a novel cleavage-polyadenylation signal (pAs1). (B) Map of B19V derived minigenome; simplified transcription map, indicating the two classes of mRNAs (mRNA 1–2), with alternative splicing forms (dashed lines) and related coding potential.

### 3.1.2. Comparative functional analysis of the pAs1 clones

From the pCH10 plasmid, three genomic inserts with progressively truncated ITRs can be amplified by PCR reaction, with the longer two also excisable by RE digestion: CH10 (nt 184-5313), spanning up to the site of dyad symmetry; CI0 (nt 245-5474), spanning within the sites of dyad symmetry; CJ0 (nt 366-5231), spanning just to the beginning of palindromic sequences. In the same way, the three modified minigenome inserts could be obtained from the pCH10 pAs1

## Generation of a functional minigenome of Parvovirus B19

plasmid. Thus, a functional comparative analysis was performed by using the purified genomic inserts obtained through *in vitro* amplification to nucleofect UT7/EpoS1 cells.

### 3.1.2.1. Nucleic acids analysis

At 8 and 24 hours post transfection (hpt), aliquots of cell culture were sampled to quantify viral nucleic acids (DNA, mRNAs) via qPCR and RT-qPCR. Results are shown in Table 2 and Figure 22.

Table 2: Quantification of viral nucleic acids in nucleofected UT7/EpoS1 cells. Target copies amount (viral DNA, total mRNA, NS1 mRNA) normalized to  $10^5$  cells, at 8 or 24 hours post transfection. Mean of duplicate determination for two different experiments.

Insert	DNA		RNA (total)		RNA (NS)	
	8 hpt	24 hpt	8 hpt	24 hpt	8 hpt	24 hpt
CH10	6.41E+06	1.73E+06	2.50E+04	6.64E+04	4.27E+02	3.99E+02
CH10-pAs1	7.39E+06	1.88E+06	7.53E+04	5.01E+05	3.97E+02	7.02E+02
CI0	9.52E+06	8.06E+05	2.34E+04	7.21E+04	1.24E+02	2.31E+02
CI0-pAs1	9.07E+06	2.53E+06	5.90E+04	2.83E+05	3.87E+02	1.72E+02
CJ0	6.21E+06	1.30E+06	5.81E+03	2.94E+04	7.63E+01	2.46E+02
CJ0-pAs1	1.10E+07	1.92E+06	7.90E+03	1.35E+04	1.17E+02	9.00E+01

## Generation of a functional minigenome of Parvovirus B19

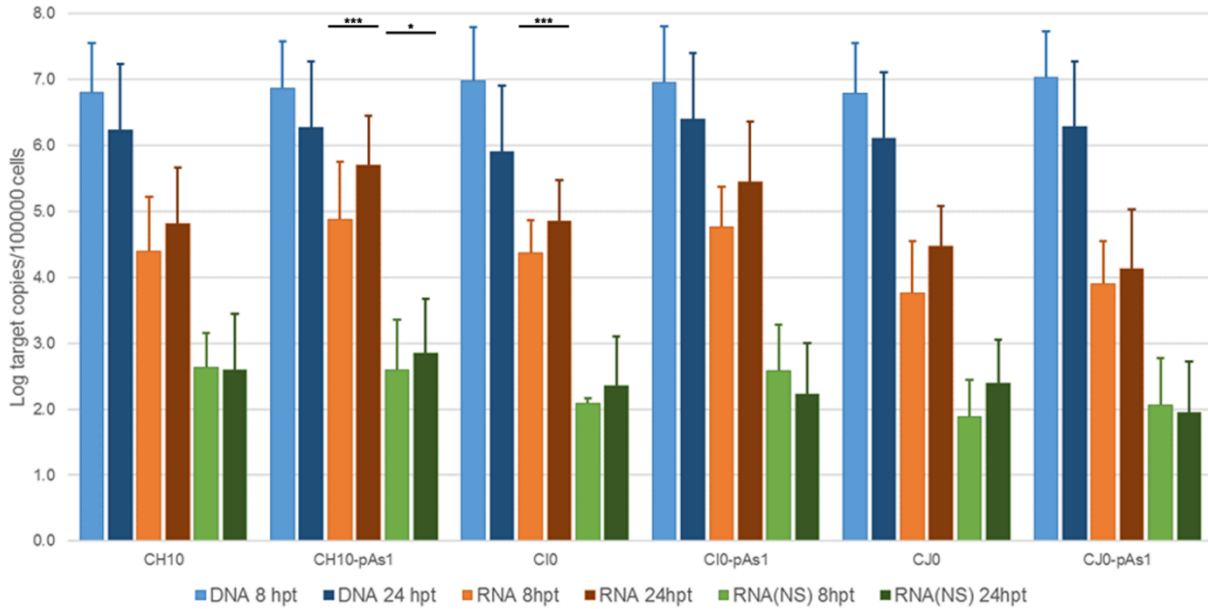


Figure 22: Viral nucleic acids in UT7/EpoS1 cells, nucleofected with CH10 and CH10-pAs1 derived inserts. Log amounts of target copies (viral DNA, total RNA, NS1 mRNA), normalized to  $10^5$  cells, at 8 and 24 hpt. Mean and std of duplicate determinations for two different experiments. Two-way ANOVA, Bonferroni post-test: \*\*\*,  $p < 0.001$ ; \*,  $p < 0.05$ .

The nucleofection efficiency was similar for all the inserts, as showed by the comparable amount of DNA that was obtained from the samples, either at 8- or 24-hpt. Owing to the large quantity of input DNA that is needed for the experiment, no significant temporal variation in the DNA amount was observed for any of the tested inserts, excluding a general decrease from the 8- to the 24-hpt (mean -0.7 log, range -1.1 – -0.57) probably as a consequence of progressive degradation of exogenous DNA.

The transcriptional activity was assessed for all transfected inserts, with viral mRNAs being detected at both time points. A general increase was seen from 8 to 24 hpt (mean 0.56 log, range -0.01–1.33) for the total mRNA and, even if to a lesser extent, for the NS mRNA as well (mean 0.08, range -0.36–0.51), with statistical significance just for CH10 pAs1. Despite some variability, these results demonstrated the early beginning and maintenance of viral transcription, implying a processing of the pre-mRNA at the novel synthetic cleavage-polyadenylation site pAs1, while preserving a balance used of splicing signals. In fact, the production of both the unspliced RNA coding for the NS1 protein and the spliced mRNAs was observed, with a pattern similar to that typically observed in the early phase of a replicative cycle.

To determine if the minigenome clones maintained the replication competence, a parallel experiment was conducted with RE excised CH10 (with BssHIII) and CI0 (with AccIII) unmodified

## Generation of a functional minigenome of Parvovirus B19

and pAs1 inserts to assess their post-nucleofection resistance to DpnI treatment. DpnI is a restriction enzyme that cuts only methylated DNA, thus digesting viral inserts directly excised from the plasmid while being unable to digest *de novo* generated DNA due to viral replication.

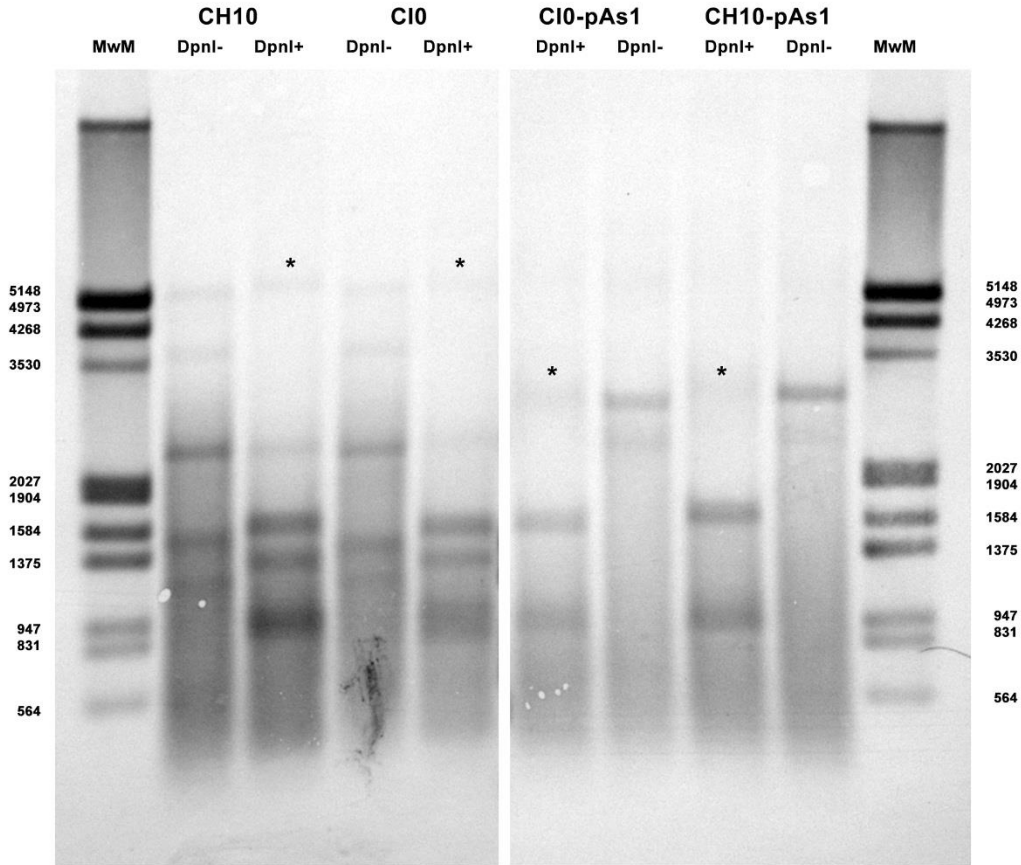


Figure 23: Southern Blot Analysis of B19V DNA obtained from UT7/EpoS1 cells nucleofected with inserts CH10 (5231 bps), CI0 (5108 bps) and CH10-pAs1 (2880 bps), CI0-pAs1 (2757 bps), collected at 24 hpt. Samples were treated by RE DpnI to distinguish *de novo* synthesized viral DNA (\*) based on different dam methylation pattern and sensitivity to RE DpnI. MwM: molecular weight marker III, Dig-labelled (Roche).

Resistance to DpnI treatment was assessed in two different ways: through a Southern Blot analysis, using a full-length DIG-labelled probe, and via qPCR using a primer pair encompassing a DpnI site within the NS gene.

Results from the Southern Blot analysis (Figure 23) showed the presence of a full-length, DpnI resistant band for all the four tested inserts. Moreover, the qPCR analysis allowed the quantification of the DpnI resistant fraction: DNA directly excised from the plasmids was resistant at 1.7% and 1.4% for CH10 and CH10 pAs1, and at 1.6% and 1.3% for CI0 and CI0 pAs1. These percentages were increased when recovering inserts from nucleofected cells, reaching 11.7% and

## ***Generation of a functional minigenome of Parvovirus B19***

15.8% for the CH10s and 8.8% and 19.0% for the CI0s, unmodified and pAs1 respectively. These data are consistent with the maintenance of the viral replication competence of nucleofected inserts, at least for CH10- and CI0-derived inserts, either complete genomes or minigenomes, a property likely due to the preservation of sequence symmetry within the ITRs and possibly relying on a hairpin-independent mechanism of DNA synthesis priming, as already shown [163].

### **3.1.2.2. Protein expression analysis**

Along with the nucleic acids, protein expression was monitored as well either by indirect immunofluorescence (IIF) and cytofluorimetric analysis, targeting the NS1 protein.

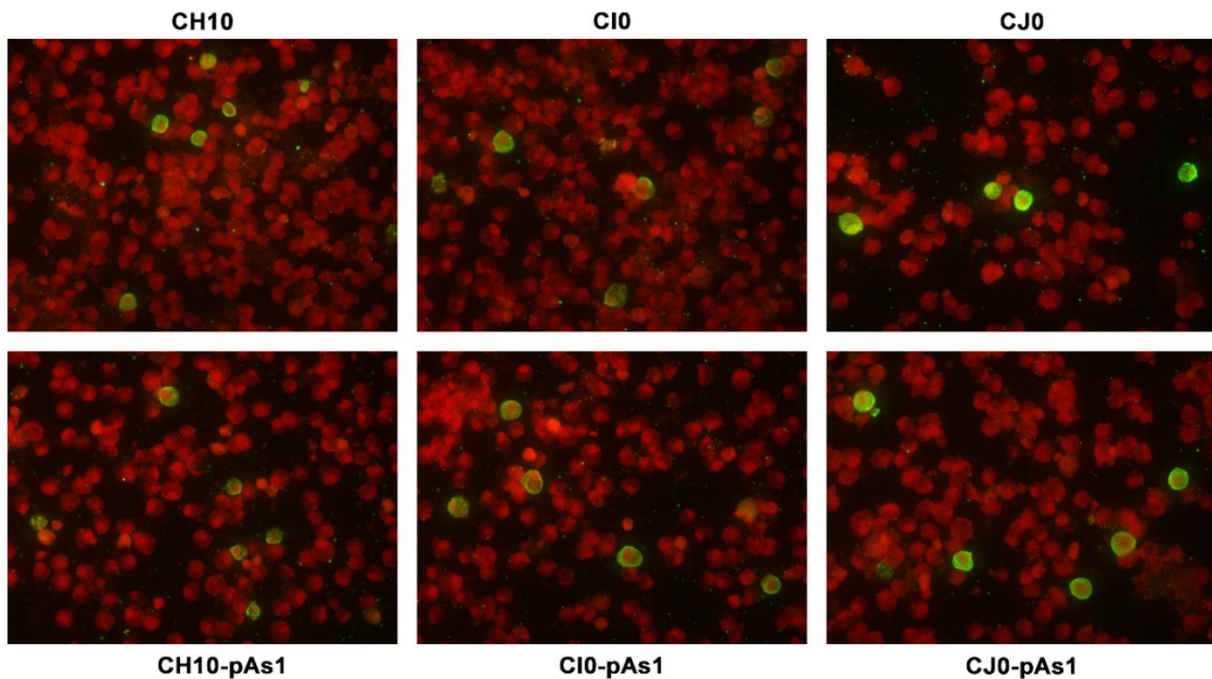


*Figure 24: UT7/EpoS1 cell nucleofected with the indicated inserts. 24 hpt anti-NS1 IIF: the protein signal is showed in green, while the general red staining is due to Evans blue staining. Original magnification 400x.*

NS1 expression was already seen at 8 hpt (data not shown), but both the number of positive cells and signal intensity increased at 24hpt (Figure 24). The intracellular distribution pattern was similar for all the tested clones, minigenome and complete ones.

## Generation of a functional minigenome of Parvovirus B19

Even if an overexpression seemed to be noticed in the minigenomes, at least for clone CI0 pAs1, a proper quantification couldn't be obtained only relying on IIF. Thus, a cytofluorimetric assay was performed at 24 hpt (Figure 25).

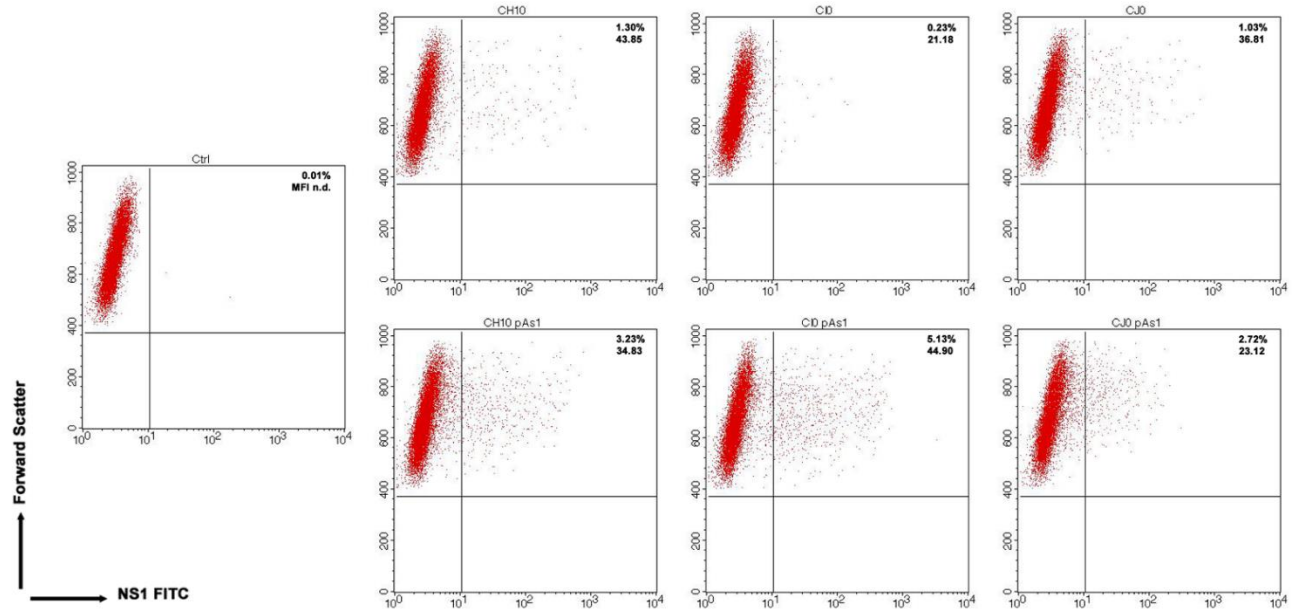


Figure 25: UT7/EpoS1 cells nucleofected with the indicated inserts (Ctrl: no DNA control) were sampled at 24 hpt, and cell population was analyzed by cytofluorimeter to determine the percentage of NS1 expressing cells. Dot plot graph on gated cell population for FSc and NS1 FITC. Reported percentage values of positive cells and geometric mean fluorescence intensity (MFI) for positive subpopulations reported as the average result of two independent determinations.

This analysis confirmed the expression of NS1 for all the tested clones, with the percentage of positive cells in the range 0.2–1.3% for the complete clone increasing to 2.6–5.0% for the derived minigenomes, the highest increase being for the CI0/CI0 pAs1 couple. These data suggest that, in a simpler genomic environment, NS1 progressive expression and accumulation was promoted in an increased portion of the cell population.

### **3.2. Genome splitting and functional complementation**

Once achieved the generation of an NS1-expressing replicating minigenome, the question arose whether it could be possible to further manipulate the B19V genomic clones, with the prospective aim of producing modified viruses that could target erythroid progenitor cells.

## ***Generation of a functional minigenome of Parvovirus B19***

To address the issue, a first strategy was to investigate whether the NS1 protein expressed by the minigenome could provide trans-complementing functions to a modified, NS1-deficient, B19V genome. To this purpose, in a complementary approach to that previously followed, we decided to edit the consensus sequence of full-length clones to avoid the expression of the NS1 protein but maintaining the coding sequences for expression of the late genes. The capacity of the CH10-pAs1 minigenome to provide complementing functions through expression of NS1 protein was thereafter tested in a subsequent series of co-transfection experiments.

### ***3.2.1. NS Knocked Out genome***

#### **3.2.1.1. Molecular Cloning**

To silence the NS1 expression, a recombinant PCR strategy was followed to introduce a mutation around the NS gene starting codon, thus mutating it into a stop codon and introducing a unique RE site (XbaI), used to check the effective mutation (Figure 26).

```
catactaaca tggagctatt
gtatgattgt acctcgataa

>>.....
  M E L

      XbaI
catactatct agaagctatt
gtatgataga tcttcgataa
```

*Figure 26: Mutation introduced in the NSKO genomic clone. Up – consensus sequence with NS1 protein sequence beginning; Down – mutated sequence with no protein prediction and XbaI site. Start to stop codon mutation is underlined in red.*

The modified sequence was then successfully cloned in the pCK10 plasmid, preserving the functionality of the complete ITRs, thus generating the new pCK10 NS Knock-Out (NSKO) plasmid.

#### **3.2.1.2. Functional analysis of NSKO genome**

As previously done with the pAs1 minigenome, the CK10 NSKO functionality was tested by nucleofecting UT7/EpoS1 cells. In this case, instead of testing NSKO inserts of different lengths, CK10 NSKO was used alone or in co-transfection with CH10 pAs1, using the unmodified CH10

## Generation of a functional minigenome of Parvovirus B19

insert as a control. Transcriptional levels and viral protein expression were monitored at 24 hpt (Figure 27).

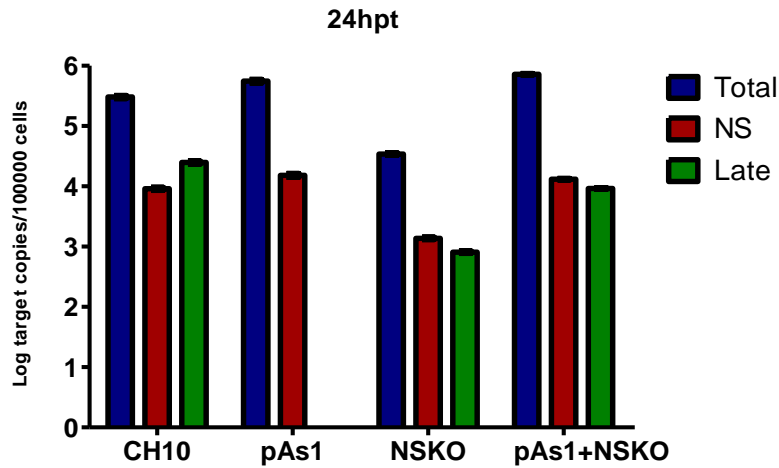


Figure 27: Transcriptional analysis of UT7/EpoS1 cell nucleofected with the indicated genomic inserts. Log amounts of target copies (total RNA, NS1 mRNA, late genes RNA), normalized to  $10^5$  cells, at 24 hpt.

The RT-qPCR analysis on the sampled cells revealed generally reduced transcriptional levels for the CK10 NSKO genomic insert when nucleofected alone (around 1 Log). The co-transfection of both CH10 pAs1 and CK10 NSKO seemed to restore the RNA amounts to levels comparable to those obtained by the control clones. It has to be noted that, in the analysis of the co-transfected cells, only the late genes could be attributed to just one of the two genomic inserts, while both could contribute to the amount of NS1 mRNAs in a ratio that could not be determined.

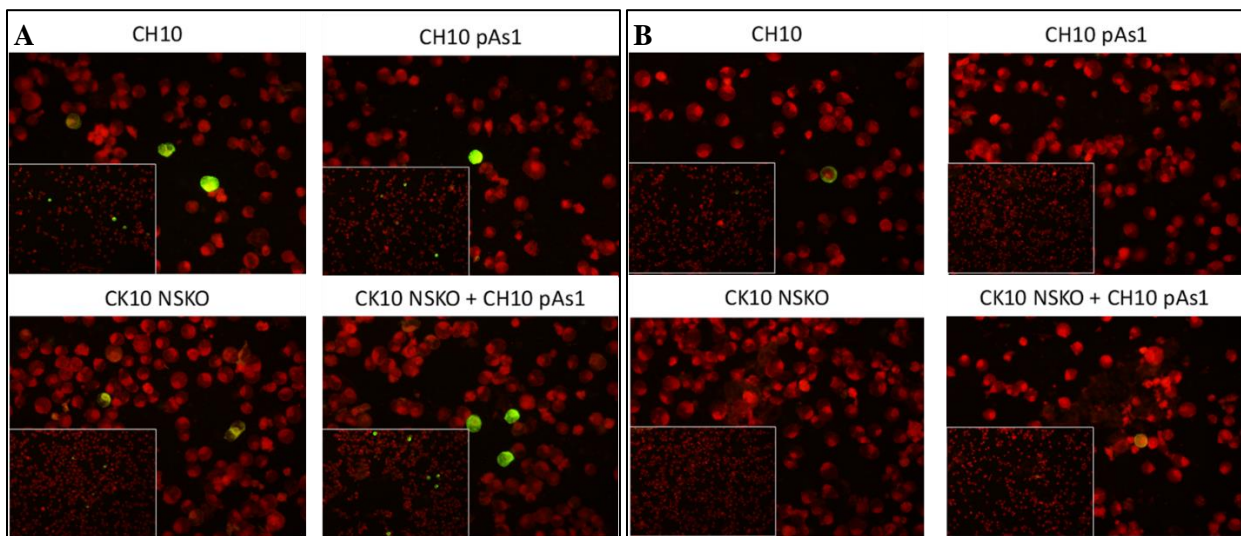
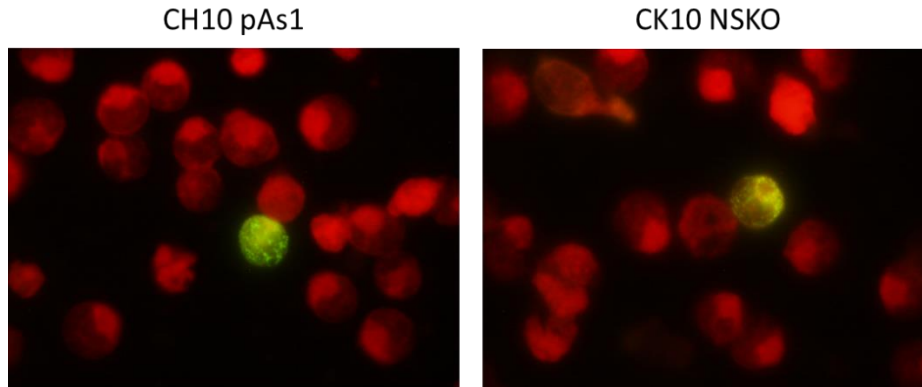


Figure 28: : UT7/EpoS1 cell nucleofected with the indicated inserts. 24 hpt IIF: A – NS1; B – VPs. Original magnifications 200x and 400x.

## ***Generation of a functional minigenome of Parvovirus B19***

At a protein level (Figure 28), the IIF analysis showed that the NS1 expression was strongly reduced in the NSKO clones, although some reactivity could still be observed. On the other hand, VP expression, generally very low could be restored in the complementing combination.



*Figure 29: Different intracellular distribution of the NS1 signal between CH10 pAs1 and CK10 NSKO nucleofected cells. Original magnification 1000x.*

Interestingly, an NS1 specific signal was detected even in NSKO nucleofected cells, though the intracellular distribution was different (Figure 29). In the unmodified and pAs1 clones, distribution of NS1 usually appears quite homogenously dispersed within the cells, while in the case of the NSKO genome the intracellular distribution of the protein presents a peculiar “moon slice” shape. This could be explained with the synthesis of a truncated form of NS1, due to the use of an alternative downstream starting codon, recognized by the carboxy-terminal domain targeting antibody. Such hypothesis will need further investigation.

However, the anti-VP IIF showed no expression of the capsid proteins in the CK10 NSKO nucleofected cells, while it was recovered if the two inserts were nucleofected together, although at a characteristically low expression yield. This low yield of VP expression after nucleofection is a known phenomenon in this cell line, and is probably related to post transcriptional inhibition within the cells [43]. Therefore, even if a truncated form of NS1 is produced by the CK10 NSKO genomic insert, this protein does not appear to be properly functional as the lack of VPs expression and the globally reduced transcriptional levels seem to imply an impairment of its activity. In any case, the presence of this unexpected expression was considered a limit and potential problem, thus an alternative strategy to silence the NS1 was followed.

### 3.2.2. NS Spliced minigenomes

#### 3.2.2.1. Molecular Cloning

In order to achieve a complete silencing of the NS1 protein, we decided to generate a second family of minigenomes by introducing a large deletion in B19V genome corresponding to the intron hosted into the NS1 gene, which is spliced when the capsid proteins are expressed. Since this intron is subject to an alternative splicing mechanism, with two different splicing acceptor sites that can be used, a recombinant PCR approach was followed to obtain two *NS Spliced* minigenomes: A1.1 and A1.2, depending on which acceptor site was used as 3' end of the deletion. The modified fragments were then cloned in the pCH10 plasmid, to preserve a symmetry with what was done with the pAs1 minigenome, obtaining the pCH10 A1.1 and A1.2 plasmids (Figure 30).

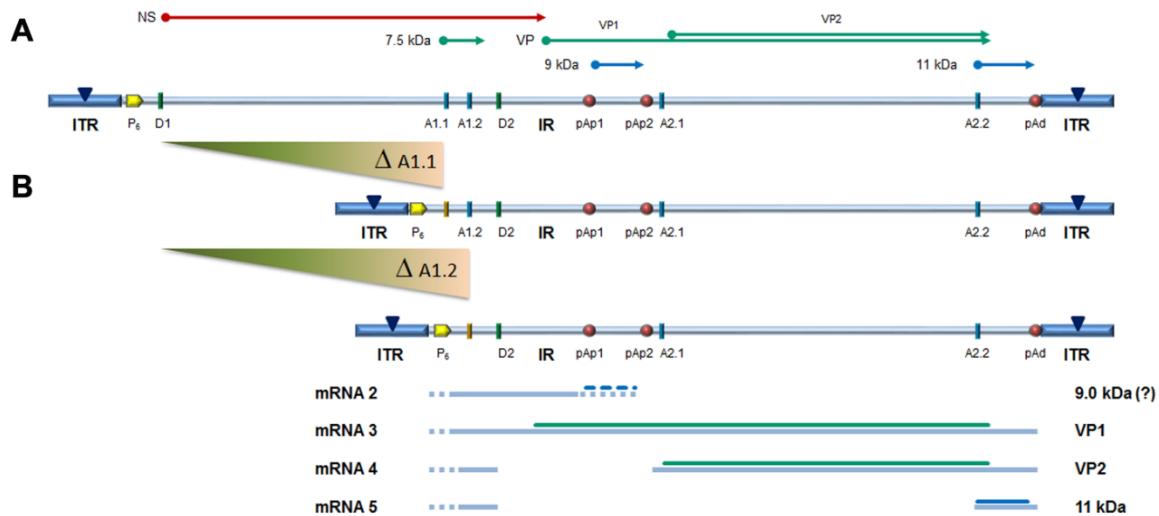


Figure 30: (A) Map of B19V genome.  $\Delta$ : deletion to remove first intron (A1.1/2). (B) Map of B19V derived minigenomes; simplified transcription map, indicating the four classes of mRNAs (mRNA 2–5), with alternative splicing/cleavage forms (dashed lines) and related coding potential.

#### 3.2.2.2. Functional analysis of *NS Spliced* minigenomes

Functional analysis of the *NS Spliced* minigenomes was performed as described previously for the NSKO genome. Results are shown in Table 3 and Figure 31.

## Generation of a functional minigenome of Parvovirus B19

Table 3: Quantitation of Viral nucleic acids in UT7/EpoS1 cells, transfected/co-transfected with CH10, CH10-pAs1 and CH10-A1.1/2 inserts. Amounts of target copies (viral DNA, total RNA, NS1 mRNA, pAd cleaved RNA, VP RNA), normalized to  $10^5$  cells, at 24 hpt. Mean of duplicate determinations for two different experiments.

Insert(s)	DNA total	RNA (total)	RNA (NS)	RNA (pAd)	RNA (VP)
CH10	1.38E+06	3.24E+05	1.95E+04	9.24E+04	5.23E+04
CH10-pAs1	2.33E+06	1.54E+06	8.09E+04	1.00E+00	1.00E+00
CH10-A1.1	1.50E+06	1.98E+03	1.00E+00	1.00E+00	1.00E+00
CH10-A1.2	1.00E+06	4.60E+03	1.00E+00	1.00E+00	1.00E+00
pAs1 + A1.1	1.78E+06	6.21E+05	5.81E+04	1.29E+04	7.97E+03
pAs1 + A1.2	1.52E+06	1.37E+05	3.37E+03	2.40E+04	8.89E+03

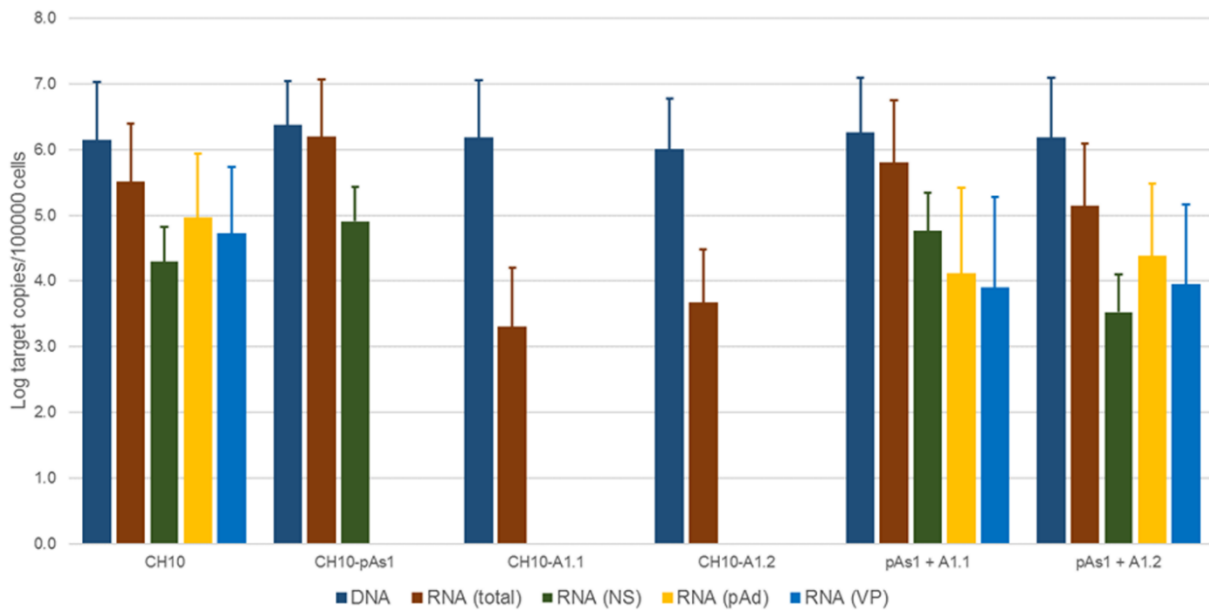


Figure 31: Viral nucleic acids in UT7/EpoS1 cells, transfected/co-transfected with CH10, CH10-pAs1 and CH10-A1.1/2 inserts. Log amounts of target copies (viral DNA, total RNA, NS1 mRNA, pAd cleaved RNA, VP RNA), normalized to  $10^5$  cells, at 24 hpt. Mean and std of duplicate determinations for two different experiments.

Nucleic acid analysis showed a similar nucleofection efficiency for all the tested clones, since comparable level of viral DNA was obtained from all the samples.

As for the NSKO genome, transcription analysis by RT-qPCR showed a general decrease in the transcriptional levels of both CH10 A1.1 and A1.2 when nucleofected alone (around 3 log), with no detection of NS1 or (pA)d transcripts, suggesting that transcriptional activity was limited to non-coding RNAs in the centre of the genome. Insert CH10 pAs1, on the other hand, confirmed its high transcriptional activity and correct mRNA processing, with about 1% of the total transcripts encoding NS1.

Co-transfection of CH10 pAs1 and the *NS Spliced* minigenomes led to a functional complementation, bringing back levels of late mRNAs to only 1 log below those of the complete

## Generation of a functional minigenome of Parvovirus B19

CH10 control insert. Despite proximally cleaved mRNAs were still the most abundant by composition, the expression of the late transcripts seemed to be rescued in co-transfected cells to a 1% of the total.

IIF analysis (Figure 32) confirmed what had been observed by RT-qPCR.

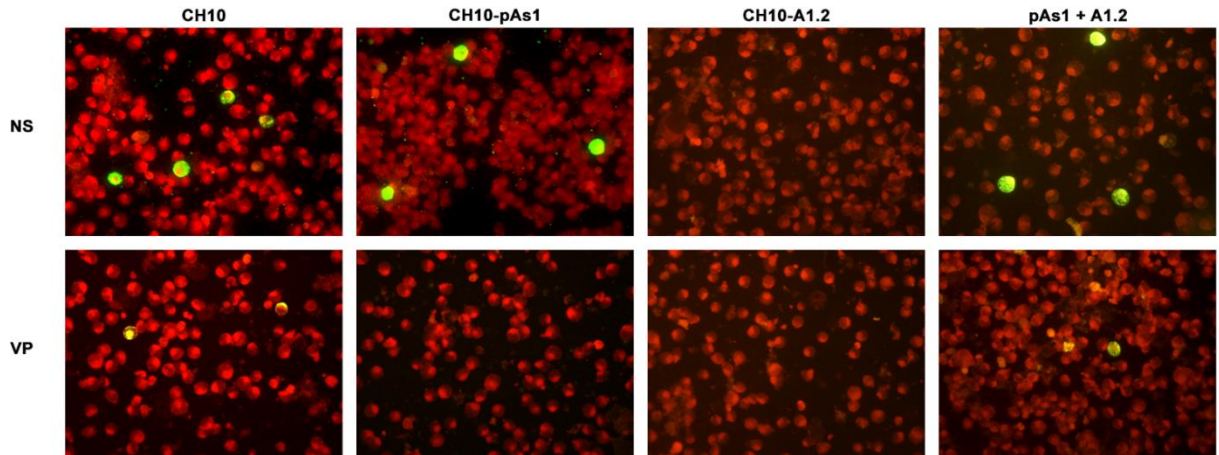


Figure 32: UT7/EpoS1 cells nucleofected with the indicated inserts were sampled at 24 hpt, and NS1 or VP1/2 proteins were detected by IIF. Results obtained for insert CH10-A1.1 were analogous to what obtained for CH10-A1.2 (not in figure). Original magnification 400x.

The expression both NS1 and, always to low extent, of VPs was observed for the CH10 control clone. The NS1 was confirmed also for the CH10 pAs1 insert, while it was not detected for the *NS Spliced* minigenomes, as expected. Capsid protein expression was not detected for the CH10 A1.1 or A1.2 alone but was recovered when co-transfected, although limited to a small number of cells. Overall, these data confirmed that the NS1 protein produced by the pAs1 minigenome is functional in complementation of defective B19V genomes, restoring the expression of the late transcripts in a pattern comparable to the standard expression profile of B19V genome and enabling the production of capsid proteins.

### 3.2.2.3. Extracellular vehiculation of minigenomes

Measurable amounts of viral DNA were detectable in the supernatants of nucleofected UT7/EpoS1 cells up to 6 days post nucleofection, not associated to cells and partially resistant to benzonase nuclease treatment. To verify whether this DNA could be transferred to susceptible EPCs, 6 dpt supernatants from the nucleofected UT7/EpoS1 cells with the different insert combinations described above were collected and added to *in vitro* differentiated EPCs as a test system.

### ***Generation of a functional minigenome of Parvovirus B19***

After a 48h course of incubation, cells were collected and the presence of viral nucleic acids and protein expression was checked. For all samples, low amounts of B19V DNA were measured (less than  $10^2$  copies /  $10^5$  cells) but no evidence of viral transcription or protein expression was found. These results imply that the vehiculation of B19V genomic material to EPCs might not be a result of transducing viral particles, with the process not being functionally relevant at a measurable extent.

Whether this transfer could be due to a simple carry-over of nuclease-resistant DNA input, or to the formation of extracellular vesicles or exosomes needs further investigations, as well as the actual formation of a limited amount of transducing viral particles.

### **3.3. Discussion**

In this project, we designed and produced a B19V minigenome simplified to replicon unit, derived from a complete competent cloned B19V genome. When nucleofected in UT7/EpoS1 cells, it proved to be competent for viral replication, transcription and NS1 protein expression. Its ability to complement B19-derived NS-deficient genomes, restoring their capacity to express capsid proteins was also demonstrated.

B19V genome was engineered to obtain a two-component system, with one element expressing the functional protein NS1 and the other one the structural proteins with complementing functions. Both the pAs1 and the *NS Spliced* genetic elements preserve the ITRs up to the site of dyad symmetry in an heterogenous flip/flop configuration, hence meeting the requirements needed for maintaining the replicative competence [163,172]. *De novo* synthesis of viral DNA was observed, as expected [163], for the complete CH10 and CI0 genomic inserts, a property that has been extended to the derived pAs1 minigenomes: a hairpin-independent mechanism of priming the DNA synthesis was previously described [15], and could be involved here.

The unique viral promoter is present in the same pattern and position in the modified minigenomes, thus linking the transcriptional efficiency to the actual expression levels of the NS1 protein, which is known to exert a strong transactivating activity [24].

Transcription is detectable for the CH10, CI0 and CJ0 inserts, either complete or pAs1, from 8hpt increasing at the late 24 hpt time point, with the pAs1 clones showing higher mRNA levels and a lower ITRs-related influence compared to their control clones. On the opposite, the CH10 A1.1 and A1.2 *NS Spliced* minigenomes showed relevant transcriptional activity only when

## ***Generation of a functional minigenome of Parvovirus B19***

complemented with a genomic element providing the NS1 protein. The deletion introduced in the pAs1 modified clones simplified the pre-mRNA, because the reduced size together with the generation of a novel cleavage-polyadenylation site abrogated the early-late transcriptional switch, thus allowing the accumulation of the left-side cassette mRNAs [26,29].

Different effects were introduced by the rearrangements to obtain the *NS Spliced* minigenomes: the large deletion of the first intron abrogated the expression of the NS1 protein but, since the splicing signals were not altered, the possibility to perform an early-late switch was not lost. Moreover, the preservation of the splicing signals in the right-side cassette allowed the production of the complete set of late genes (VP1, VP2, 11-kDa), that was experimentally demonstrated in the presence of NS1. However, the contribution of both transcriptional templates to the production of short, proximally cleaved and spliced mRNAs likely led to an increase in the amount of these transcripts compared to the complete genome, thus reducing the VP-encoding mRNAs to suboptimal levels.

Distinct considerations can be made for the CK10 NSKO genome. In this case, no invasive alteration was performed on the genome sequence, but a targeted mutation to transform the starting codon of the NS1 gene into a stop codon. Hence, the whole set of viral transcripts could be produced, depending on the basal activity of the promoter and the ability of the NS1 provided by the pAs1 elements to enhance it. Experimental results showed that NS1 silencing in the NSKO genome was not complete, likely due to the presence of alternative starting codons in frame within the gene. However, the strong reduction in the transcriptional levels associated with NSKO nucleofected cells suggest that the truncated protein was not totally functional, likely due to the lack of some NLS or an impairment in the DNA binding domain: indeed, the intracellular distribution of the truncated protein appeared different from that of the wild-type NS1. However, the carboxy-terminal transactivation domain could still be partially active, thus justifying the detected transcription of the late genes, even if replication and related switch are possibly lacking. A further characterization of the truncated product by Western Blot analysis, to understand whether one or more isoforms are generated and the extension of their truncation, will be object of future studies..

The present work, that was recently published [173], reached several goals and showed some critical limitations inherent to the system.

## ***Generation of a functional minigenome of Parvovirus B19***

A replicating minigenome was generated, able to replicate, transcribe and overexpress the NS1 protein. Such a minigenome could be considered a useful tool to study the NS1 function in a simplified genomic environment, regarding its interaction with host cell partners or looking for molecules showing an antiviral effect.

A functional complementation between defective minigenomes was demonstrated, by restoring VPs expression in NS-deficient inserts. This property paves the way for editing B19V genome with less stringent structural constraints, allowing e.g. the modification of cis-acting signals, the mutation or addition of expression tags to viral genes, or the insertion of heterologous reported genes to better characterize B19V lifecycle within the cellular environment.

Ideally, the presence of two complementing genetic units within a same cell opens the possibility for packaging and producing a pseudoviral progeny, but no generation of transducing viral particles was not observed in our experiments: this is the major limit of the present work.

UT7/EpoS1 cells, used for nucleofection experiments, are the best cell line currently available to study B19V, but nucleofection efficiency is low. A complete genome nucleofected in these cells could generate a viral progeny, that needs to be used to infect EPCs as an amplifier system to obtain high viral titers. In the case of complementing units, transducing viral particles would not take advantage of such a system. However, within the inherent limits of the system – B19V is notoriously as an exigent virus – the generation of engineered virus specifically targeting a selected cell population such the EPCs would be of translational interest, so further intense research is still required to achieve this goal.

#### 4. Study of the role of APOBEC3B on B19V genome

APOBEC3s are a family of cytidine deaminases introducing mutations in viral genomes, thus exerting a role as innate immune effectors. Their preferred motif is a 5'-TC (only exception is A3G, which prefers 5'-CC), where the deamination converts the cytosine into a uracil, thus introducing a C to T transition at the following replicative cycle.

Recently, a wide bioinformatic analysis made by my hosting group at the University of Namur analyzed more than 33400 human viruses genomes looking for those shaped by APOBEC3s activity [42]. Interestingly, among the 22% of viruses that showed an impact by A3s, B19V demonstrated to be strongly footprinted on both genome strands.

Indeed, a strong depletion of 5'-NTC motifs was shown, where the deaminated C is at the third position of a codon (Figure 33).

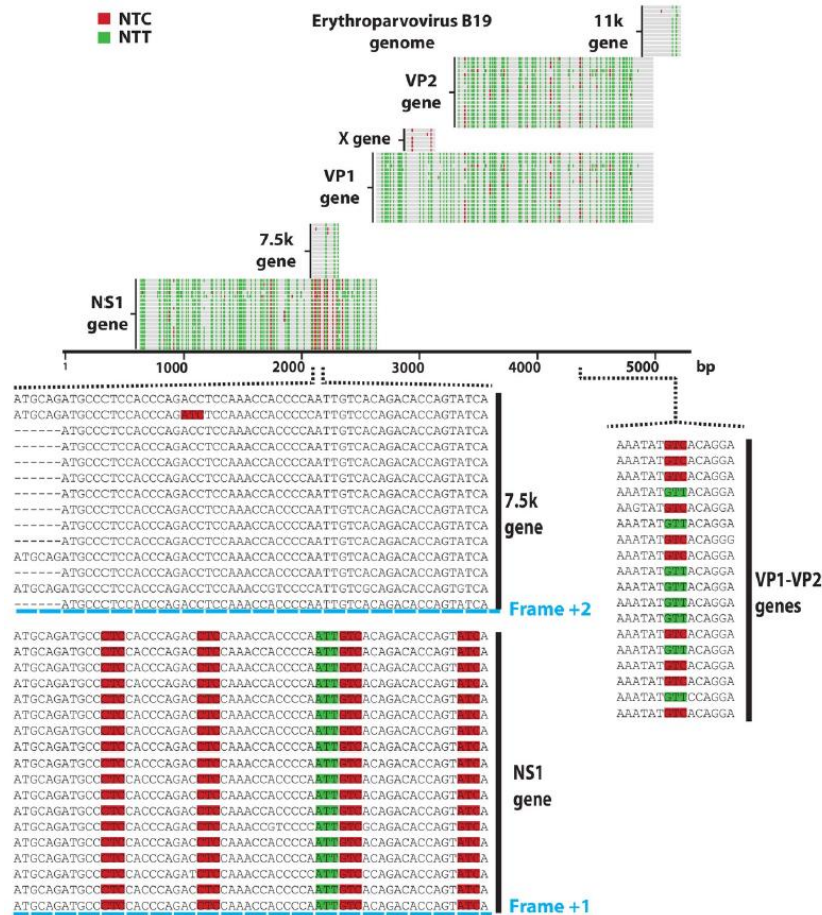


Figure 33: Coding sequences (NS1, 7.5k, VP1, X, VP2 and 11k) from 18 full-length B19 erythroparvovirus were depicted by grey lines overlaid by red marks to symbolize NTC and green marks to position NTT codons. Zoom-in detailed a 60 bp-long sequence from the NS1 and 7.5k genes (from nucleotide 1723 to 1783). A second zoom-in detailed a 15 bp-long sequence from the VP1-VP2 genes (from nucleotide 3973 to 3987) [42].

## *Study of the role of APOBEC3B on B19V genome*

In such a context, a C to T transition would introduce a synonym mutation without altering the protein sequence. So it's possible to notice how B19V genome is generally depleted of 5'NTC motifs, with the only exception of those regions where two coding sequences overlap on different frames: those Cs that are in third position on one frame are in the first or second position on the other one, thus their deamination would lead to missense or nonsense mutations. This information looks particularly interesting with regards to the 7.5-kDa protein: its actual expression and role are still unknown, but the preservation of 5'-NTCs in the NS1 frame seems to suggest some functionality of this ORF.

To test in vitro the role of A3B, the constitutively expressed nuclear A3, on B19V, I edited the UT7/EpoS1 cell line to silence A3B expression, looking for differences in viral behavior.

### **4.1. Test of A3s expression in UT7/EpoS1**

At first, since nothing was known about APOBEC3s expression in the UT7/EpoS1 cell line, an expression analysis on these cells was performed by RT-qPCR and Western Blot.

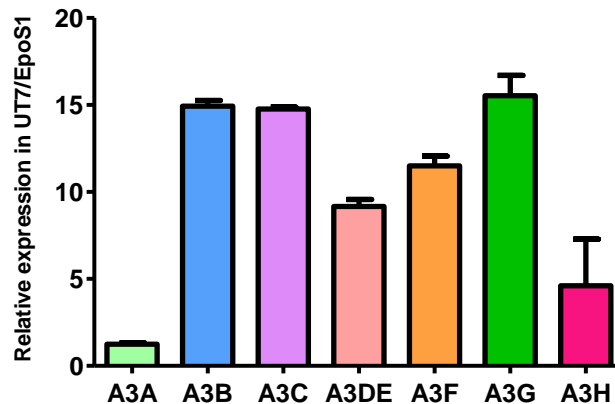


*Figure 34: Relative expression of the different A3 genes in UT7/EpoS1. Each gene expression has been compared to the expression of the GAPDH HK gene. Values of  $20-\Delta Ct$  are plotted.*

The RT-qPCR analysis showed a relevant expression of A3B, A3C and A3G, while A3A and A3H seemed to be the least expressed (Figure 34).

## Study of the role of APOBEC3B on B19V genome

By Western Blot analysis, A3B, A3C and A3G expression was confirmed (Figure 38). It is important to notice that, in our hypothesis, the main effector on B19V genome, due to the nuclear localization, should be A3B. However, the only available antibody able to label A3B recognizes also A3G, even more abundantly expressed in the UT7/EpoS1 cells.

To verify whether those A3s were functionally active inside the cells, a UT7/EpoS1 cell lysate was used in a deamination test (DT), incubating it in peculiar conditions in the presence of a fluorescent DNA probe containing a single cytidine. Owing to the reagents in the reaction mixture, if the cytidine is deaminated the probe is broken, resulting shorter on an urea-polyacrylamide gel.

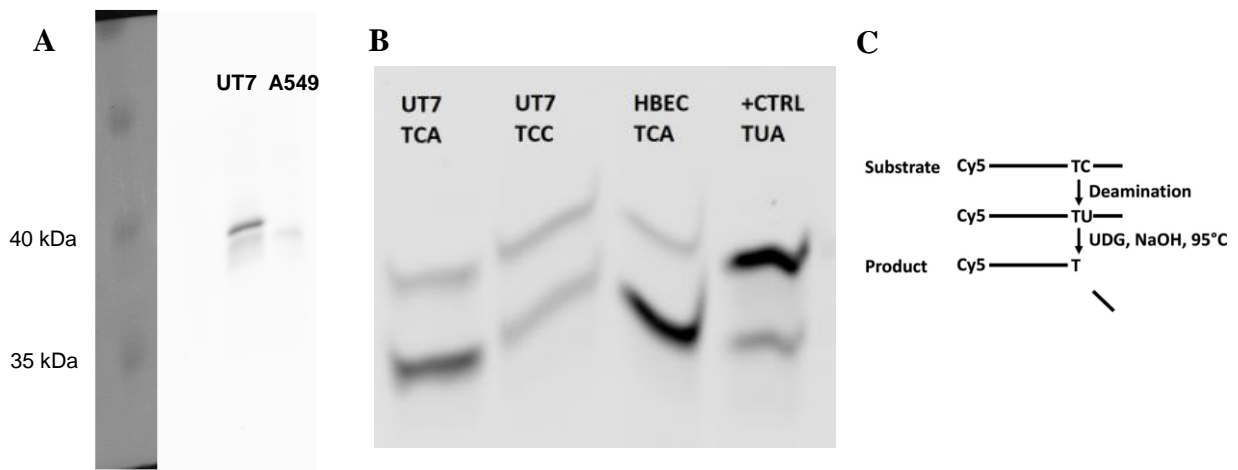


Figure 35: A3s expression in UT7/EpoS1. A – Western Blot analysis of A3B (37-kDa) and A3G (40-kDa), comparing with the control lung cell line A549, transduced to constitutively express A3B; B – Deamination test (DT) of a UT7/EpoS1 lysate, compared with a Human Bronchial Epithelial Cells (HBEC) lysate; C – schematic description of the DT.

The DT proved the activity of the A3s in the cell line, as showed by the generation of a shorter band in all the tested samples (Figure 35).

A3B can be expressed in the cells in four different isoforms, regulated by alternative splicing and mainly depending on the cell type. So, at last, an isoform characterization of A3B was performed by RT-PCR checking the resulting amplicons by agarose gel electrophoresis (Figure 36).

## Study of the role of APOBEC3B on B19V genome



Figure 36: Isoform characterization of A3B in UT7/EpoS1 cells. Left – Representation of the 4 A3B isoforms with the different possible outcomes of the two RT-PCRs to identify them; Right – RT-PCRs on exons 4-6 (left) and 7-8 (right) in UT7/EpoS1 cells. MWM goes down from 1000 bps decreasing by 100 bps per band.

This experiment showed the presence of the peculiar 327/234 bps bands combination, thus identifying isoform A3B-201 as the one expressed in this cell line.

### 4.2. A3B silencing in UT7/EpoS1 cells

In order to strongly silence A3B expression in UT7/EpoS1 cells, HEK239T cells were transfected with a mixture of lentiviral constructs expressing 3 different shRNAs targeting A3B or a scrambled shRNA. Lentiviral vectors thus produced were then used to transduce UT7/EpoS1 cells.

Transduced cells were kept under puromycin selection at different concentrations and monitored for the expression of the reporter gene mCherry, encoded in the lentiviral construct, to obtain a pure population of silenced cells.

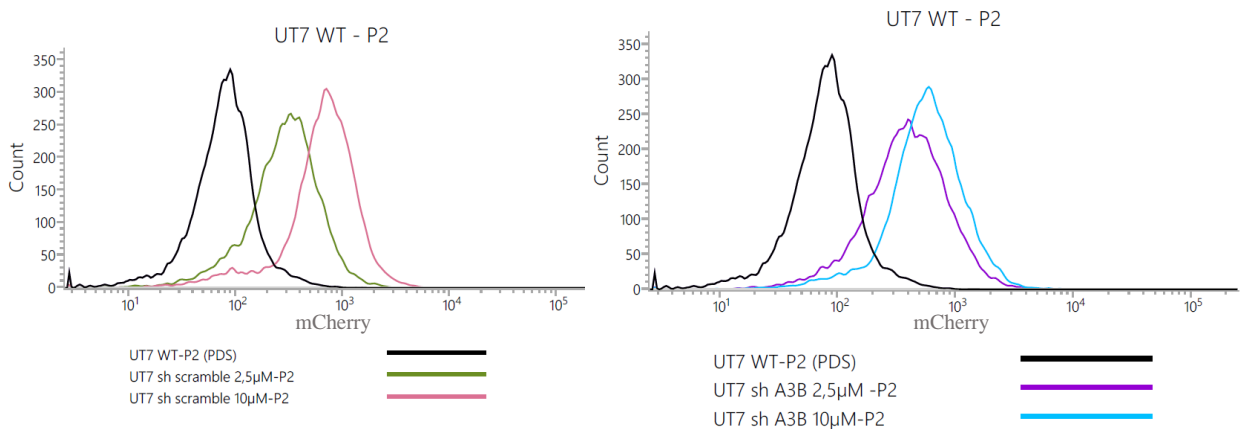


Figure 37: FACS analysis of transduced and wild-type UT7/EpoS1 cells. mCherry expression was monitored for Ut7-ShScramble (left) and UT7-ShA3B (right) at two different puromycin concentrations.

The cytofluorimetric analysis showed that a higher puromycin concentration improved the selection of a pure population of transduced cells after two weeks of selection (Figure 37). Selected cells were then tested for A3B expression, in order to confirm target silencing.

By Western Blot analysis, a specific reduction of A3B was noticed in the UT7-ShA3B transduced cells, while no reduction was detected in the scrambled control. This reduced expression of A3B determines a strong reduction in the deaminase activity of the cell lysate, as proven by the DT (Figure 38). Overall, these data confirm the establishment of a modified UT7/EpoS1 cell line with strongly reduced A3B levels.

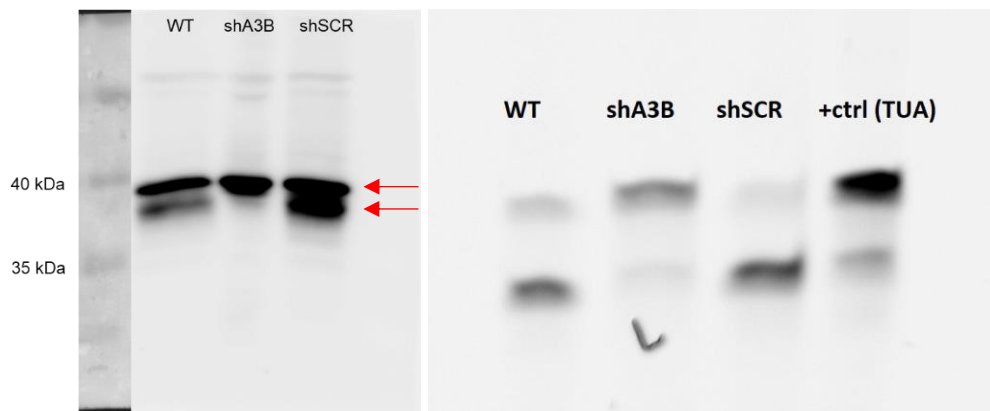


Figure 38: Western Blot (left) and deamination (right) test on the transduced UT7/EpoS1 cells. The reduction in A3B expression in the UT7-ShA3B cells goes side by side with the loss of deamination efficiency.

### **4.3. B19V–A3B interplay in nucleofected UT7/EpoS1**

The three UT7 cell lines (*wild type*, shA3B and shScr) were nucleofected with the viral genomic insert CK10 and the cells were analyzed to assess differences in the viral and A3B transcriptional levels, as well as capsid protein expression A3B variations by RT-qPCR and IIF. Due to the high amount of DNA needed for the nucleofection, no information on viral replication within the cells could be obtained. To evaluate putative induction effects on A3B by the mere presence of exogenous DNA, a linearized pcDNA3.1 was used in mock-nucleofected cells as a control.

*Study of the role of APOBEC3B on B19V genome*

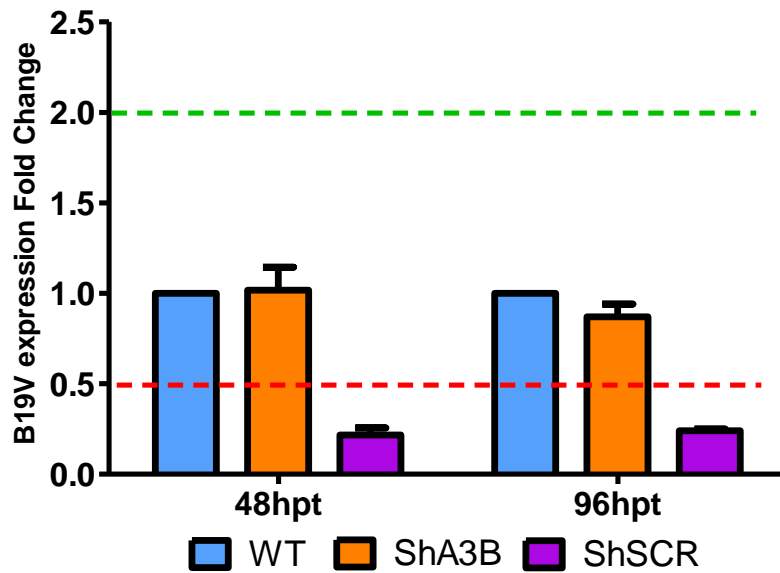


Figure 39: B19V expression fold change, normalized on WT cells.

No differences in viral transcription were detected in the shA3B cell line compared to the *wild type* at the two time points analyzed, 48 and 96 hpt, while a small but statistically significant decrease was detected in the -shScrambled cells: this variation, however, does not appear to be A3B-related, and further investigation would be needed to determine its cause (Figure 39). A3B silencing was confirmed in the UT7-shA3B compared to the *wild type* or the -shScrambled, but no significant variation was noticed in cells nucleofected with the viral insert compared to the plasmid control. To check whether any difference was visible at a protein level, an IIF analysis on both A3B and the VPs was performed: VPs expression is normally considered typical of a replicating viral genome, thus decreases in their expression could reflect an A3B antiviral activity.

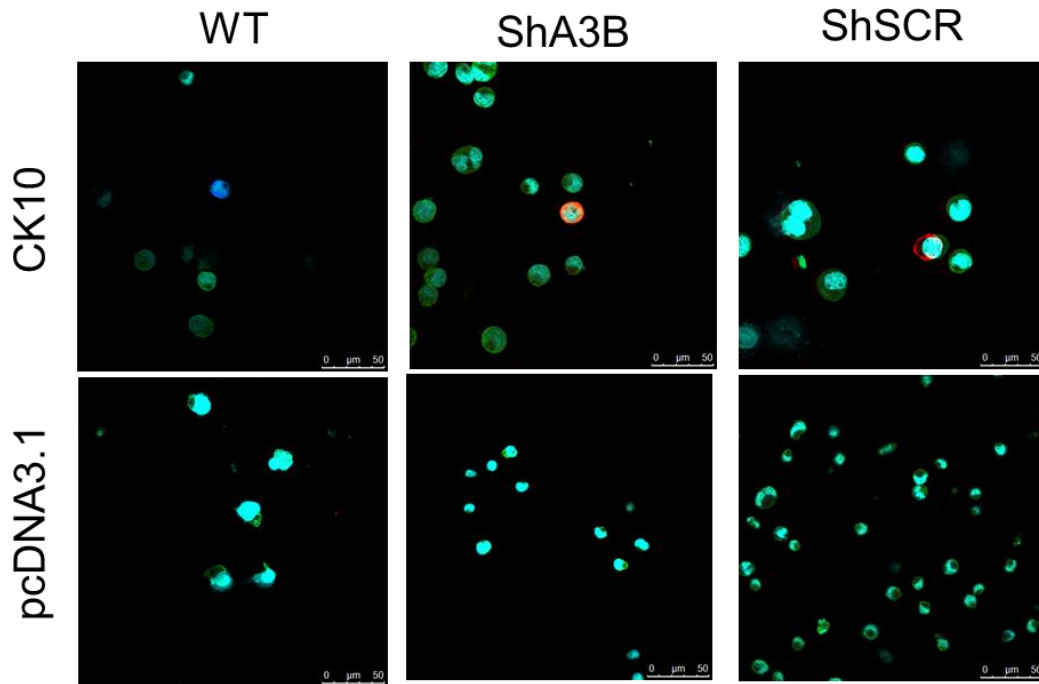


Figure 40: IIF analysis of nucleofected UT7/EpoS1 at 48 hpt. Color legend: cyan – DAPI; green – A3B/G; dark blue/red – VPs. Original magnification: 630X.

The IIF analysis, shown in Figure 40, was not really informative. On one hand, the reactivity of our antibody with both A3B and A3G was an issue, because the high expression levels of A3G in UT7/EpoS1 hid the silencing of A3B in the shA3B edited cells. On the other hand, the low efficiency of the nucleofection technique yielded a very small number of VPs positive cells, thus making putative differences within the positive cells compared to the negative ones hard to notice. Overall, these preliminary results did not highlighted any relevant difference in the viral general transcription levels between A3B silenced or non-silenced UT7/EpoS1, nor any variation in A3B expression comparing cells nucleofected with CK10 viral insert or a control plasmid.

However, the high amounts of dsDNA used for the nucleofection are not the best target to assess A3B effect on the viral genome, that usually enters the cells in much lower quantity and as a single-stranded molecule. Moreover, the low efficiency inherent to the technique has proved to be an issue while evaluating statistically significant differences in infected cells compared to the non-infected ones.

#### 4.4. B19V–A3B interplay in infected UT7/EpoS1

To investigate the role of A3B in a context more similar to a natural one, the 3 UT7/EpoS1 cell lines were infected with a CK10 B19V viral stock and viral replication, transcription and protein expression were analyzed.

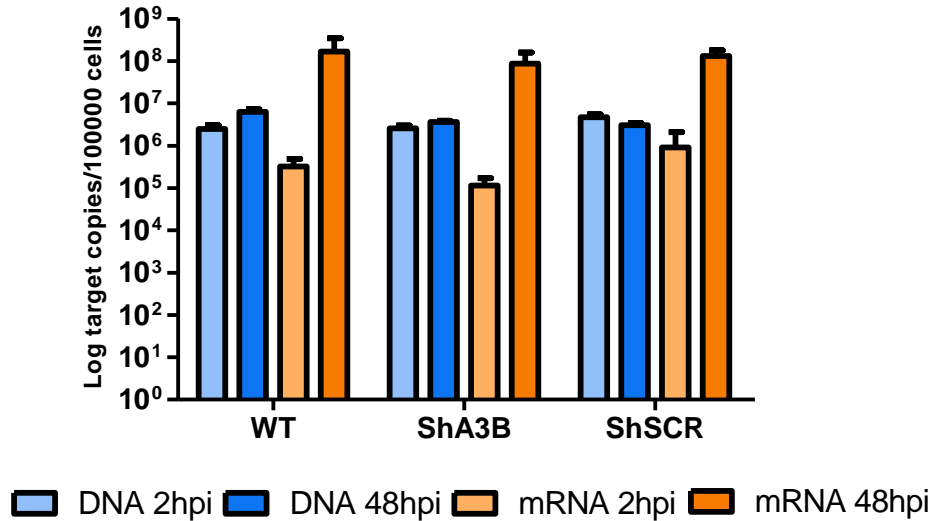


Figure 41: B19V nucleic acid analysis UT7/EpoS1 cell lines, infected with CK10 B19V. Log amounts of target copies, normalized to 10<sup>5</sup> cells..

The nucleic acid analysis on B19V was conducted at two different time points, 2 and 48 hours post infection (hpi), verifying the amounts of both viral DNA and total mRNAs.

Viral DNA amounts indicate remained comparable between the two time points, thus suggesting that only a portion of viral genomic input was actively replicating and compensating the general effect of exogenous DNA degradation (Figure 41).

At a transcriptional level, the increased amounts of viral transcripts detected at 48 hpi compared to the to 2 hpi indicated that viral genome was actually expressed in all the three analyzed cell lines. However, no significant difference was noticed either for replication or transcriptional efficiency among the three UT7/EpoS1 cell lines.

*Study of the role of APOBEC3B on B19V genome*

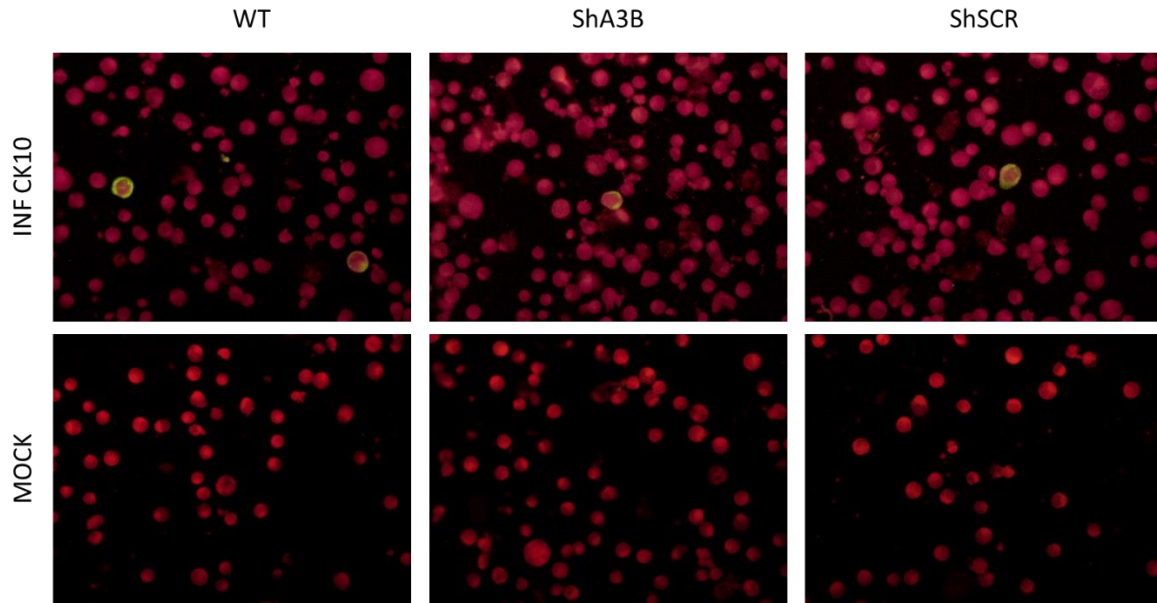


Figure 42: Anti-VPs IIF analysis of infected and mock-infected cells. Original magnification 400x

To assess whether any difference in capsid protein expression was detectable within cells, cells were analyzed by IIF at 48 hpi (Figure 42).

VPs were expressed in *wild type* UT7/EpoS1 as well as in the shRNA edited ones but, once again, no significant differences were detected between them.

On the other hand, the variation of A3B expression following B19V infection was evaluated, by quantifying A3B transcripts and comparing their amounts in infected vs non-infected cells.

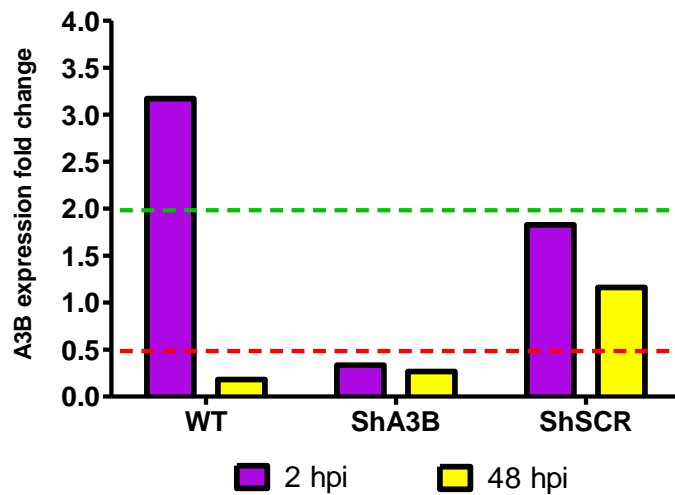


Figure 43: Fold change expression of A3B in B19V infected vs non-infected cells. Values higher than 2 indicate an upregulation of gene expression, while values below 0.5 represent a downregulation.

## ***Study of the role of APOBEC3B on B19V genome***

This analysis showed a modest inductor effect of B19V infection on A3B in *wild-type* UT7/EpoS1 cells at 2 hpi, followed by a downregulation at 48 hpi (Figure 43). For the silenced cells, the analysis of A3B downregulation should take into consideration that this variation, although statistically significant, is detected by qPCR at very low expression levels, thus the biological relevance of the reduced expression is probably low. At last, the UT7/EpoS1-ShScr cells do not seem to show relevant alterations of A3B expression due to B19V infection, even if a trend of upregulation can be noticed at 2 hpi similarly to what happens in *wild type* cells. Overall, some effect of B19V on A3B expression has been detected in UT7/EpoS1 *wild type* cells infected by Parvovirus B19, but this data should be considered preliminary and confirmed with independent analyses and different techniques.

### **4.5. Discussion**

APOBEC3s are a family of cytidine deaminases acting as important innate immune intracellular effectors, whose antiviral role has been demonstrated for viruses of different species. Recently, a bioinformatic analysis on a vast database of viral genomic sequences has pointed out how Parvovirus B19 genome is strongly depleted of 5'-NTC motives, which are the preferred target of A3s deamination activity [42]. In particular, due to its nuclear localization, A3B seemed to be the principal suspect to have footprinted B19V genome, whose lifecycle takes place mainly within the nucleus.

With the goal of verifying whether A3B could still exert a strong activity in editing B19V genome, which could open possibilities of targeting the protein to enhance its antiviral effect in B19V infections, I spent a period in the University of Namur in a collaborative study, to generate useful cellular models in which to study this interplay.

The UT7/EpoS1 cell line was proven to constitutively express A3B, thus its expression could be silenced to study viral behavior in absence of this protein. Lentiviral vectors expressing A3B-targeting shRNAs, as well as scrambled controls, were used to edit the cells; then, transduced cells were carefully selected to obtain a pure population of silenced cells. These cells achieved a strong reduction of A3B expression, that went side by side with the loss of deaminase activity.

## *Study of the role of APOBEC3B on B19V genome*

The three cell lines thus obtained (UT7/EpoS1 *wild-type*, -ShA3B and -ShScrambled) were used to study viral behavior in presence or absence of the protein and, at the same time, A3B variations due to the presence of viral genome.

In nucleofection experiments, no significant variation of viral transcription was noticed in silenced cells compared to the *wild type*, but a small reduction not related to A3B expression was detected in -shScrambled cells, that will be further evaluated. On the other hand, no variation of A3B expression was noticed in cells nucleofected with B19V CK10 genomic clone compared to plasmid controls, either at transcriptional or translational level. Technical issues inherent to the nucleofection technique prevented an appropriate evaluation of viral replication: on one hand, the high amounts of DNA needed for the nucleofection saturated qPCR signal preventing a proper quantification of replication; on the other hand, the low number of positive cells made a statistical analysis of VP expressing cells impossible to achieve.

Infections of the 3 cell lines with a CK10 viral stock took place in Bologna at my return. No significant variation of B19V transcriptional or replicative activity was noticed within the different cell types, nor VPs seemed to differ. Regarding A3B expression modest transcriptional variations associated to B19V have been seen for *wild type* cells but not for the -ShScrambled ones. This difference of behavior between the two lines deserves further investigations, in order to confirm this B19V associated variations also at the protein level, with independent analyses.

Overall, these data show no evidence of APOBEC3B activity towards B19V at present moment, at least in UT7/EpoS1 cells. An investigation on EPCs, that represent a better cellular model for B19V infection, would be interesting but, due to their nature of primary differentiating cells, a stable gene silencing in such population is technically unfeasible.

Our experiments shed new light on the bioinformatic prediction. It is reasonable to assume that A3B had an important role in editing B19V genome during its evolution, as demonstrated by the strong depletion of 5'-NTCs motifs, hence nearly exhausting its antiviral potential on this template. The number of 5'-NTC codons left on B19V genome appears to be now very small, and as a consequence, the susceptibility of B19V to A3B is reduced to irrelevant levels. Therefore, this may represent a limit to A3B antiviral effectiveness while being a selective advantage for the virus.

### 5. Conclusions

Parvovirus B19 is among the smallest pathogenic human viruses presently known, with its 5996 bps long genome encapsidated into a 22 nm icosahedral capsid. Nevertheless, much of its lifecycle mechanisms still have to be properly characterized: structural information has been determined only for the capsid shell, but the N-terminal domain of the VP1 (VP1u) remains largely unknown; the identity of the main viral receptor, for a long time attributed to globoside, is currently under debate, with an unknown receptor for the VP1u as principal candidate; the roles of the two main non-structural proteins have been partially determined, as well as some putative information on NS1 domains, but structural information are missing and the two minor proteins are almost just predicted. Moreover, a better characterization of virus-host interactions would allow the identification of novel putative targets, in order to identify specific antiviral drugs that are still missing.

A strong limitation in the study of B19V has always been its lack of adaptation to *in vitro* growth, thus making patients-derived viremic sera necessary to research. Furthermore, few cell lines can support viral replication and even the most used among them, UT7/EpoS1, only yields very low amounts of viral progeny. Hence, the best cellular model is still represented by primary EPCs obtained through *in vitro* differentiation from peripheral blood.

Recently, a synthetic approach pursued in our laboratory has led to the development of a functional genomic clone, CK10, that has proven able to replicate in UT7/EpoS1 cells giving rise to an infectious viral progeny, that can be successfully propagated in EPCs [163]. Moreover, progressive truncation of the ITRs in the synthetic sequence has elucidated the role of these sequences in preserving replicative competence. The use of a synthetic virus presents several advantages: first, the need for a patient-derived viral stock can be overcome and the use of native virus reduced, if anything, to a control role; second, the complete knowledge of the genome sequence would reduce sample variability among different experiments; third, cloned genomes can be edited to perform sequence-function studies.

During this work, CK10 genomic clone and its derived viral progeny have been used to investigate the interplay between B19V and an innate immune effector such as APOBEC3B, whose role during viral evolution, showed by bioinformatic analysis, suggested an active and present effect of this protein in the deamination of the viral genome, with potential antiproliferative consequence.

Furthermore, the genomic clone with ITRs extended up to the sites of dyad symmetry (CH10) was edited to split viral expression in a two-component system. This led to the production of a functional replicating minigenome, named pAs1, which is able to overexpress the main non-structural protein NS1 and to complement NS1-deficient genomes or minigenomes. Such a system could be used as a tool to deepen the knowledge about NS1 role and cellular partners within the cell, as well as to look for molecules with potential antiviral activity targeting NS1, in a simpler genomic environment. On the other hand, the generation of this two-component system serves as a proof-of-concept of B19V genome plasticity: this could open the way to subsequent genomic editing by, for example, adding expression tags to viral proteins or expressing heterologous genes. Further intense research work will be needed to improve these preliminary results in B19V genome editing, but the generation of engineered virus specifically targeting a selected population, such as the EPCs, would be of relevant interest in a translational perspective.

## **6. Materials and Methods**

### **6.1. Bacterial strains**

- **Library efficiency DH5 $\alpha$  Competent cells (Invitrogen):** *E. coli* strain suitable for cloning experiments, blue/white screening and efficient transformation of large plasmids. They bear no resistance genes, so are suitable with every selection marker. S.O.C. medium is required during transformation procedure.
- **SURE 2 Supercompetent cells (Agilent technologies):** *E. coli* strain engineered to allow cloning of DNA fragments considered “unclonable”, with great efficiency. SURE cells lack elements catalyzing the rearrangement and deletion of secondary and tertiary nucleic acid sequences, so they have been used when B19V hairpin sequences were included in the plasmid. They are kanamycin, tetracycline and chloramphenicol resistant and require NZY+ broth during transformation procedure.

Both strains lack ribonuclease and endonuclease to ensure the stability and improve the quality of purified plasmids.

### **6.2. Bacterial media**

In order to fit to the diverse steps of the experiment, different media were used:

- LB Agar is a solid medium used for plating. It's composed of: 1% tryptone, 0,5% yeast extract, 1% NaCl, 100  $\mu$ L NaOH 1 M in 100 mL of medium, 1,5% agar and antibiotics ([kanamycin]<sub>final</sub> = 50  $\mu$ g/mL; [ampicillin]<sub>final</sub> = 100  $\mu$ g/mL). Plates were preheated at 37°C for about 1 h before utilization; thus reaching the ideal temperature for bacterial growing and preventing condensation.
- S.O.C. or NZY+ broth were added to the bacterial cellular suspension during transformation procedure to allow a quick recovery: 1) SOC medium is made of: 2% Tryptone, 0,5% yeast extract, 10 mM NaCl, 2,5 mM KCl, 10 mM MgSO<sub>4</sub>, 10 mM MgCl<sub>2</sub>, 20 mM glucose; 2) NZY+ broth is made of: 1% casein digest (NZ amine), 0,5% NaCl, and 0,5% yeast extract. They were both pre-heated at 37°C before utilization.

- LB medium is a liquid broth used for bacterial growth. It is composed as follows: 1% tryptone, 0,5% yeast extract, 1% NaCl, NaOH 1 mM. Antibiotics were added until their final concentration: kanamycin 50 µg/mL, ampicillin 100 µg/mL. Bacteria grew in this medium at 30°C or 37°C for 16-18 h and in continuous agitation.

### **6.3. Molecular cloning**

Cloning strategies were planned *in silico* using Clone Manager 9 software to manage plasmid sequences and simulate restriction endonuclease cleavage, ligations, PCRs and mutagenesis profiles.

Enzymatic reactions were performed using restriction enzymes (REs) in order to screen the transformed bacteria colonies, to separate the vectors and the inserts for the subsequent ligase reactions or the transfection reactions. Different *FastDigest* enzymes were used provided by *ThermoFisher Scientific*: AccIII, BamHI, BssHIII, Eco47III, EcoRI, NotI, SacI, SalI, ScaI, SmaI, XmaI, XbaI, and XhoI. For each digestion reaction, plasmid DNA was incubated together with the enzyme (1 U) in 1:10 diluted FastDigest buffer (*ThermoFisher Scientific*) and water, till the final volume of 20 µL, at 37°C for at least 30 minutes. Double digestions were performed as the single ones but using multiple enzymes within the same reactions, except for those involving XmaI: this enzyme requires a specific buffer (Cfr9I buffer, *ThermoFisher Scientific*), thus making necessary a purification step between the two digestions. Following the incubation, digestions were checked by gel electrophoresis before following steps.

Purified vectors and inserts were then used for the ligation reaction. Ligations were performed using the T4 DNA ligase enzyme (Roche): vector and insert DNA were incubated together with T4 DNA ligase (1 U) in 1X ligation buffer (50 mM Tris-HCl, 10 mM dithioerythritol, 500 µg/mL BSA, pH 7,6; also containing ATP as cofactor's enzyme) overnight at 16°C. Both vectors and inserts had sticky ends, due to the digestion by the restriction enzymes, and they were in a molar ratio of 1:3 or 1:5 or respectively, to ensure a major probability of specific binding.

In addition to the reactions between the insert and the vector, a ligase reaction was done with all the reagents except the insert and used as negative control. A negative control indicated if the plasmid (vector) could close itself without insert and have the ability to form colonies after transformation of bacteria.

## ***Material and Methods***

In the course of the experimental workflow, several plasmids were generated. Plasmid composition and cloning strategies are indicated in the following Table 4, Figure 44, Figure 45 and Figure 46.

*Table 4: Plasmids generated with indication of backbone, insert and cloning steps.*

<b>Clone</b>	<b>Backbone (pEX, CI, CH, CK)</b>	<b>Genomic Insert</b>	<b>Cloning terminal sites</b>	<b>Cloning steps</b>
pCH10 pAs1	pCH	CH10 pAs1	BssHII-BssHII	pCH10 vector + CH0-MR pAs1 insert from pCH0-MR pAs1 w/ EcoRI-XmaI
<i>pCH0-MR pAs1</i>	pCH0R	CH0-MR pAs1	SmaI-BssHII	pCH0R pAs1 vector + MpAs1 fragment from pEX-A128-MpAs1 w/ XmaI-BamHI (eurofins)
<i>pCH0-R pAs1</i>	pCH0R	CH0-R pAs1	BamHI-BssHII	pCH0R vector + CH0R pAs1 insert from pEX-CI0-pAs1 w/ BamHI-AccIII
pEX-CI0 pAs1	pEX	CI0 pAs1	AccIII-AccIII	pEX-A128-MpAs1 vector + CI0-L insert from CI0-LM w/ XhoI-XmaI
pCH10 A1.1 NS Spliced	pCH	CH10 A1.1	BssHII-BssHII	pCH0-R vector + CH1-LM A1.1 from pCH1-LM A1.1 w/ BamHI-SalI/XhoI
<i>pCH1-L D1</i> <sup>1</sup>	pCI	CH1-L D1	BssHII-NotI	pCI0-L vector + amplicon 1 (pMA Fw – D1 Rev from pCH1-LM) w/ EcoRI-NotI

<sup>1</sup> = Clone is formally a pCH, due to BssHII extensions, but it's build on a CI backbone (KanR)

<i>pCH1-LM A1.1 NS Spliced<sup>1</sup></i>	pCI	CH1-LM A1-1	BssHII-BamHI	pCH1-L D1 vector + amplicon 2 A1.1 (A1.1 Fw – pMA Rev from pCH1-LM) w/ NotI-BamHI
pCH10 A1.2 NS Spliced	pCH	CH10 A1.2	BssHII-BssHII	pCH0-R vector + CH1-LM A1.2 insert from pCH1-LM A1.2 w/ BamHI-SalI/XhoI
<i>pCH1-LM A1.2 NS Spliced<sup>1</sup></i>	pCI	CH1-LM A1-2	BssHII-BamHI	pCH1-L D1 vector + amplicon 2 A1.2 (A1.2 Fw – pMA Rev from pCH1-LM) w/ NotI-BamHI
pCK10 NSKO	pCK	CK10 NSKO	SacI-SacI	pCK0-R vector + CK1-LM NSKO insert from pCK1- LM NSKO w/ SalI/XhoI-BamHI
<i>pCK1-LM NSKO<sup>2</sup></i>	pCK	CK1-LM NSKO	SacI-BamHI	pCK1-LM vector + CH1-LM NSKO insert from pCH1- LM NSKO w/ BssHII-BamHI
<i>pCH1-LM NSKO<sup>2</sup></i>	pCH	CH1-LM NSKO	BssHII-BamHI	pCH1-LM vector + amplicon 3 <sup>3</sup> NSKO w/ EcoRI-SmaI
pEX-A128- MpAs1	pEX-A128	MpAs1	XmaI-AccIII	Purchased from Eurofins Genomics

<sup>2</sup> = Sequence analysis showed 4 mutations, considered irrelevant: one in the 5' non-coding region (not within the promoter), a silent one and 2 missense (on the whole NS1 sequence, Thr332Ala, Leu442Leu, Phe496Leu)

<sup>3</sup>= Amplicon 3 comes from self-priming PCR reaction of amplicons 1 NSKO and 2 NSKO on pCH1-LM template. Amplicon 1 w/ primer pair pMA Fw – Mut Rev, Amplicon 2 w/ Mut Fw – R2355. The two amplicons have been joined in PCR, column purified and 10 µL used as template for subsequent PCR w/ external primer pair pMA FW – R2355.

## Material and Methods

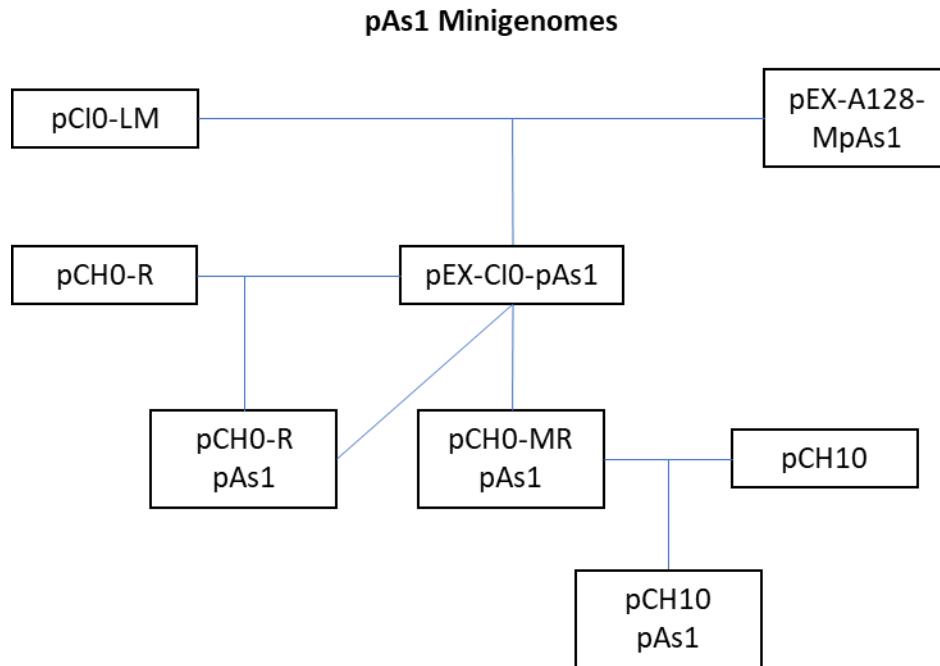


Figure 44: Flowchart of the cloning strategy for the pAs1 minigenomes

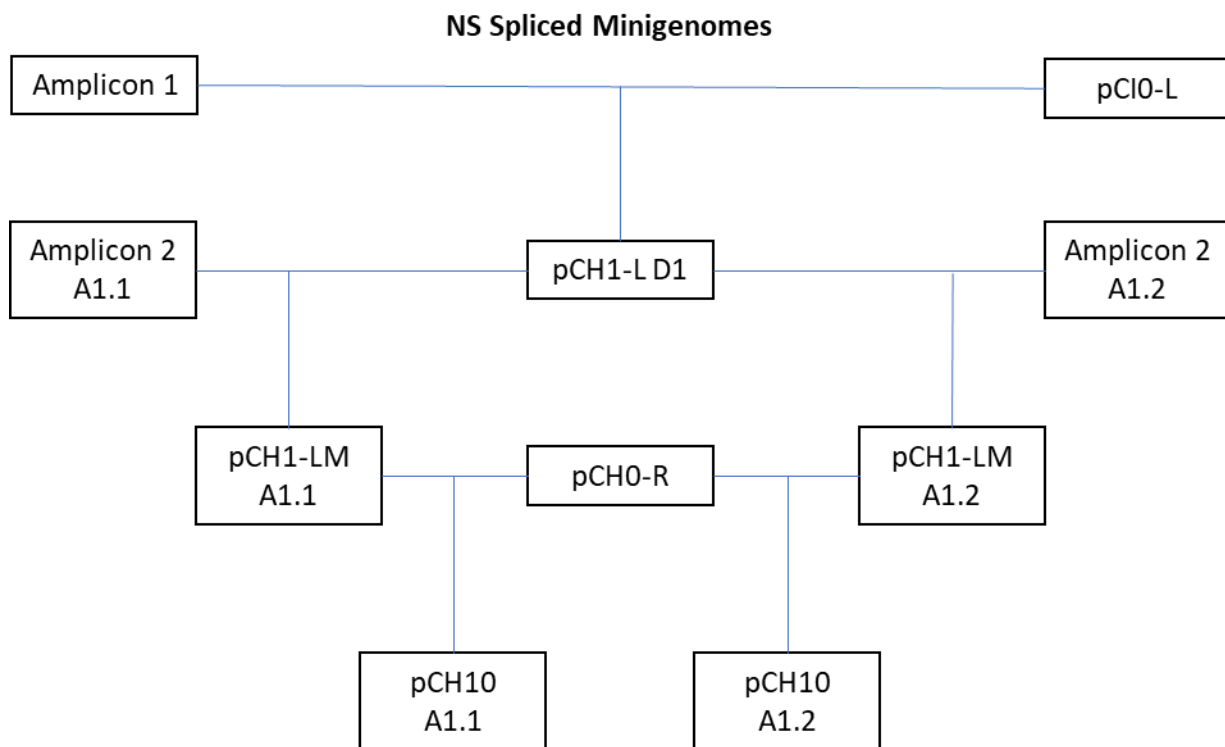


Figure 45: Flowchart of the cloning strategy for the NS Spliced minigenomes

## NSKO Genomes

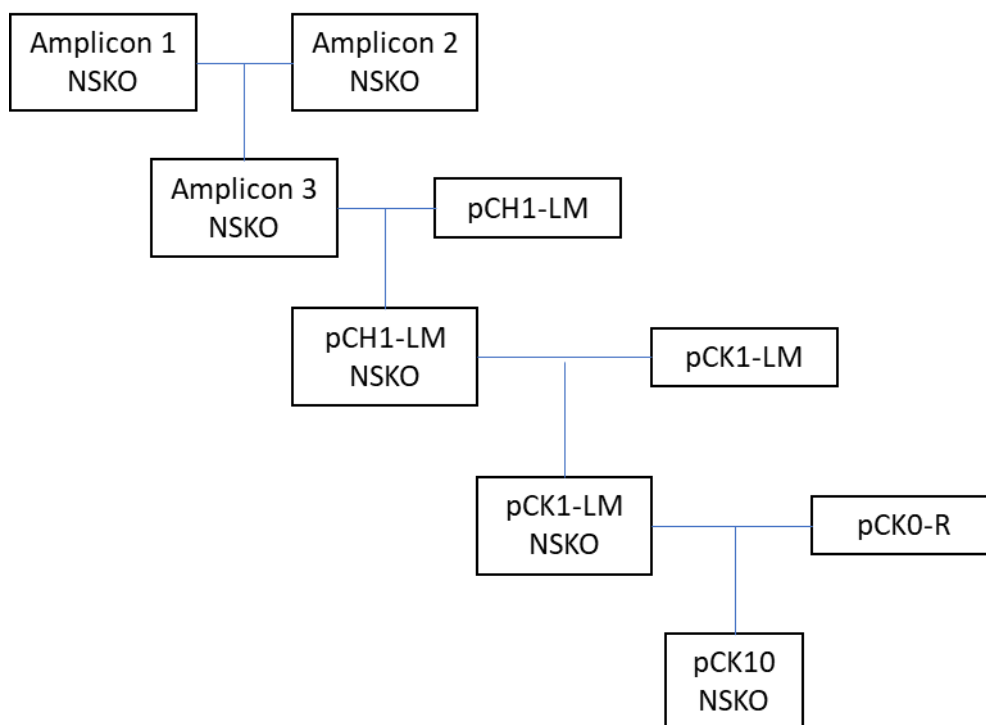


Figure 46: Flowchart of the cloning strategy for the NSKO genomes

#### **6.4. Bacterial transformation and growth**

10 ng of plasmid DNA or 2  $\mu$ L of a ligation reaction were used to transform 20  $\mu$ L of competent bacterial cells. The cell suspension was then kept on ice for 30 minutes, shocked at 42°C for 30-45 seconds (depending on the strain) and kept on ice again for 2 minutes. Eventually, the suspension was added with 80  $\mu$ L of S.O.C. or NZY+ medium (depending on the strain) and incubated at 37°C for 1 h rocking. Cellular suspension was disseminated on a Petri plate containing selective medium and incubated at 30°C or 37°C O/N.

Transformed bacterial colonies were recovered from the selective solid medium and expanded in 5 mL of LB liquid broth with antibiotics (kanamycin or ampicillin). Selected colonies were further expanded in 100 mL of LB liquid broth with antibiotics for medium-scale plasmid preparation.

### **6.5. Plasmid miniprep and midiprep systems**

*PureYield Plasmid Miniprep System* and *PureYield Plasmid Midiprep System* (Promega) were used to purify plasmid DNA, both based on a rapid silica-membrane column purification method. Their main difference is the culture volume to process: the miniprep system purifies plasmid from a maximum of 3 mL of culture volume, while the midiprep system purifies 50 to 250 mL culture volume.

The miniprep system was used for an early screening of the transformed bacterial colonies recovered from the plates; on the other hand, the midiprep system was used to generate a plasmid stock from the selected colony after expansion in 100 mL, which could then be used for subsequent vector/insert preparations or as a PCR template.

The isolated and purified plasmid DNAs were quantified via UV spectrophotometry and checked by RE digestion, evaluating the size of the derived fragments by agarose gel electrophoresis. As a further confirmation, when PCR amplification was needed during cloning strategy, plasmids were sequenced.

### **6.6. DNA fragments purification**

To purify digested plasmids or PCR fragments, either in solution or from agarose gel, *Wizard SV Gel and PCR cleanup system* (Promega) was used. This kit provides silica columns that bind DNA with the help of a *DNA binding solution*, that can be used to dissolve agarose bands as well. Purified DNA was then eluted in nuclease-free water and quantified via UV spectrophotometry.

### **6.7. Cells**

Different eukaryotic cell systems were used:

- UT7/EpoS1 cells: cancer cell line derived by a human adult acute megakaryoblastic leukemia. Cells grow in suspension in IMDM (Cambrex) supplemented with 10% FBS, 1% L-Gln, 1% pen-strep and 2 U/mL Epo  $\alpha$  (Eprex, Janssen), at 37°C and 5% CO<sub>2</sub> and densities between  $2 \times 10^5$  and  $10^6$  cell/mL.

- Erythroid Progenitor Cells: EPCs were generated through *in vitro* differentiation of peripheral blood mononuclear cells (PBMCs), obtained from leukocyte-enriched buffy coats of healthy blood donors, available for institutional research purposes according to the policy approved by the local Ethical Committee (S.Orsola-Malpighi University Hospital). PBMCs were isolated using centrifugation in Ficoll-Plaque Plus (GE Healthcare Bio-Sciences AB) density gradient and cultured in IMDM (Lonza) supplemented with 20% serum substitute BIT 9500 (StemCell Technologies), 900 ng/mL ferrous sulphate, 90 ng/mL ferric nitrate, 1  $\mu$ M hydrocortisone (Sigma-Aldrich), 3 U/mL Epo  $\alpha$  (Eprex, Janssen), 5 ng/mL IL-3, 20 ng/mL Stem Cell Factor (SCF; Life Technologies), 2 mM L-Gln and 1% pen-strep. Cells were infected when at day 8 of *in vitro* growth and differentiation.
- HEK293T: derived from a human embryo kidney, it's a highly transfectable cell line transformed by SV40 T-antigen. They're competent to replicate viral vectors bearing the SV40 origin of replication, giving high titers in producing retroviruses. They were kept in DMEM medium supplemented with 10% FBS and 1% L-Gln and used for transfection when at 70% confluency.

## **6.8. Endpoint PCRs**

In order to amplify DNA fragments to be used in nucleofection experiments or during molecular cloning steps, the *Expand High Fidelity<sup>PLUS</sup> System* (Roche) was used with the “Longpan” amplification profile (Table 5) and different primer pairs. *Clone manager 9* software was used to determine the correct annealing temperature for each primer pair.

All the reactions were set up in 50  $\mu$ L total volume, according to manufacturer's instruction and using 5 ng of DNA as a template.

The following Table 5 and Table 6 recap the amplification profile the primers used.

## Material and Methods

Table 5: Longpan amplification profile

Step	Temperature	Time	Number of cycles
Initial Denaturation	94°C	2'	1
Denaturation	94°C	15''	10
Annealing	Various	30''	
Elongation	68/72°C	1'/kb	
Denaturation	94°C	15''	20
Annealing	Various	30''	
Elongation	68/72°C	1'/kb + 5''/cycle	
Final elongation	72°C	7'	1
Cooling	10°C	Indefinitely	1

Table 6: Primer list for endpoint PCRs. Lower case indicates mismatches, underlined bases indicate introduced RE site.

Primer Name	Primer sequence (5'→3')	Target (5')	Function
pMA Fw	CGCGACGTAATACGACTCAC	Plasmid backbone	Introducing deletion of the first intron
D1 Reverse	cgcg <u>ggccg</u> CCTGTTAGTTAGCTCACAAAAACAGC	Splicing donor D1	
A1-1 Forward	gcgg <u>ggccgc</u> ATGCCCTCCACCCAGACCTCCAAACC	Splicing acceptor A1.1	
A1-2 Forward	gcgg <u>ggccgc</u> GCGCCTGGAACACTGAAACC	Splicing acceptor A1.2	
pMA Rev	CAGGTTTCCCGACTGGAAAG	Plasmid backbone	
HH1	CGCCGCTTGTCTTAGTGTCAAGGC	Flip ITR, within dyad symmetry	Amplifying CH10 insert
HH0	CGCCGCTTGATCTTAGTGGCACGTC	Flop ITR, within dyad symmetry	
HI0	GCGTCCGGAAGTCCC GCCC ACCGGAA	ITRs, before isomerism	Amplifying CI0 insert

HJ0	GCGTCCGGAGTCTTCTTTTAAATTTT	ITRs, stem	Amplifying CJ0 insert
Mut Fw	GTTAACATACTA <u>CtaGa</u> AGCTATTTAGAGGGGTG	14 nt upstream NS1 ATG	NS1 ATG
Mut Rev	CTAAATAGCT <u>CtaGa</u> TAGTATGTTAACAAGTAG	11 nt downstream NS1 ATG	KO, with pMA Fw
R2355	GAAACTGGTCTGCCAAAGGT	Central exon	

### **6.9. Nucleofection of UT7/EpoS1 cells**

UT7/EpoS1 cells were nucleofected using the *Amaxa Nucleofector II* device, set on program T-20, and Kit V Nucleofector Reagent, both supplied by Lonza. Cells were passed 1:2 the day before, then washed twice in PBS and nucleofected with a DNA ratio of 1 µg/10<sup>6</sup> cells for each genomic insert. After nucleofection, cells were plated in a cell culture plate with complete medium at 37°C and 5% CO<sub>2</sub> and analyzed as previously described.

### **6.10. Infection of UT7/EpoS1 cells or EPCs**

UT7/EpoS1 cells were split 1:2 the day before infection, while EPCs were used at day 8 of *in vitro* differentiation. Cells were washed in PBS and incubated in presence of a viral stock, to achieve the desired MOI of 10<sup>3</sup>, or of 6 dpt supernatant, for 2 hours at a cellular density of 10<sup>7</sup> cells/mL. After two hours, cells were washed twice in PBS and plated at 37°C and 5% CO<sub>2</sub> with complete medium until the subsequent analyses.

### **6.11. Generation of Lentiviral vectors**

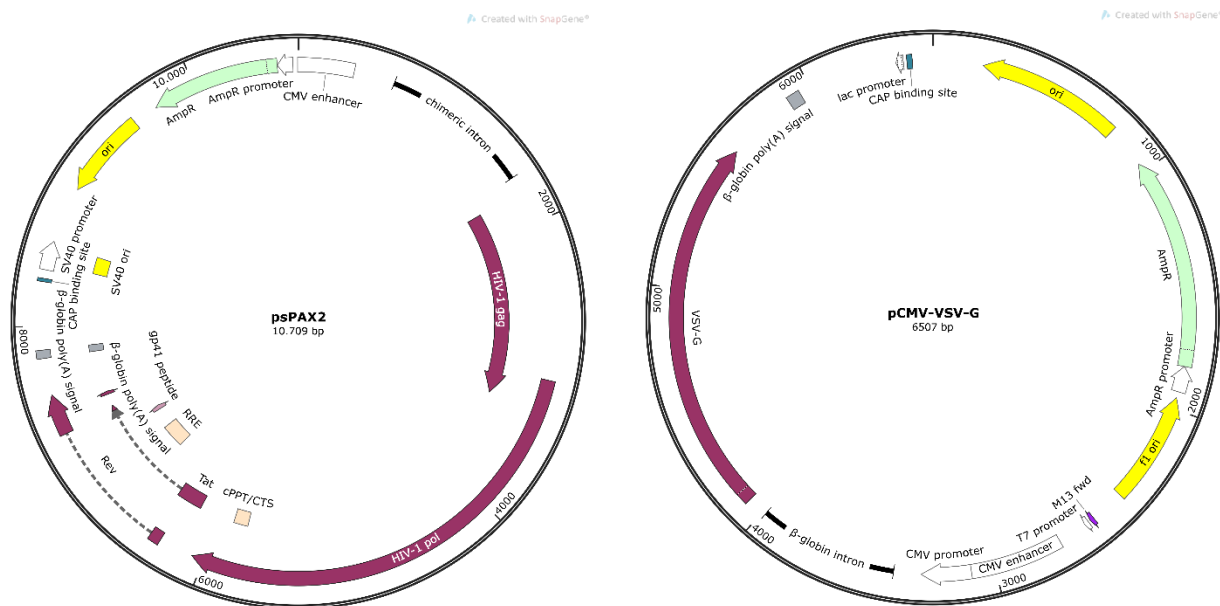
In second generation lentiviral vectors, three plasmids need to be transfected into producer cells to originate lentiviruses: a transfer plasmid (the pSicoR plasmids described below), bearing the transgene flanked by the LTRs; a packaging plasmid (psPAX2) encoding Gag, Pol, Rev and Tat; an envelope plasmid (pCMV-VSV-G), encoding the envelope protein, which is usually VSV-G (Vesicular Stomatitis Virus protein G) for its wide infectivity.

HEK293T cells were used for transfection when 70% confluent. Transfection mixture was prepared in 500 µL of Opti-MEM medium (ThermoFisher Scientific) supplemented with 16 µL of

## Material and Methods

Lipofectamine 2000 (ThermoFisher Scientific) and with the following plasmids: 0,4 µg of pCMV-VSV-G; 3,6 µg of psPAX2; 4 µg of pSicoR\_EF1a\_mCherry\_T2A\_Puro\_sh-scrambled or 4 µg of a plasmid mixture of pSicoR\_EF1a\_mCherry\_T2A\_Puro\_shA3B\_754, pSicoR\_EF1a\_mCherry\_T2A\_Puro\_shA3B\_1061 and pSicoR\_EF1a\_mCherry\_T2A\_Puro\_shA3B\_1467. Three different plasmids were used to target A3B transcript with different shRNAs binding in different positions, in order to maximize the silencing effect. Cells were then kept in culture in a BSL3 facility with UT7/EpoS1 complete medium to allow lentiviral production.

Plasmid maps are shown in the following Figure 47.



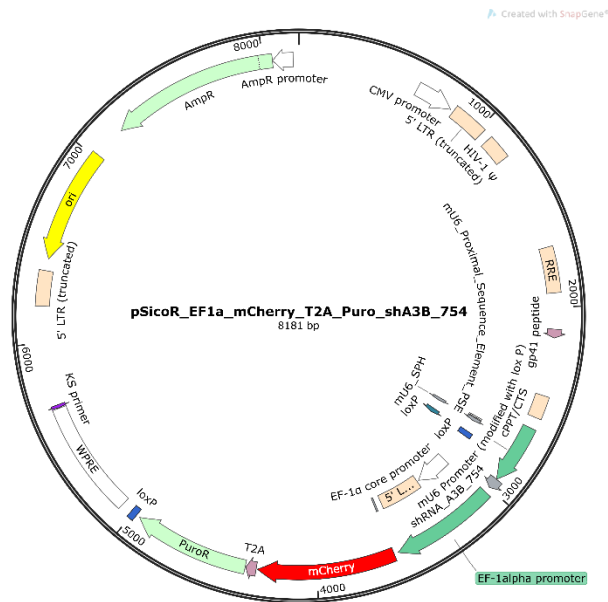


Figure 47: Plasmids used in the generation of the lentiviral vectors. Just one of the three pSicoR plasmid is shown.

## 6.12. Lentiviral transduction of UT7/EpoS1 cells

At 48 and 72 hours post transfection, cell free supernatant from transfected HEK293T cells was collected and used as inoculum to transduce UT7/EpoS1 cells, which were resuspended in it at a cell density of  $5 \times 10^5$  cells/mL and placed in culture at 37°C and 5% CO<sub>2</sub> in a BSL3 facility.

## 6.13. Selection of edited UT7/EpoS1 cells

At 48 hours post transduction, cells were resuspended in complete fresh medium enriched with 2,5 µg/mL puromycin to select transduced cells. Cells were kept in a BSL3 facility for at least 3 passages, then checked for the presence of lentiviruses in the supernatant (using the *qPCR Lentivirus Titration Kit* (Applied Biological Materials)) before moving them to a BSL2 laboratory. The expression of mCherry was then checked by flow cytometry (FACSVerse, Becton Dickinson) using a Texas Red filter, to determine the percentage of transduced cells.

## 6.14. Nucleic acid extraction

Nucleic acid extraction was performed using 2 different systems: *Viral Total Nucleic Acids* kit with *Maxwell 16 automatic extractor* (Promega) and *RNeasy Micro* (Qiagen).

## ***Material and Methods***

The first system was used for almost all nucleic acid analyses, and it takes advantage of an automatic extractor with a cartridge-based system. Cell pellets are lysed with the supplied Lysis Buffer and Proteinase K, for 10 minutes at 56°C and 750 rpm in a thermomixer. Lysed samples are then loaded into the kit cartridge, following manufacturer's instructions, and eluted in water at a ratio of 100 µL/10<sup>5</sup> cells. This kit can elute cellular and viral nucleic acids, preserving both DNA and RNA.

Only for the post-nucleofection RT-qPCR analysis of the UT7 cells in the A3B-related project, the column-based *RNeasy Micro* kit was used. 4x10<sup>5</sup> cells were lysed following manufacturer's instruction and the purified RNA was eluted in a final volume of 14 µL, thus having a highly concentrated RNA solution.

### **6.15. qPCR analysis**

qPCR analysis was performed using the *Maxima Sybr Green qPCR Master Mix 2X* (ThermoFisher Scientific), on a *RotorGene-Q* (Qiagen) machine.

This kit provides a 2X master mix containing all the reagents but the primers: in particular, a hot start Taq DNA polymerase (activated after 10 minutes at 95°C) and the SYBR Green I fluorescent dye ( $\lambda_{\text{excitation}}= 494 \text{ nm}$  and  $\lambda_{\text{emission}}= 521 \text{ nm}$ ). Reaction mixture was prepared according to the manufacturer's instruction, in a final volume of 20 µL and using 5 µL of 10-fold diluted nucleic acid extract. Two replicates were made per each qPCR reaction.

*Table 7: List and function of qPCR primers.*

<b>Primer name</b>	<b>Sequence 5'→3'</b>	<b>DNA target</b>
R2210	CGCCTGGAACACTGAAACCC	Virus DNA
R2355	GAAACTGGTCTGCCAAAGGT	
DpnI 1801 Fw	CTTGGTGGTCTGGGATGAAG	For DpnI assay
DpnI 1801 Rev	TACTCCAGGCACAGCTACAC	
18Sfor	CGGACAGGATTGACAGATTG	Genomic 18S rDNA
18Srev	TGCCAGAGTCTCGTTCGTTA	

Amplification profile:

	Temperature	Time	Cycles
Initial Taq activation	95°C	10'	1
Denaturation	95°C	15''	40
Annealing	60°C	30''	
Elongation and acquisition	72°C	30''	

To confirm amplicon specificity, the PCR products were subjected to a slow denaturation (“melting curve analysis”). The melting point (T<sub>m</sub>) was evaluated by a different profile: from 95°C the temperature was reduced to 65°C then increased to 95°C with a shift of 0,1°C/sec. Values previously obtained for external standards were employed to build a calibration curve, enabling concentration calculation by interpolation within this reference curve. GraphPad Prism 5.00 software for Windows (GraphPad Software, San Diego California, USA) was used to carry out data analysis.

### **6.16. RT-qPCR analysis**

Viral and cellular mRNAs were quantified via RT-qPCR using *QuantiNova*<sup>®</sup> *SYBR Green RT-PCR Kit* (Qiagen) to evaluate transcription levels. This kit serves as a fast tool to quantify transcripts in a single-step reaction. Nucleic acid extracts were pre-treated with *Turbo DNA-free kit* (ThermoFisher Scientific) to remove DNA. For the virus, a region within the central exon, common to all transcripts, was amplified in order to confirm that the genome was transcriptionally active; furthermore, specific mRNAs were considered for this analysis. Two replicates were made per each reaction.

The following Table 8 and Table 9 recap the reaction mixture setup and the thermal profile.

*Table 8: QuantiNova reaction mixture setup*

<b>Reagent</b>	<b>Volume/reaction</b>
Template (DNase-treated RNA, 10-fold diluted)	5 µL

## Material and Methods

2x QuantiNova SYBR Green RT-PCR Master Mix	10 µL
QN SYBR Green RT-MIX	0,2 µL
10x Primer Mix (containing 10 µM of each primer)	1 µL
RNase-Free Water	Up to 20 µL

Table 9: QuantiNova thermal profile

Step	Temperature	Time	N° of Cycles
Reverse transcription	50°C	10'	1
PCR initial activation step	95°C	2'	1
Denaturation	95°C	5''	40
Combined annealing and extension	60°C	10''	
Melting curve analysis	60°C to 95°C (0,5 °C steps)	-	1

Only for the characterization of APOBEC3s expression in the UT7/EpoS1 cells and for the post-nucleofection analysis in the A3B project, a different kit was used. 500 ng of TurboDNase-treated RNA were retrotranscribed using the *iScript cDNA synthesis kit* (Bio-Rad) following the manufacturer's instructions, then three different dilutions (10-, 30- and 90-fold) were analysed per each sample using the *Takyon No Rox SYBR MasterMix dTTP Blue UF-NSMT* (Eurogentec) on a Bio-Rad *CFX Connect Real-Time PCR System* machine, in a final volume of 10 µL following manufacturer's extraction for reaction setup and amplification profile.

All the primers used are listed in the Table 10 below.

Table 10: RT-qPCR primers

Primers	Primer sequence (5'→3')	mRNA
R2210	CGCCTGGAACACTGAAACCC	Viral central exon, total RNA
R2355	GAAACTGGTCTGCCAAAGGT	
R1882	GCGGGAACACTACAACAAC	NS1 mRNA
R2033	GTCCCAGCTTTGTGCATTAC	
R4869	ATATGACCCACAGCTACAG	VPs mRNA
R5014	TGGGCGTTTAGTTACGCATC	

R4899	ACACCACAGGCATGGATACG	(pA)d cleaved mRNAs
R5014	TGGGCGTTTAGTTACGCATC	
A3A_RTqPCR_Fw	GAGAAGGGACAAGCACATGG	A3A mRNA
A3A_RTqPCR_Rv	TGGATCCATCAAGTGTCTGG	
A3B_RTqPCR_Fw	GACCCTTTGGTCCTTCGAC	A3B mRNA
A3B_RTqPCR_Rv	GCACAGCCCCAGGAGAAG	
A3C_RTqPCR_Fw	AGCGCTTCAGAAAAGAGTGG	A3C mRNA
A3C_RTqPCR_Rv	AAGTTTCGTTCCGATCGTTG	
A3DE_RTqPCR_Fw	ACCCAAACGTCAGTCGAATC	A3DE mRNA
A3DE_RTqPCR_Rv	CACATTTCTGCGTGGTTCTC	
A3F_RTqPCR_Fw	CCGTTTGGACGCAAAGAT	A3F mRNA
A3F_RTqPCR_Rv	CCAGGTGATCTGGAAACACTT	
A3G_RTqPCR_Fw	CCGAGGACCCGAAGGTTAC	A3G mRNA
A3G_RTqPCR_Rv	TCCAACAGTGCTGAAATTCG	
A3H_RTqPCR_Fw	AGCTGTGGCCAGAAGCAC	A3H mRNA
A3H_RTqPCR_Rv	CGGAATGTTTCGGCTGTT	
TBP_RTqPCR_Fw	ACCTAAAGACCATTGCACTTCG	TBP mRNA
TBP_RTqPCR_Rv	CATATTTTCTTGCTGCCAGTCTG	
GAPDH_RTqPCR_Fw	ATTCCCATCACCATCTTCCAG	GAPDH mRNA
GAPDH_RTqPCR_Rv	CAGAGATGATGACCCTTTTGG	

### **6.17. A3B isoform identification**

500ng of UT7/EpoS1 RNA extract, Turbo DNase pre-treated, were retrotranscribed using the *iScript cDNA synthesis kit* (Bio-Rad) following the manufacturer's instructions, then 0,5  $\mu$ L of cDNA were used to setup two different PCR reactions (*GoTaq G2*, Promega), to identify the A3B isoform expressed in the cells. The following Table 11, Table 12 and Table 13 recap information regarding the reactions.

## ***Material and Methods***

Table 11: GoTaq 2 reaction mixture

5x Green buffer	10 $\mu$ L
dNTPs mix 20mM	0.5 $\mu$ L
GoTaq DNA Pol	0.25 $\mu$ L
Primer Mix 10 $\mu$ L	2.5 $\mu$ L
DNA	0.5 $\mu$ L
H2O	36.75 $\mu$ L
<b>Total volume</b>	<b>50<math>\mu</math>L</b>

Table 12: GoTaq G2 amplification profile

<b>Step</b>	<b>Temperature</b>	<b>Time</b>	<b>Cycles</b>
Initial denaturation	95°C	2'	1
Denaturation	95°C	30''	40
Annealing	63/66 °C	30''	
Extension	72 °C	10''	
Cooling	10°C	$\infty$	1

Table 13: Primer sequences to identify A3B isoform. See results section further details.

<b>Primer Name</b>	<b>Primer sequence (5'→3')</b>
A3B_exon_4_Fw	ATGCCTTGGTACAAATTCGATG
A3B_exon_6_Rv	CCAAGTGACCCTGTAGATCTGG
A3B_exon_7_Fw	CTTTGTGTACCGCCAGGGAT
A3B_exon_8_Rv	TTTGCTGGTGTCTGTGAGCA

### **6.18. IIF analysis**

For detection of viral proteins by immunofluorescence, aliquots of  $5 \times 10^4$  cells were spotted on glass slides and fixed with 1:1 acetone:methanol for 10 min at -20°C. For detection of NS1 protein, cells were incubated with the human monoclonal antibody MAb1424 (kindly supplied by Dr. Susanne Modrow [174]) (1:100 in PBS/FCS 10%), then with an anti-human FITC-conjugated secondary antibody (Dako, 1:20 in PBS/FCS 10%). For detection of VP proteins, cells were incubated with a monoclonal mouse antibody against VP1 and VP2 proteins (MAb8293, Chemicon, Merck Millipore) (1:200 in PBS/BSA 1%), then with AlexaFluor488 anti-mouse secondary antibodies (Life Technologies) (1:1000 in PBS/BSA 1%).

For the co-detection of A3B and VP proteins, cells were incubated with the mix of primary monoclonal antibodies mouse anti-VPs (MAb8293) and rabbit anti-human APOBEC3B (5210-87-13, catalog number 12397, from Reuben Harris and obtained through the NIH AIDS Reagent Program, Division of AIDS, NIAID, NIH [175]), diluted in permeabilization buffer (eBioscience,

Invitrogen) + 2% goat serum 1:200 and 1:250 respectively. Then, cells were incubated with secondary antibodies anti-mouse AlexaFluor647 and anti-rabbit AlexaFluor488 in permeabilization buffer + 2% goat serum 1:1000 and DAPI 1:10000.

### **6.19. Flow cytometry analysis**

Cell populations were analyzed for expression of viral proteins by using flow cytometry (FACSCalibur, Becton Dickinson). Aliquots of  $10^6$  cells were fixed in PBS/formaldehyde 0.5% O/N at 4°C, permeabilized in PBS/saponin 0.2% at RT while rocking for 45 min and incubated in suspension with antibodies diluted in PBS/FCS 2% (1:100 NS primary; 1:40 anti-human FITC secondary). Data were analyzed using the Cell Quest Pro Software (Becton Dickinson).

### **6.20. Southern Blot analysis**

Viral extracts from nucleofected UT7/EpoS1 cells were analyzed by Southern Blot assay. Samples were digested by DpnI RE to distinguish de novo synthesized viral DNA based on different *Dam* methylation pattern. Following cleavage, the DNA fragments were separated by an electrophoresis agarose gel run. To denature and prepare the DNA before transfer, the gel was washed twice by Gel Denaturation solution (0.6 M NaCl, 0.4 M NaOH) for 20 minutes at RT and once in Gel Transfer solution (0.6 M NaCl, 8 mM NaOH) for 20 minutes at RT. For transblotting, the DNA molecules were transferred by capillarity from the gel to a positively charged nylon membrane for 90 minutes at RT using the *Turboblotter* system (Schleiner & Schuell), then fixed by UV for 3 minutes. The membrane was subsequently washed for 10 minutes in STE 1X (0.15 M NaCl, 10 mM TrisCl – pH 7.5, 1 mM EDTA) on a shaker and hybridized with 50 ng of DIG labeled-B19V probe which was diluted in 5 mL of hybridization solution (*DIG Easy Hyb Granules*; Roche) over night at 45°C in hybridizer. Before the addition, the DIG labeled-B19V probe was denatured at 95°C for 5 minutes.

The following day, the membrane was washed twice with Wash Buffer 1 (STE 1X, 0,1% SDS) for 10 minutes rocking at RT, twice with Wash Buffer 2 (STE 0,1X, 0,1% SDS) for 30 minutes at 65°C in hybridizer and then incubated with anti-DIG AP-conjugated antibody, diluted 1:10.000 in Buffer 2 for 30 minutes rocking at RT. The surplus of antibody was removed two 30 minutes long washes with Buffer 1 (0.1 M TrisCl - pH 7.5, 0.15 M NaCl) rocking on a shaker. A 30 minutes

## ***Material and Methods***

wash with Buffer 3 (0.1 M TrisCl - pH 9.5, 0.1 M NaCl, 0.05 M MgCl<sub>2</sub>) at RT was performed before adding NBT/BCIP substrate of the alkaline phosphatase, in order to reach the pH 9 requested by the enzyme. Then, the membrane was incubated with NBT/BCIP diluted 1:50 in Buffer 3. DNA fragments were detected as purple bands on the membrane due to the reaction of the alkaline phosphatase with its substrate. Finally, the enzyme reaction was stopped by water. DNA molecules length was evaluated by using *DIG labeled-Marker III* (Roche).

### **6.21. Western Blot analysis**

2x10<sup>6</sup> cells were resuspended in 150 µL of RIPA buffer (0,05 M Tris-Cl pH 8, 0,15 M NaCl, 1% NP-40, 0,5% deoxycholate, 0,1% SDS, 0,01 mM PMSF, cOmplete protease inhibitor (Roche) 1X, Triton 1X) and lysed by sonication for 15 cycles of 30 sec on/30 sec off using Bioruptor Pico device (Diagenode) at 4°C. After sonication, cell debris were pelleted at 14000 rpm at 4°C, then the protein concentration in the supernatant was quantified using *Pierce BCA protein assay kit* (ThermoFisher Scientific).

To perform the SDS-PAGE, 30 µg of protein solution per sample, previously denatured at 95°C for 5 minutes in SDS-containing loading buffer, were loaded on a 10 or 12% tris-glycine polyacrylamide gel and run at 120V for 2,5 hours. Proteins were then transferred to a PVDF membrane using a tank transferring system in Transfer Buffer (50 mM Tris, 200 mM glycine, 20% methanol), for 2h at 200V and 200mA.

Membranes were then blocked in the proper blocking solution for 1h and then incubated with primary antibodies diluted in blocking solution O/N at 4°C rocking. The following day, after three washes for 10 minutes in TBS-Tween 0,1%, membranes were incubated with secondary HRP-conjugated antibodies diluted in blocking solution rocking for 1 hour at RT. After three 15 minutes long washes in TBS-Tween 0,1%, membranes were incubated with the revelation solution (*SuperSignal West Femto Maximum Sensitivity Substrate*, ThermoFisher Scientific) and analyzed with an *ImageQuant LAS 4000* imager (GE Healthcare Bio-Sciences AB).

Table 14: Western Blot targets and relative antibodies and blocking solutions.

<b>Target</b>	<b>Primary antibody (dilution)</b>	<b>HRP-secondary antibody (dilution)</b>	<b>Blocking solution (in TBS-Tween 0,1%)</b>
A3A/B/G	Rabbit anti human A3B monoclonal 12397 (1:1000)	Anti-Rabbit, Dako (1:2000)	BSA 5%
A3C	Rabbit anti human A3C, Proteintech (1:1000)	Anti-Rabbit, Dako (1:2000)	Milk 4%
A3F	Rabbit anti human A3F monoclonal 12399 (1:20)	Anti-Rabbit, Dako (1:2000)	BSA 5%
A3H	Mouse anti human A3H P3A3-A10 (1:1000)	Anti-Mouse, Dako (1:2000)	BSA 5%
HSP90	Rabbit anti HSP90AB1 (Sigma-Aldrich)	Anti-Rabbit, Dako (1:2000)	BSA 5%

## **6.22. Deamination Test**

Cells were collected and washed in PBS, then resuspended in HED buffer (20mM HEPES [pH 7.4], 5mM EDTA, 1mM dithiothreitol [DTT], 10% glycerol) supplemented with cOmplete protease inhibitor cocktail (Roche). Cells were then submitted to one freeze/thaw cycle and sonicated for 15 cycles of 30 sec on/30 sec off using Bioruptor Pico device (Diagenode) at 4°C. Cell lysates were spun down at 14,000 rpm for 15 min to remove cell debris. Proteins were quantified using Pierce BCA protein assay kit (ThermoFisher Scientific). 50 µg of proteins was incubated overnight at 37°C with 1 pmol of a fluorescent oligonucleotide substrate (59-ATTATTATTATTCAAATGGATTTATTTATTTATTTATTTATTTATTT-Cy5-39), 1mM ZnCl<sub>2</sub>, 0,025 units uracil DNA glycosylase (NEB), 2 µl 10X uracil DNA glycosylase (UDG) buffer (NEB), and 100 µg/ml RNase A (ThermoFisher Scientific). Reaction mixture was treated with 50mM NaOH and heated to 95°C for 10 min to cleave DNA probes at the abasic site. Reaction mixture was then neutralized with 50mM HCl and mixed with 1.25X formamide buffer. Substrates (43 bases long) from products (30 bases long) were separated on a 15% Tris-borate-EDTA (TBE)-urea gel. The Cy5-labeled substrates and deamination products were detected using *ImageQuant LAS4000* imager (GE Healthcare Bio-Sciences AB).

## 7. References

1. Cossart, Y.E.; Cant, B.; Field, A.M.; Widdows, D. PARVOVIRUS-LIKE PARTICLES IN HUMAN SERA. *Lancet* **1975**, *305*, 72–73, doi:10.1016/S0140-6736(75)91074-0.
2. Cotmore, S.F.; Agbandje-McKenna, M.; Chiorini, J.A.; Mukha, D. V.; Pintel, D.J.; Qiu, J.; Soderlund-Venermo, M.; Tattersall, P.; Tijssen, P.; Gatherer, D.; et al. The family Parvoviridae. *Arch. Virol.* **2014**, *159*, 1239–1247, doi:10.1007/s00705-013-1914-1.
3. Péntzes, J.J.; Söderlund-Venermo, M.; Canuti, M.; Eis-Hübinger, A.M.; Hughes, J.; Cotmore, S.F.; Harrach, B. Reorganizing the family Parvoviridae: a revised taxonomy independent of the canonical approach based on host association. *Arch. Virol.* **2020**, *165*, 2133–2146, doi:10.1007/s00705-020-04632-4.
4. Servant, A.; Laperche, S.; Lallemand, F.; Marinho, V.; De Saint Maur, G.; Meritet, J.F.; Garbarg-Chenon, A. Genetic diversity within human erythroviruses: identification of three genotypes. *J. Virol.* **2002**, *76*, 9124–34, doi:10.1128/jvi.76.18.9124-9134.2002.
5. Hübschen, J.M.; Mihneva, Z.; Mentis, A.F.; Schneider, F.; Aboudy, Y.; Grossman, Z.; Rudich, H.; Kasymbekova, K.; Sarv, I.; Nedeljkovic, J.; et al. Phylogenetic analysis of human parvovirus B19 sequences from eleven different countries confirms the predominance of genotype 1 and suggests the spread of genotype 3b. *J. Clin. Microbiol.* **2009**, *47*, 3735–3738, doi:10.1128/JCM.01201-09.
6. Liefeldt, L.; Plentz, A.; Klempa, B.; Kershaw, O.; Endres, A.S.; Raab, U.; Neumayer, H.H.; Meisel, H.; Modrow, S. Recurrent high level parvovirus B19/genotype 2 viremia in a renal transplant recipient analyzed by real-time PCR for simultaneous detection of genotypes 1 to 3. *J. Med. Virol.* **2005**, *75*, 161–169, doi:10.1002/jmv.20251.
7. Candotti, D.; Etiz, N.; Parsyan, A.; Allain, J.-P. Identification and Characterization of Persistent Human Erythrovirus Infection in Blood Donor Samples. *J. Virol.* **2004**, *78*, 12169–12178, doi:10.1128/JVI.78.22.12169-12178.2004.
8. Ekman, A.; Hokynar, K.; Kakkola, L.; Kantola, K.; Hedman, L.; Bonden, H.; Gessner, M.; Aberham, C.; Norja, P.; Miettinen, S.; et al. Biological and Immunological Relations among Human Parvovirus B19 Genotypes 1 to 3. *J. Virol.* **2007**, *81*, 6927–6935, doi:10.1128/JVI.02713-06.
9. Parsyan, A.; Szmargd, C.; Allain, J.-P.; Candotti, D. Identification and genetic diversity of

- two human parvovirus B19 genotype 3 subtypes. *J. Gen. Virol.* **2007**, *88*, 428–431, doi:10.1099/vir.0.82496-0.
10. Norja, P.; Eis-Hübinger, A.M.; Söderlund-Venermo, M.; Hedman, K.; Simmonds, P. Rapid Sequence Change and Geographical Spread of Human Parvovirus B19: Comparison of B19 Virus Evolution in Acute and Persistent Infections. *J. Virol.* **2008**, *82*, 6427–6433, doi:10.1128/JVI.00471-08.
  11. Shackelton, L.A.; Holmes, E.C. Phylogenetic Evidence for the Rapid Evolution of Human B19 Erythrovirus. *J. Virol.* **2006**, *80*, 3666–3669, doi:10.1128/JVI.80.7.3666-3669.2006.
  12. Cotmore, S.F.; McKie, V.C.; Anderson, L.J.; Astell, C.R.; Tattersall, P. Identification of the major structural and nonstructural proteins encoded by human parvovirus B19 and mapping of their genes by procaryotic expression of isolated genomic fragments. *J. Virol.* **1986**, *60*, 548–557.
  13. Mietzsch, M.; Pénczes, J.J.; Agbandje-Mckenna, M. Twenty-five years of structural parvovirology. *Viruses* **2019**, *11*, doi:10.3390/v11040362.
  14. Gallinella, G. Parvovirus B19 Achievements and Challenges. *ISRN Virol.* **2013**, *2013*.
  15. Guan, W.; Wong, S.; Zhi, N.; Qiu, J. The Genome of Human Parvovirus B19 Can Replicate in Nonpermissive Cells with the Help of Adenovirus Genes and Produces Infectious Virus. *J. Virol.* **2009**, *83*, 9541–9553, doi:10.1128/JVI.00702-09.
  16. Cotmore, S.F.; Tattersall, P. Parvoviruses: Small Does Not Mean Simple. *Annu. Rev. Virol.* **2014**, *1*, 517–537, doi:10.1146/annurev-virology-031413-085444.
  17. Tewary, S.K.; Zhao, H.; Deng, X.; Qiu, J.; Tang, L. The human parvovirus B19 non-structural protein 1 N-terminal domain specifically binds to the origin of replication in the viral DNA. *Virology* **2014**, *449*, 297–303, doi:10.1016/j.virol.2013.11.031.
  18. Sanchez, J.L.; Romero, Z.; Quinones, A.; Torgeson, K.R.; Horton, N.C. DNA Binding and Cleavage by the Human Parvovirus B19 NS1 Nuclease Domain. *Biochemistry* **2016**, *55*, 6577–6593, doi:10.1021/acs.biochem.6b00534.
  19. Blundell, M.C.; Beard, C.; Astell, C.R. In Vitro Identification of a B19 Parvovirus Promoter. **1987**, *538*, 534–538.
  20. Ozawa, K.; Ayub, J.; Hao, Y.S.; Kurtzman, G.; Shimada, T.; Young, N. Novel transcription map for the B19 (human) pathogenic parvovirus. *J. Virol.* **1987**, *61*, 2395–2406.
  21. Raab, U.; Bauer, B.; Gigler, A.; Beckenlehner, K.; Wolf, H.; Modrow, S. Cellular

- transcription factors that interact with p6 promoter elements of parvovirus B19. *J. Gen. Virol.* **2001**, *82*, 1473–1480, doi:10.1099/0022-1317-82-6-1473.
22. Blundell, M.C.; Astell, C.R. A GC-box motif upstream of the B19 parvovirus unique promoter is important for in vitro transcription. *J. Virol.* **1989**, *63*, 4814–23.
  23. Ganaie, S.S.; Qiu, J. Recent Advances in Replication and Infection of Human Parvovirus B19. *Front. Cell. Infect. Microbiol. | www.frontiersin.org* **2018**, *1*, 166, doi:10.3389/fcimb.2018.00166.
  24. Gareus, R.; Gigler, A.; Hemauer, A.; Leruez-Ville, M.; Morinet, F.; Wolf, H.; Modrow, S. Characterization of cis -Acting and NS1 Protein-Responsive Elements in the p6 Promoter of Parvovirus B19. *J. Virol.* **1998**, *72*, 609–616, doi:10.1128/JVI.72.1.609-616.1998.
  25. Doerig, C.; Hirt, B.; Antonietti, J.P.; Beard, P. Nonstructural protein of parvoviruses B19 and minute virus of mice controls transcription. *J. Virol.* **1990**, *64*, 387–96.
  26. Yoto, Y.; Qiu, J.; Pintel, D.J. Identification and Characterization of Two Internal Cleavage and Polyadenylation Sites of Parvovirus B19 RNA. *J. Virol.* **2006**, *80*, 1604–1609, doi:10.1128/jvi.80.3.1604-1609.2006.
  27. Bonvicini, F.; Filippone, C.; Manaresi, E.; Zerbini, M.; Musiani, M.; Gallinella, G. Functional analysis and quantitative determination of the expression profile of human parvovirus B19. *Virology* **2008**, *381*, 168–177, doi:10.1016/j.virol.2008.09.002.
  28. Guan, W.; Cheng, F.; Huang, Q.; Kleiboeker, S.; Qiu, J. Inclusion of the Central Exon of Parvovirus B19 Precursor mRNA Is Determined by Multiple Splicing Enhancers in both the Exon and the Downstream Intron. *J. Virol.* **2011**, *85*, 2463–2468, doi:10.1128/jvi.01708-10.
  29. Guan, W.; Cheng, F.; Yoto, Y.; Kleiboeker, S.; Wong, S.; Zhi, N.; Pintel, D.J.; Qiu, J. Block to the production of full-length B19 virus transcripts by internal polyadenylation is overcome by replication of the viral genome. *J. Virol.* **2008**, *82*, 9951–63, doi:10.1128/JVI.01162-08.
  30. Qiu, J.; Söderlund-Venermo, M.; Young, N.S. Human Parvoviruses. *Clin. Microbiol. Rev.* **2017**, *30*, 43–113, doi:10.1128/CMR.00040-16.
  31. Liu, J.M.; Green, S.W.; Shimada, T.; Young, N.S. A block in full-length transcript maturation in cells nonpermissive for B19 parvovirus. *J. Virol.* **1992**, *66*, 4686–4692.
  32. Bua, G.; Manaresi, E.; Bonvicini, F.; Gallinella, G. Parvovirus B19 Replication and

- Expression in Differentiating Erythroid Progenitor Cells. *PLoS One* **2016**, *11*, e0148547, doi:10.1371/journal.pone.0148547.
33. Ozawa, K.; Young, N. Characterization of capsid and noncapsid proteins of B19 parvovirus propagated in human erythroid bone marrow cell cultures. *J. Virol.* **1987**, *61*, 2627–2630, doi:10.1128/jvi.61.8.2627-2630.1987.
  34. Momoeda, M.; Wong, S.; Kawase, M.; Young, N.S.; Kajigaya, S. A putative nucleoside triphosphate-binding domain in the nonstructural protein of B19 parvovirus is required for cytotoxicity. *J. Virol.* **1994**, *68*, 8443–8446, doi:10.1128/jvi.68.12.8443-8446.1994.
  35. Lou, S.; Luo, Y.; Cheng, F.; Huang, Q.; Shen, W.; Kleiboeker, S.; Tisdale, J.F.; Liu, Z.; Qiu, J. Human parvovirus B19 DNA replication induces a DNA damage response that is dispensable for cell cycle arrest at phase G2/M. *J. Virol.* **2012**, *86*, 10748–58, doi:10.1128/JVI.01007-12.
  36. Raab, U.; Beckenlehner, K.; Lowin, T.; Niller, H.H.; Doyle, S.; Modrow, S. NS1 protein of parvovirus B19 interacts directly with DNA sequences of the p6 promoter and with the cellular transcription factors Sp1/Sp3. *Virology* **2002**, *293*, 86–93, doi:10.1006/viro.2001.1285.
  37. Morita, E.; Nakashima, A.; Asao, H.; Sato, H.; Sugamura, K. Human Parvovirus B19 Nonstructural Protein (NS1) Induces Cell Cycle Arrest at G1 Phase. *J. Virol.* **2003**, *77*, 2915–2921, doi:10.1128/JVI.77.5.2915.
  38. St Amand, J.; Astell, C.R. Identification and characterization of a family of 11-kDa proteins encoded by the human parvovirus B19. *Virology* **1993**, *192*, 121–31.
  39. Chen, A.Y.; Zhang, E.Y.; Guan, W.; Cheng, F.; Kleiboeker, S.; Yankee, T.M.; Qiu, J. The small 11kDa nonstructural protein of human parvovirus B19 plays a key role in inducing apoptosis during B19 virus infection of primary erythroid progenitor cells. ... **2010**.
  40. Xu, P.; Chen, A.Y.; Ganaie, S.S.; Cheng, F.; Shen, W.; Wang, X.; Kleiboeker, S.; Li, Y.; Qiu, J. The 11-Kilodalton Nonstructural Protein of Human Parvovirus B19 Facilitates Viral DNA Replication by Interacting with Grb2 through Its Proline-Rich Motifs. *J. Virol.* **2018**, *93*, 1–15, doi:10.1128/jvi.01464-18.
  41. Luo, W.; Astell, C.R. A Novel Protein Encoded by Small RNAs of Parvovirus B19. *Virology* **1993**, *195*, 448–455, doi:10.1006/viro.1993.1395.
  42. Poulain, F.; Lejeune, N.; Willemart, K.; Gillet, N.A. Footprint of the host restriction factors

- APOBEC3 on the genome of human viruses. *PLoS Pathog.* **2020**, *16*, 1–30, doi:10.1371/JOURNAL.PPAT.1008718.
43. Pallier, C.; Greco, a; Le Junter, J.; Saib, a; Vassias, I.; Morinet, F. The 3' untranslated region of the B19 parvovirus capsid protein mRNAs inhibits its own mRNA translation in nonpermissive cells. *J. Virol.* **1997**, *71*, 9482–9489.
  44. Ozawa, K.; Ayub, J.; Young, N. Translational regulation of B19 parvovirus capsid protein production by multiple upstream AUG triplets. *J. Biol. Chem.* **1988**, *263*, 10922–6.
  45. Pillet, S.; Annan, Z.; Fichelson, S.; Morinet, F. Identification of a nonconventional motif necessary for the nuclear import of the human parvovirus B19 major capsid protein (VP2). *Virology* **2003**, *306*, 25–32, doi:10.1016/S0042-6822(02)00047-8.
  46. Kawase, M.; Momoeda, M.; Young, N.S.; Kajigaya, S. Modest truncation of the major capsid protein abrogates B19 parvovirus capsid formation. *J. Virol.* **1995**, *69*, 6567–71.
  47. Kajigaya, S.; Fujii, H.; Field, A.; Anderson, S.; Rosenfeld, S.; Anderson, L.J.; Shimada, T.; Young, N.S. Self-assembled B19 parvovirus capsids, produced in a baculovirus system, are antigenically and immunogenically similar to native virions. *Proc. Natl. Acad. Sci.* **1991**, *88*, 4646–4650, doi:10.1073/pnas.88.11.4646.
  48. Leisi, R.; Di Tommaso, C.; Kempf, C.; Ros, C. The receptor-binding domain in the VP1u region of parvovirus B19. *Viruses* **2016**, *8*, 61, doi:10.3390/v8030061.
  49. Dorsch, S.; Kaufmann, B.; Schaible, U.; Prohaska, E.; Wolf, H.; Modrow, S. The VP1-unique region of parvovirus B19: amino acid variability and antigenic stability. *J. Gen. Virol.* **2001**, *82*, 191–199, doi:10.1099/0022-1317-82-1-191.
  50. Bleker, S.; Sonntag, F.; Kleinschmidt, J.A. Mutational Analysis of Narrow Pores at the Fivefold Symmetry Axes of Adeno-Associated Virus Type 2 Capsids Reveals a Dual Role in Genome Packaging and Activation of Phospholipase A2 Activity. *J. Virol.* **2005**, *79*, 2528–2540, doi:10.1128/JVI.79.4.2528-2540.2005.
  51. Brown, K.E.; Anderson, S.M.; Young, N.S. Erythrocyte P antigen: cellular receptor for B19 parvovirus. *Science* **1993**, *262*, 114–117, doi:10.1126/science.8211117.
  52. Brown, K.E.; Hibbs, J.R.; Gallinella, G.; Anderson, S.M.; Lehman, E.D.; McCarthy, P.; Young, N.S. Resistance to parvovirus B19 infection due to lack of virus receptor (erythrocyte P antigen). *N. Engl. J. Med.* **1994**, *330*, 1192–6, doi:10.1056/NEJM199404283301704.

53. Bieri, J.; Ros, C. Globoside Is Dispensable for Parvovirus B19 Entry but Essential at a Postentry Step for Productive Infection. *J. Virol.* **2019**, *93*, 1–15, doi:10.1128/jvi.00972-19.
54. Bieri, J.; Leisi, R.; Bircher, C.; Ros, C. Human parvovirus B19 interacts with globoside under acidic conditions as an essential step in endocytic trafficking. *PLOS Pathog.* **2021**, *17*, e1009434, doi:10.1371/journal.ppat.1009434.
55. Leisi, R.; Nordheim, M. Von; Ros, C.; Kempf, C. The VP1u receptor restricts parvovirus B19 uptake to permissive erythroid cells. *Viruses* **2016**, *8*, doi:10.3390/v8100265.
56. Leisi, R.; Ruprecht, N.; Kempf, C.; Ros, C. Parvovirus B19 Uptake Is a Highly Selective Process Controlled by VP1u, a Novel Determinant of Viral Tropism. *J. Virol.* **2013**, *87*, 13161–13167, doi:10.1128/JVI.02548-13.
57. Ros, C.; Gerber, M.; Kempf, C. Conformational Changes in the VP1-Unique Region of Native Human Parvovirus B19 Lead to Exposure of Internal Sequences That Play a Role in Virus Neutralization and Infectivity. *J. Virol.* **2006**, *80*, 12017–12024, doi:10.1128/JVI.01435-06.
58. Bonsch, C.; Zuercher, C.; Lieby, P.; Kempf, C.; Ros, C. The Globoside Receptor Triggers Structural Changes in the B19 Virus Capsid That Facilitate Virus Internalization. *J. Virol.* **2010**, *84*, 11737–11746, doi:10.1128/JVI.01143-10.
59. Harbison, C.E.; Chiorini, J.A.; Parrish, C.R. The parvovirus capsid odyssey: from the cell surface to the nucleus. *Trends Microbiol.* **2008**, *16*, 208–214, doi:10.1016/j.tim.2008.01.012.
60. Manaresi, E.; Gallinella, G. Advances in the development of antiviral strategies against parvovirus B19. *Viruses* **2019**, *11*, doi:10.3390/v11070659.
61. Caliaro, O.; Marti, A.; Ruprecht, N.; Leisi, R.; Subramanian, S.; Hafenstein, S.; Ros, C. Parvovirus B19 uncoating occurs in the cytoplasm without capsid disassembly and it is facilitated by depletion of capsid-associated divalent cations. *Viruses* **2019**, *11*, doi:10.3390/v11050430.
62. Chen, A.Y.; Kleiboeker, S.; Qiu, J. Productive Parvovirus B19 Infection of Primary Human Erythroid Progenitor Cells at Hypoxia Is Regulated by STAT5A and MEK Signaling but not HIF $\alpha$ . *PLoS Pathog.* **2011**, *7*, e1002088, doi:10.1371/journal.ppat.1002088.
63. Luo, Y.; Kleiboeker, S.; Deng, X.; Qiu, J. Human Parvovirus B19 Infection Causes Cell Cycle Arrest of Human Erythroid Progenitors at Late S Phase That Favors Viral DNA

- Replication. *J. Virol.* **2013**, *87*, 12766–12775, doi:10.1128/JVI.02333-13.
64. Chen, A.Y.; Guan, W.; Lou, S.; Liu, Z.; Kleiboeker, S.; Qiu, J. Role of Erythropoietin Receptor Signaling in Parvovirus B19 Replication in Human Erythroid Progenitor Cells. *J. Virol.* **2010**, *84*, 12385–12396, doi:10.1128/JVI.01229-10.
65. Morita, E.; Tada, K.; Chisaka, H.; Asao, H.; Sato, H.; Yaegashi, N.; Sugamura, K. Human parvovirus B19 induces cell cycle arrest at G(2) phase with accumulation of mitotic cyclins. *J. Virol.* **2001**, *75*, 7555–63, doi:10.1128/JVI.75.16.7555-7563.2001.
66. Filippone, C.; Franssila, R.; Kumar, A.; Saikko, L.; Kovanen, P.E.; Söderlund-Venermo, M.; Hedman, K. Erythroid progenitor cells expanded from peripheral blood without mobilization or preselection: Molecular characteristics and functional competence. *PLoS One* **2010**, *5*, doi:10.1371/journal.pone.0009496.
67. Takahashi, T.; Ozawa, K.; Takahashi, K.; Asano, S.; Takaku, F. Susceptibility of human erythropoietic cells to B19 parvovirus in vitro increases with differentiation. *Blood* **1990**, *75*, 603–610.
68. Ganaie, S.S.; Zou, W.; Xu, P.; Deng, X.; Kleiboeker, S.; Qiu, J. Phosphorylated STAT5 directly facilitates parvovirus B19 DNA replication in human erythroid progenitors through interaction with the MCM complex. *PLOS Pathog.* **2017**, *13*, e1006370, doi:10.1371/journal.ppat.1006370.
69. Wong, S.; Zhi, N.; Filippone, C.; Keyvanfar, K.; Kajigaya, S.; Brown, K.E.; Young, N.S. Ex Vivo-Generated CD36+ Erythroid Progenitors Are Highly Permissive to Human Parvovirus B19 Replication. *J. Virol.* **2008**, *82*, 2470–2476, doi:10.1128/JVI.02247-07.
70. Luo, Y.; Lou, S.; Deng, X.; Liu, Z.; Li, Y.; Kleiboeker, S.; Qiu, J. Parvovirus B19 Infection of Human Primary Erythroid Progenitor Cells Triggers ATR-Chk1 Signaling, Which Promotes B19 Virus Replication. *J. Virol.* **2011**, *85*, 8046–8055, doi:10.1128/JVI.00831-11.
71. Wan, Z.; Zhi, N.; Wong, S.; Keyvanfar, K.; Liu, D.; Raghavachari, N.; Munson, P.J.; Su, S.; Malide, D.; Kajigaya, S.; et al. Human parvovirus B19 causes cell cycle arrest of human erythroid progenitors via deregulation of the E2F family of transcription factors. *J. Clin. Invest.* **2010**, *120*, 3530–44, doi:10.1172/JCI41805.
72. Young, N.S.; Mortimer, P.P.; Moore, J.G.; Humphries, R.K. Characterization of a virus that causes transient aplastic crisis. *J. Clin. Invest.* **1984**, *73*, 224–230, doi:10.1172/JCI111195.

73. Yaegashi, N.; Niinuma, T.; Chisaka, H.; Uehara, S.; Moffatt, S.; Tada, K.; Iwabuchi, M.; Matsunaga, Y.; Nakayama, M.; Yutani, C.; et al. Parvovirus B19 infection induces apoptosis of erythroid cells in vitro and in vivo. *J. Infect.* **1999**, *39*, 68–76.
74. Moffatt, S.; Yaegashi, N.; Tada, K.; Tanaka, N.; Sugamura, K. Human Parvovirus B19 Nonstructural (NS1) Protein Induces Apoptosis in Erythroid Lineage Cells. *J. Virol.* **1998**, *72*, 3018–3028, doi:10.1128/JVI.72.4.3018-3028.1998.
75. Sol, N.; Le Junter, J.; Vassias, I.; Freyssinier, J.M.; Thomas, A.; Prigent, A.F.; Rudkin, B.B.; Fichelson, S.; Morinet, F. Possible interactions between the NS-1 protein and tumor necrosis factor alpha pathways in erythroid cell apoptosis induced by human parvovirus B19. *J Virol* **1999**, *73*, 8762–8770.
76. Bua, G.; Gallinella, G. How does parvovirus B19 DNA achieve lifelong persistence in human cells? *Future Virol.* **2017**, *12*, 549–553, doi:10.2217/fvl-2017-0079.
77. Pyöriä, L.; Toppinen, M.; Mäntylä, E.; Hedman, L.; Aaltonen, L.M.; Vihinen-Ranta, M.; Ilmarinen, T.; Söderlund-Venermo, M.; Hedman, K.; Perdomo, M.F. Extinct type of human parvovirus B19 persists in tonsillar B cells. *Nat. Commun.* **2017**, *8*, doi:10.1038/ncomms14930.
78. Schmidt-Lucke, C.; Spillmann, F.; Bock, T.; Kühl, U.; Van Linthout, S.; Schultheiss, H.; Tschöpe, C. Interferon Beta Modulates Endothelial Damage in Patients with Cardiac Persistence of Human Parvovirus B19 Infection. *J. Infect. Dis.* **2010**, *201*, 936–945, doi:10.1086/650700.
79. Schmidt-Lucke, C.; Zobel, T.; Schrepfer, S.; Kuhl, U.; Wang, D.; Klingel, K.; Becher, P.M.; Fechner, H.; Pozzuto, T.; Van Linthout, S.; et al. Impaired Endothelial Regeneration Through Human Parvovirus B19–Infected Circulating Angiogenic Cells in Patients With Cardiomyopathy. *J. Infect. Dis.* **2015**, *212*, 1070–1081, doi:10.1093/infdis/jiv178.
80. Duechting, A.; Tschöpe, C.; Kaiser, H.; Lamkemeyer, T.; Tanaka, N.; Aberle, S.; Lang, F.; Torresi, J.; Kandolf, R.; Bock, C.-T. Human parvovirus B19 NS1 protein modulates inflammatory signaling by activation of STAT3/PIAS3 in human endothelial cells. *J. Virol.* **2008**, *82*, 7942–52, doi:10.1128/JVI.00891-08.
81. Kerr, J.R. Pathogenesis of human parvovirus B19 in rheumatic disease. *Ann. Rheum. Dis.* **2000**, *59*, 672–683, doi:10.1136/ard.59.9.672.
82. Adamson-Small, L.A.; Ignatovich, I. V.; Laemmerhirt, M.G.; Hobbs, J.A. Persistent

- parvovirus B19 infection in non-erythroid tissues: Possible role in the inflammatory and disease process. *Virus Res.* **2014**, *190*, 8–16, doi:10.1016/j.virusres.2014.06.017.
83. Xu, H.; Hao, S.; Zhang, J.; Chen, Z.; Wang, H.; Guan, W. The formation and modification of chromatin-like structure of human parvovirus B19 regulate viral genome replication and RNA processing. *Virus Res.* **2017**, *232*, 134–138, doi:10.1016/j.virusres.2017.03.001.
84. Janovitz, T.; Wong, S.; Young, N.S.; Oliveira, T.; Falck-Pedersen, E. Parvovirus B19 integration into human CD36+ erythroid progenitor cells. *Virology* **2017**, *511*, 40–48, doi:10.1016/j.virol.2017.08.011.
85. Bonvicini, F.; Manaresi, E.; Di Furio, F.; de Falco, L.; Gallinella, G. Parvovirus B19 DNA CpG dinucleotide methylation and epigenetic regulation of viral expression. *PLoS One* **2012**, *7*, doi:10.1371/journal.pone.0033316.
86. Zakrzewska, K.; Cortivo, R.; Tonello, C.; Panfilo, S.; Abatangelo, G.; Giuggioli, D.; Ferri, C.; Corcioli, F.; Azzi, A. Human parvovirus B19 experimental infection in human fibroblasts and endothelial cells cultures. *Virus Res.* **2005**, *114*, 1–5, doi:10.1016/j.virusres.2005.05.003.
87. Arvia, R.; Margheri, F.; Stincarelli, M.A.; Laurenzana, A.; Fibbi, G.; Gallinella, G.; Ferri, C.; Del Rosso, M.; Zakrzewska, K. Parvovirus B19 activates in vitro normal human dermal fibroblasts: a possible implication in skin fibrosis and systemic sclerosis. *Rheumatology* **2020**, *59*, 3526–3532, doi:10.1093/rheumatology/keaa230.
88. Kerr, J.R. The role of parvovirus B19 in the pathogenesis of autoimmunity and autoimmune disease. *J. Clin. Pathol.* **2016**, *69*, 279–291, doi:10.1136/jclinpath-2015-203455.
89. Anderson, M.J.; Higgins, P.G.; Davis, L.R.; Willman, J.S.; Jones, S.E.; Kidd, I.M.; Pattison, J.R.; Tyrrell, D.A.J. Experimental Parvoviral Infection in Humans. *J. Infect. Dis.* **1985**, *152*, 257–265, doi:10.1093/infdis/152.2.257.
90. Anderson, L.J.; Tsou, C.; Parker, R.A.; Chorba, T.L.; Wulff, H.; Tattersall, P.; Mortimer, P.P. Detection of antibodies and antigens of human parvovirus B19 by enzyme-linked immunosorbent assay. *J. Clin. Microbiol.* **1986**, *24*, 522–526, doi:10.1128/jcm.24.4.522-526.1986.
91. Erdman, D.D.; Usher, M.J.; Tsou, C.; Caul, E.O.; Gary, G.W.; Kajigaya, S.; Young, N.S.; Anderson, L.J. Human parvovirus B19 specific IgG, IgA, and IgM antibodies and DNA in serum specimens from persons with erythema infectiosum. *J. Med. Virol.* **1991**, *35*, 110–

- 115, doi:10.1002/jmv.1890350207.
92. Söderlund, M.; Brown, C.S.; Spaan, W.J.M.; Hedman, L.; Hedman, K. Epitope type-specific igg responses to capsid proteins vp1 and vp2 of human parvovirus b19. *J. Infect. Dis.* **1995**, *172*, 1431–1436, doi:10.1093/infdis/172.6.1431.
  93. Corcoran, A.; Mahon, B.P.; Doyle, S. B cell memory is directed toward conformational epitopes of parvovirus B19 capsid proteins and the unique region of VP1. *J. Infect. Dis.* **2004**, *189*, 1873–1880, doi:10.1086/382963.
  94. von Poblitzki, A.; Hemauer, A.; Gigler, A.; Puchhammer-Stöckl, E.; Heinz, F.X.; Pont, J.; Laczika, K.; Wolf, H.; Modrow, S. Antibodies to the nonstructural protein of parvovirus B19 in persistently infected patients: implications for pathogenesis. *J. Infect. Dis.* **1995**, *172*, 1356–9.
  95. Ennis, O.; Corcoran, A.; Kavanagh, K.; Mahon, B.; Doyle, S. Baculovirus expression of parvovirus B19 (B19V) NS1: utility in confirming recent infection. *J. Clin. Virol.* **2001**, *22*, 55–60, doi:10.1016/S1386-6532(01)00168-8.
  96. von Poblitzki, A.; Gerdes, C.; Reischl, U.; Wolf, H.; Modrow, S. Lymphoproliferative responses after infection with human parvovirus B19. *J. Virol.* **1996**, *70*, 7327–30.
  97. Norbeck, O.; Isa, A.; Pohlmann, C.; Broliden, K.; Kasprovicz, V.; Bowness, P.; Klenerman, P.; Tolfvenstam, T. Sustained CD8+ T-cell responses induced after acute parvovirus B19 infection in humans. *J. Virol.* **2005**, *79*, 12117–12121, doi:10.1128/JVI.79.18.12117.
  98. Tolfvenstam, T.; Oxenius, A.; Price, D.A.; Shacklett, B.L.; Spiegel, H.M.; Hedman, K.; Norbeck, O.; Levi, M.; Olsen, K.; Kantzanou, M.; et al. Direct ex vivo measurement of CD8(+) T-lymphocyte responses to human parvovirus B19. *J. Virol.* **2001**, *75*, 540–543.
  99. Isa, A.; Lundqvist, A.; Lindblom, A.; Tolfvenstam, T.; Broliden, K. Cytokine responses in acute and persistent human parvovirus B19 infection. *Clin. Exp. Immunol.* **2007**, *147*, 419–425, doi:10.1111/j.1365-2249.2006.03286.x.
  100. Kleinman, S.H.; Glynn, S.A.; Lee, T.-H.; Tobler, L.H.; Schlumpf, K.S.; Todd, D.S.; Qiao, H.; Yu, M.W.; Busch, M.P. A linked donor-recipient study to evaluate parvovirus B19 transmission by blood component transfusion. *Blood* **2009**, *114*, 3677–3683, doi:10.1182/blood-2009-06-225706.
  101. Juhl, D.; Özdemir, M.; Dreier, J.; Görg, S.; Hennig, H. Look-back study on recipients of Parvovirus B19 (B19V) DNA-positive blood components. *Vox Sang.* **2015**, *109*, 305–311,

doi:10.1111/vox.12295.

102. Norja, P.; Hokynar, K.; Aaltonen, L.-M.; Chen, R.; Ranki, A.; Partio, E.K.; Kiviluoto, O.; Davidkin, I.; Leivo, T.; Eis-Hubinger, A.M.; et al. Bioportfolio: Lifelong persistence of variant and prototypic erythrovirus DNA genomes in human tissue. *Proc. Natl. Acad. Sci.* **2006**, *103*, 7450–7453, doi:10.1073/pnas.0602259103.
103. Manning, A.; Willey, S.J.; Bell, J.E.; Simmonds, P. Comparison of Tissue Distribution, Persistence, and Molecular Epidemiology of Parvovirus B19 and Novel Human Parvoviruses PARV4 and Human Bocavirus. *J. Infect. Dis.* **2007**, *195*, 1345–1352, doi:10.1086/513280.
104. Brown, K.E. Haematological consequences of parvovirus B19 infection. *Bailliere's Best Pract. Res. Clin. Haematol.* **2000**, *13*, 245–259, doi:10.1053/beha.1999.0071.
105. Musiani, M.; Zerbini, M.; Gentilomi, G.; Plazzi, M.; Gallinella, G.; Venturoli, S. Parvovirus b19 clearance from peripheral blood after acute infection. *J. Infect. Dis.* **1995**, *172*, 1360–1363, doi:10.1093/infdis/172.5.1360.
106. Young, N.S.; Abkowitz, J.L.; Luzzatto, L. New Insights into the Pathophysiology of Acquired Cytopenias. *Hematology* **2000**, *2000*, 18–38, doi:10.1182/asheducation-2000.1.18.
107. Koduri, P.R. Parvovirus B19-Related Anemia in HIV-Infected Patients. *AIDS Patient Care STDS* **2000**, *14*, 7–11, doi:10.1089/108729100318082.
108. Broliden, K.; Tolfvenstam, T.; Ohlsson, S.; Henter, J.I. Persistent B19 parvovirus infection in pediatric malignancies. *Med. Pediatr. Oncol.* **1998**, *31*, 66–72, doi:10.1002/(SICI)1096-911X(199808)31:2<66::AID-MPO4>3.0.CO;2-X.
109. Lindblom, A.; Heyman, M.; Gustafsson, I.; Norbeck, O.; Kaldensjö, T.; Vernby, A.; Henter, J.-I.; Tolfvenstam, T.; Broliden, K. Parvovirus B19 infection in children with acute lymphoblastic leukemia is associated with cytopenia resulting in prolonged interruptions of chemotherapy. *Clin. Infect. Dis.* **2008**, *46*, 528–536, doi:10.1086/526522.
110. Gallinella, G.; Manaresi, E.; Venturoli, S.; Grazi, G.L.; Musiani, M.; Zerbini, M. Occurrence and clinical role of active parvovirus B19 infection in transplant recipients. *Eur. J. Clin. Microbiol. Infect. Dis.* **1999**, *18*, 811–3.
111. Chorba, T.; Coccia, P.; Holman, R.C.; Tattersall, P.; Anderson, L.J.; Sudman, J.; Young, N.S.; Kurczynski, E.; Saarinen, U.M.; Moir, R. The role of parvovirus B19 in aplastic crisis

- and erythema infectiosum (fifth disease). *J. Infect. Dis.* **1986**, *154*, 383–393.
112. Anderson, M.J.; Jones, S.E.; Fisher-Hoch, S.P.; Lewis, E.; Hall, S.M.; Bartlett, C.L.R.; Cohen, B.J.; Mortimer, P.P.; Pereira, M.S. Human Parvovirus, the cause of erythema infectiosum (fifth disease)? *Lancet* 1983, *321*, 1378.
  113. Pozzuto, T.; von Kietzell, K.; Bock, T.; Schmidt-Lucke, C.; Poller, W.; Zobel, T.; Lassner, D.; Zeichhardt, H.; Weger, S.; Fechner, H. Transactivation of human parvovirus B19 gene expression in endothelial cells by adenoviral helper functions. *Virology* **2011**, *411*, 50–64, doi:10.1016/j.virol.2010.12.019.
  114. Bonvicini, F.; La Placa, M.; Manaresi, E.; Gallinella, G.; Gentilomi, G.A.; Zerbini, M.; Musiani, M. Parvovirus B19 DNA is commonly harboured in human skin. *Dermatology* **2010**, *220*, 138–142, doi:10.1159/000277431.
  115. Drago, F.; Ciccarese, G.; Broccolo, F.; Javor, S.; Parodi, A. Atypical exanthems associated with Parvovirus B19 (B19V) infection in children and adults. *J. Med. Virol.* **2015**, *87*, 1981–1984, doi:10.1002/jmv.24246.
  116. Smitha, S.B.; Libowa, L.F.; Elstona, D.M.; Bernerta, R.A.; Warschaw, K.E. Gloves and socks syndrome: Early and late histopathologic features. *J. Am. Acad. Dermatol.* **2002**, *47*, 749–754, doi:10.1067/mjd.2002.124612.
  117. Zerbini, M.; Musiani, M.; Venturoli, S.; Gallinella, G.; Gibellini, D.; Gentilomi, G.; La Placa, M. Different syndromes associated with B19 parvovirus viraemia in paediatric patients: Report of four cases. *Eur. J. Pediatr.* **1992**, *151*, 815–817, doi:10.1007/BF01957931.
  118. White, D.G.; Mortimer, P.P.; Blake, D.R.; Woolf, A.D.; Cohen, B.J.; Bacon, P.A. Human Parvovirus arthropaty. *Lancet* **1985**, *325*, 419–421, doi:10.1016/S0140-6736(85)91145-6.
  119. Reid, D.M.; Brown, T.; Reid, T.M.S.; Rennie, J.A.N.; Eastmond, C.J. Human Parvovirus-associated arthritis: a clinical and laboratory description. *Lancet* **1985**, *325*, 422–425, doi:10.1016/S0140-6736(85)91146-8.
  120. Moore, T.L. Parvovirus-associated arthritis. *Curr. Opin. Rheumatol.* **2000**, *12*, 289–294, doi:10.1097/00002281-200007000-00010.
  121. Ray, N.B.; Nieva, D.R.; Seftor, E.A.; Khalkhali-Ellis, Z.; Naides, S.J. Induction of an invasive phenotype by human parvovirus B19 in normal human synovial fibroblasts. *Arthritis Rheum* **2001**, *44*, 1582–1586, doi:10.1002/1529-0131(200107)44:7<1582::AID-

ART281>3.0.CO;2-E.

122. Meyer, O. Parvovirus B19 and autoimmune diseases. *Joint. Bone. Spine* **2003**, *70*, 6–11.
123. von Landenberg, P.; Lehmann, H.W.; Modrow, S. Human parvovirus B19 infection and antiphospholipid antibodies. *Autoimmun. Rev.* 2007, *6*, 278–285.
124. Jordan, J.A.; Deloia, J.A. Globoside expression within the human placenta. *Placenta* **1999**, *20*, 103–108, doi:10.1053/plac.1998.0353.
125. Wegner, C.C.; Jordan, J.A. Human parvovirus B19 VP2 empty capsids bind to human villous trophoblast cells in vitro via the globoside receptor. *Infect. Dis. Obstet. Gynecol.* **2004**, *12*, 69–78, doi:10.1080/10647440400009912.
126. Pasquinelli, G.; Bonvicini, F.; Foroni, L.; Salfi, N.; Gallinella, G. Placental endothelial cells can be productively infected by Parvovirus B19. *J. Clin. Virol.* **2009**, *44*, 33–38, doi:10.1016/j.jcv.2008.10.008.
127. Lamont, R.F.; Sobel, J.D.; Vaisbuch, E.; Kusanovic, J.P.; Mazaki-Tovi, S.; Kim, S.K.; Uldbjerg, N.; Romero, R. Parvovirus B19 infection in human pregnancy. *BJOG* **2011**, *118*, 175–86, doi:10.1111/j.1471-0528.2010.02749.x.
128. O'Malley, A.; Barry-Kinsella, C.; Hughes, C.; Kelehan, P.; Devaney, D.; Mooney, E.; Gillan, J. Parvovirus Infects Cardiac Myocytes in Hydrops Fetalis. *Pediatr. Dev. Pathol.* **2003**, *6*, 414–420, doi:10.1007/s10024-001-0269-x.
129. Bonvicini, F.; Bua, G.; Gallinella, G. Parvovirus B19 infection in pregnancy — awareness and opportunities. *Curr. Opin. Virol.* **2017**, *27*, 8–14, doi:10.1016/j.coviro.2017.10.003.
130. Bock, C.-T.; Klingel, K.; Kandolf, R. Human Parvovirus B19–Associated Myocarditis. *N. Engl. J. Med.* **2010**, *362*, 1248–1249, doi:10.1056/NEJMc0911362.
131. Molina, K.M.; Garcia, X.; Denfield, S.W.; Fan, Y.; Morrow, W.R.; Towbin, J.A.; Frazier, E.A.; Nelson, D.P. Parvovirus B19 Myocarditis Causes Significant Morbidity and Mortality in Children. *Pediatr. Cardiol.* **2013**, *34*, 390–397, doi:10.1007/s00246-012-0468-4.
132. Kühl, U.; Pauschinger, M.; Bock, T.; Klingel, K.; Schwimmbeck, C.P.; Seeberg, B.; Krautwurm, L.; Poller, W.; Schultheiss, H.P.; Kandolf, R. Parvovirus B19 infection mimicking acute myocardial infarction. *Circulation* **2003**, *108*, 945–950, doi:10.1161/01.CIR.0000085168.02782.2C.
133. Bültmann, B.D.; Klingel, K.; Sotlar, K.; Bock, C.T.; Baba, H.A.; Sauter, M.; Kandolf, R. Fatal parvovirus B19-associated myocarditis clinically mimicking ischemic heart disease:

- An endothelial cell-mediated disease. *Hum. Pathol.* **2003**, *34*, 92–95, doi:10.1053/hupa.2003.48.
134. Verdonschot, J.; Hazebroek, M.; Merken, J.; Debing, Y.; Dennert, R.; Brunner-La Rocca, H.-P.; Heymans, S. Relevance of cardiac parvovirus B19 in myocarditis and dilated cardiomyopathy: review of the literature. *Eur. J. Heart Fail.* **2016**, *18*, 1430–1441, doi:10.1002/ejhf.665.
135. Rigopoulos, A.G.; Klutt, B.; Matiakis, M.; Apostolou, A.; Mavrogeni, S.; Noutsias, M. Systematic Review of PCR Proof of Parvovirus B19 Genomes in Endomyocardial Biopsies of Patients Presenting with Myocarditis or Dilated Cardiomyopathy. *Viruses* **2019**, *11*, 566, doi:10.3390/v11060566.
136. Barah, F.; Vallely, P.J.; Cleator, G.M.; Kerr, J.R. Neurological manifestations of human parvovirus B19 infection. *Rev. Med. Virol.* **2003**, *13*, 185–199, doi:10.1002/rmv.388.
137. Barah, F.; Whiteside, S.; Batista, S.; Morris, J. Neurological aspects of human parvovirus B19 infection: a systematic review. *Rev. Med. Virol.* **2014**, *24*, 154–168, doi:10.1002/rmv.1782.
138. Douvoyiannis, M.; Litman, N.; Goldman, D.L. Neurologic Manifestations Associated with Parvovirus B19 Infection. *Clin. Infect. Dis.* **2009**, *48*, 1713–1723, doi:10.1086/599042.
139. Tonnellier, M.; Bessereau, J.; Carbonnell, N.; Guidet, B.; Méritet, J.F.; Kerr, J.R.; Monnier-Cholley, L.; Offenstadt, G.; Maury, E. A possible parvovirus B19 encephalitis in an immunocompetent adult patient. *J. Clin. Virol.* **2007**, *38*, 186–187, doi:10.1016/j.jcv.2006.11.004.
140. Gallinella, G. The clinical use of parvovirus B19 assays: recent advances. *Expert Rev. Mol. Diagn.* **2018**, *18*, 821–832, doi:10.1080/14737159.2018.1503537.
141. Bansal, G.P.; Hatfield, J.A.; Dunn, F.E.; Kramer, A.A.; Brady, F.; Riggin, C.H.; Collett, M.S.; Yoshimoto, K.; Kajigaya, S.; Young, N.S. Candidate Recombinant Vaccine for Human B19 Parvovirus. *J. Infect. Dis.* **1993**, *167*, 1034–1044, doi:10.1093/infdis/167.5.1034.
142. Ballou, W.R.; Reed, J.L.; Noble, W.; Young, N.S.; Koenig, S. Safety and Immunogenicity of a Recombinant Parvovirus B19 Vaccine Formulated with MF59C.1. *J. Infect. Dis.* **2003**, *187*, 675–678, doi:10.1086/368382.
143. Bernstein, D.I.; El Sahly, H.M.; Keitel, W.A.; Wolff, M.; Simone, G.; Segawa, C.; Wong,

- S.; Shelly, D.; Young, N.S.; Dempsey, W. Safety and immunogenicity of a candidate parvovirus B19 vaccine. *Vaccine* **2011**, *29*, 7357–7363, doi:10.1016/j.vaccine.2011.07.080.
144. Chandramouli, S.; Medina-Selby, A.; Coit, D.; Schaefer, M.; Spencer, T.; Brito, L.A.; Zhang, P.; Otten, G.; Mandl, C.W.; Mason, P.W.; et al. Generation of a parvovirus B19 vaccine candidate. *Vaccine* **2013**, *31*, 3872–3878, doi:10.1016/j.vaccine.2013.06.062.
145. Yawn, B.P.; Buchanan, G.R.; Afenyi-Annan, A.N.; Ballas, S.K.; Hassell, K.L.; James, A.H.; Jordan, L.; Lanzkron, S.M.; Lottenberg, R.; Savage, W.J.; et al. Management of Sick Cell Disease. *JAMA* **2014**, *312*, 1033, doi:10.1001/jama.2014.10517.
146. Bonvicini, F.; Bua, G.; Conti, I.; Manaresi, E.; Gallinella, G. Hydroxyurea inhibits parvovirus B19 replication in erythroid progenitor cells. *Biochem. Pharmacol.* **2017**, doi:10.1016/j.bcp.2017.03.022.
147. McGann, P.T.; Ware, R.E. Hydroxyurea therapy for sickle cell anemia. *Expert Opin. Drug Saf.* **2015**, *14*, 1749–1758, doi:10.1517/14740338.2015.1088827.
148. Hankins, J.S.; Penkert, R.R.; Lavoie, P.; Tang, L.; Sun, Y.; Hurwitz, J.L.; Hankins, J. Original Research Parvovirus B19 infection in children with sickle cell disease in the hydroxyurea era. *Exp. Biol. Med.* **2016**, *241*, 749–754, doi:10.1177/1535370216636723.
149. Bonvicini, F.; Bua, G.; Manaresi, E.; Gallinella, G. Antiviral effect of cidofovir on parvovirus B19 replication. *Antiviral Res.* **2015**, *113*, 11–18, doi:10.1016/j.antiviral.2014.11.004.
150. Bonvicini, F.; Bua, G.; Manaresi, E.; Gallinella, G. Enhanced inhibition of parvovirus B19 replication by cidofovir in extendedly exposed erythroid progenitor cells. *Virus Res.* **2016**, *220*, 47–51, doi:10.1016/j.virusres.2016.04.002.
151. Bua, G.; Conti, I.; Manaresi, E.; Sethna, P.; Foster, S.; Bonvicini, F.; Gallinella, G. Antiviral activity of brincidofovir on parvovirus B19. *Antiviral Res.* **2019**, *162*, 22–29, doi:10.1016/j.antiviral.2018.12.003.
152. Marty, F.M.; Winston, D.J.; Chemaly, R.F.; Mullane, K.M.; Shore, T.B.; Papanicolaou, G.A.; Chittick, G.; Brundage, T.M.; Wilson, C.; Morrison, M.E.; et al. A Randomized, Double-Blind, Placebo-Controlled Phase 3 Trial of Oral Brincidofovir for Cytomegalovirus Prophylaxis in Allogeneic Hematopoietic Cell Transplantation. *Biol. Blood Marrow Transplant.* **2019**, *25*, 369–381, doi:10.1016/j.bbmt.2018.09.038.
153. Chan-Tack, K.; Harrington, P.; Bensman, T.; Choi, S.-Y.; Donaldson, E.; O’Rear, J.;

- McMillan, D.; Myers, L.; Seaton, M.; Ghantous, H.; et al. Benefit-risk assessment for brincidofovir for the treatment of smallpox: U.S. Food and Drug Administration's Evaluation. *Antiviral Res.* **2021**, *195*, 105182, doi:10.1016/j.antiviral.2021.105182.
154. Harris, L.M.; Merrick, C.J. G-Quadruplexes in Pathogens: A Common Route to Virulence Control? *PLOS Pathog.* **2015**, *11*, e1004562, doi:10.1371/journal.ppat.1004562.
155. Lane, A.N.; Chaires, J.B.; Gray, R.D.; Trent, J.O. Stability and kinetics of G-quadruplex structures. *Nucleic Acids Res.* **2008**, *36*, 5482–5515, doi:10.1093/nar/gkn517.
156. Lavezzo, E.; Berselli, M.; Frasson, I.; Perrone, R.; Palù, G.; Brazzale, A.R.; Richter, S.N.; Toppo, S. G-quadruplex forming sequences in the genome of all known human viruses: A comprehensive guide. *PLoS Comput. Biol.* **2018**, *14*, doi:10.1371/journal.pcbi.1006675.
157. Bua, G.; Tedesco, D.; Conti, I.; Reggiani, A.; Bartolini, M.; Gallinella, G. No G-Quadruplex Structures in the DNA of Parvovirus B19: Experimental Evidence versus Bioinformatic Predictions. *Viruses* **2020**, *12*, doi:10.3390/v12090935.
158. Xu, P.; Ganaie, S.S.; Wang, X.; Wang, Z.; Kleiboeker, S.; Horton, N.C.; Heier, R.F.; Meyers, M.J.; Tavis, J.E.; Qiu, J. Endonuclease Activity Inhibition of the NS1 Protein of Parvovirus B19 as a Novel Target for Antiviral Drug Development. *Antimicrob. Agents Chemother.* **2019**, *63*, doi:10.1128/AAC.01879-18.
159. Ning, K.; Roy, A.; Cheng, F.; Xu, P.; Kleiboeker, S.; Escalante, C.R.; Wang, J.; Qiu, J. High throughput screening identifies inhibitors for parvovirus B19 infection of human erythroid progenitor cells. *J. Virol.* **2021**, doi:10.1128/jvi.01326-21.
160. Hattangadi, S.M.; Wong, P.; Zhang, L.; Flygare, J.; Lodish, H.F. From stem cell to red cell: regulation of erythropoiesis at multiple levels by multiple proteins, RNAs, and chromatin modifications. *Blood* **2011**, *118*, 6258–6268, doi:10.1182/blood-2011-07-356006.
161. Merryweather-Clarke, A.T.; Atzberger, A.; Soneji, S.; Gray, N.; Clark, K.; Waugh, C.; McGowan, S.J.; Taylor, S.; Nandi, A.K.; Wood, W.G.; et al. Global gene expression analysis of human erythroid progenitors. *Blood* **2011**, *117*, e96-108, doi:10.1182/blood-2010-07-290825.
162. Zhi, N.; Zádori, Z.; Brown, K.E.; Tijssen, P. Construction and sequencing of an infectious clone of the human parvovirus B19. *Virology* **2004**, *318*, 142–152, doi:10.1016/j.virol.2003.09.011.
163. Manaresi, E.; Conti, I.; Bua, G.; Bonvicini, F.; Gallinella, G. A Parvovirus B19 synthetic

- genome: sequence features and functional competence. *Virology* **2017**, *508*, 54–62, doi:10.1016/j.virol.2017.05.006.
164. Sparrer, K.M.J.; Gack, M.U. Intracellular detection of viral nucleic acids. *Curr. Opin. Microbiol.* **2015**, *26*, 1–9, doi:10.1016/J.MIB.2015.03.001.
165. Prelli Bozzo, C.; Kmiec, D.; Kirchhoff, F. When good turns bad: how viruses exploit innate immunity factors. *Curr. Opin. Virol.* **2022**, *52*, 60–67, doi:10.1016/J.COVIRO.2021.11.009.
166. Willems, L.; Gillet, N.A. APOBEC3 interference during replication of viral genomes. *Viruses* **2015**, *7*, 2999–3018, doi:10.3390/v7062757.
167. Hirabayashi, S.; Shirakawa, K.; Horisawa, Y.; Matsumoto, T.; Matsui, H.; Yamazaki, H.; Sarca, A.D.; Kazuma, Y.; Nomura, R.; Konishi, Y.; et al. APOBEC3B is preferentially expressed at the G2/M phase of cell cycle. *Biochem. Biophys. Res. Commun.* **2021**, *546*, 178–184, doi:10.1016/j.bbrc.2021.02.008.
168. Harris, R.S.; Dudley, J.P. APOBECs and virus restriction. *Virology* **2015**, *479–480*, 131–145, doi:10.1016/j.virol.2015.03.012.
169. Tattersall, P.; Ward, D.C. Rolling hairpin model for replication of parvovirus and linear chromosomal DNA. *Nature* **1976**, *263*, 106–9, doi:10.1038/263106a0.
170. Bonvicini, F.; Filippone, C.; Delbarba, S.; Manaresi, E.; Zerbini, M.; Musiani, M.; Gallinella, G. Parvovirus B19 genome as a single, two-state replicative and transcriptional unit. *Virology* **2006**, *347*, 447–454, doi:10.1016/j.virol.2005.12.014.
171. Guan, W.; Huang, Q.; Cheng, F.; Qiu, J. Internal polyadenylation of the parvovirus B19 precursor mRNA is regulated by alternative splicing. *J. Biol. Chem.* **2011**, *286*, 24793–24805, doi:10.1074/jbc.M111.227439.
172. Luo, Y.; Qiu, J. Human parvovirus B19: A mechanistic overview of infection and DNA replication. *Future Virol.* **2015**, *10*.
173. Reggiani, A.; Avati, A.; Valenti, F.; Fasano, E.; Bua, G.; Manaresi, E.; Gallinella, G. A Functional Minigenome of Parvovirus B19. *Viruses* **2022**, *14*, 84, doi:10.3390/v14010084.
174. Gigler, A.; Dorsch, S.; Hemauer, A.; Williams, C.; Kim, S.; Young, N.S.; Zolla-Pazner, S.; Wolf, H.; Gorny, M.K.; Modrow, S. Generation of neutralizing human monoclonal antibodies against parvovirus B19 proteins. *J. Virol.* **1999**, *73*, 1974–9.
175. Leonard, B.; McCann, J.L.; Starrett, G.J.; Kosyakovsky, L.; Luengas, E.M.; Molan, A.M.;

Burns, M.B.; McDougale, R.M.; Parker, P.J.; Brown, W.L.; et al. The PKC/NF- $\kappa$ B Signaling Pathway Induces APOBEC3B Expression in Multiple Human Cancers. *Cancer Res.* **2015**, *75*, 4538–4547, doi:10.1158/0008-5472.CAN-15-2171-T.